Università degli Studi di Padova

Dipartimento di Ingegneria dell'informazione

Corso di Laurea Magistrale in Ingegneria dell'Automazione

Tesi di Laurea Magistrale in Ingegneria dell'Automazione

Robust Control Design of an Active Steering System in Heavy Vehicles

Author:
Marco Ombrella

Advisor:
Prof. Maria Elena Valcher
Co-Advisor:
Prof. Paolo Falcone

A.Y. 2013-2014

December 2, 2014

To my parents Franco and Nadia

and to my brother Giovanni,

for their support and for believing in me.

Abstract

This thesis focuses on the design of steering control strategies in long combination of heavy vehicles. In particular, we consider the problem of controlling the steering angle of the axles of a unit called dolly, connecting a truck and a semi-trailer in a so called "Nordic combination" that has a total length of 25 meters and a weight of about 60 tons. The control problem can be stated as the problem of tracking a desired wheel angle with desired performance in a given ranges of vehicle speed and road friction.

Designing a model-based control law is challenging due to the strong nonlinearities stemming from the interaction between the road and the tire contact patch. The thesis contribution are the designs of a (i) simple Proportional-Integral (PI) controller and (ii) a Linear Parameter Varying (LPV) controller, based on Linear Matrix Inequalities (LMI) techniques. Contribution (i) aims at showing the limitation of a simple linear controller, while the objective of contribution (ii) is to propose a design framework for low level steering control strategies operating in wide ranges of speed and road friction.

Acknowledgements

I would like to express my gratitude to my Swedish supervisor Paolo Falcone, that kindly offered me the opportunity to do the thesis at Chalmers University of Technology, because without his availability I could not have had the chance to live this awesome experience. I want also thank him for his help and patience during the time I spent in Sweden.
I would like to acknowledge to Hakan Köroğlu for the "LMI Robust Stability" course that he made when I was in Chalmers, because that course was really helpful for the development of my thesis. Besides, I want to say thank him for his availability to help me in the last part of my thesis, he explained me different way to solve the problem and he was really kind to spend some of his time with me for work at my problem.
I am very grateful to my Italian supervisor Maria Elena Valcher because she contacted and asked Paolo if I could have go to Chalmers to made my master thesis. I want also to say thank to her becuase she was really helpful with me and she supported me during the whole period.
Special thanks to my landlady Ann-Britt Edlund for her availability to host me in her apartament during my permanence in Göthenburg. Furthermore, I want to say "thank you" to her because she was really kind with me and she showed me the tipical Swedish mid-summer day.
Another special thanks, I want to spend to two awesome people that I met in Göthenburg, during my permanence, Hannes Oeding and Ledion Daja. Thank you guys for every single moment spent together, for every afterwork, dinner, party, barbecue, beer, travel... so thank you very much because if my experience in Sweden was unforgettable it is only because of your.

Now let me write in Italian because it is my language and I can better express my feelings. Vorrei ringraziare tutte le persone che mi sono state vicine in questi lunghi anni di studio e fatica. Vorrei ringraziare tutti gli amici che ci sono sempre stati, nei momenti belli, ma soprattutto voglio ringraziare tutti quelli che mi hanno aiutato nei momenti brutti. Per questo voglio ringraziare tutti i miei amici di San Donà di Piave, sia quelli di vecchia data che mi conoscono da una vita, sia quelli che conosco da pochi anni. In particolare voglio ringraziare Gianluca, per essermi stato sempre vicino nonostante il mio carattere un pò solitario, grazie per aver mantenuto viva la nostra amicizia nonostante la distanza. So che su un amico come te posso sempre contare. Voglio inoltre ringraziare tutti gli amici e compagni di corso che ho incontrato a Padova, i miei cinque anni e mezzo in questa fantastica città non sarebbero stati gli stessi senza di voi. Grazie davvero per tutti i momenti che abbiamo passato insieme. In particolare, vorrei ringraziare Lucia per quello che ha fatto in quest'ultimo anno e mezzo per me. Penso che senza il tuo aiuto non sarei riuscito ad arrivare dove sono arrivato ora.
Vorrei ringraziare, inoltre, tutti i coinquilini che ho avuto in questi anni di vita Patavina che con molta pazienza mi hanno supportato, e sopportato, in ogni momento e mi hanno fatto vivere a pieno la vita universitaria. Grazie a Moreno, Alessandro, Luca, Nicola, Giacomo, Gennaro, Matteo, Luca, Daniele, Mattia, Lorenzo e Francesca per tutto quello che avete fatto per me. Un'altra persona che devo ringraziare davvero di cuore, per la suo supporto in questi ultimi anni è Giulia. Da sempre mi aiuti mi ascolti e mi consigli nel modo migliore e mi sei stata molto vicina in un momento particolare della mia vita. Grazie per tutto quello che hai sempre fatto e sono sicuro continuerai a fare. Oltre a loro

vorrei ringraziare una persona conosciuta neanche un anno fa, ma che mi è stata molto vicina durante il periodo all'estero con i suoi mille messaggi e le mille chiamate in Skype. Grazie Angelo per tutto questo.
Un grazie davvero speciale va alla mia amica, Marta, che, nonostante tutte le difficoltà che un amicizia può incontrare, è sempre stata presente in ogni momento della mia vita. Lei è stata l'Amica che mi ha sempre aiutato quando ne avevo bisogno, ha sempre avuto le parole giuste per ogni situazione e c'è sempre stata in ogni periodo della mia vita. Grazie davvero di cuore.
Volevo anche di ringraziare una persona che mi è stata accanto in questi ultimi travagliati mesi e mi ha fornito tutto il supporto necessario per portare a termine i miei studi. Grazie Eleonora.
Infine, voglio ringraziare la mia famiglia per il supporto che mi ha sempre dato. In particolare voglio ringraziare Riccardo, mio cugino, perchè è stato come un fratello maggiore, mi ha sempre aiutato e mi è stato vicino in ogni momento importante della mia vita.
Un grazie davvero speciale a mio fratello Giovanni. Grazie per quello che, anche se inconsciamente, hai fatto per me. Senza di te non sarei stato la persona che sono diventato, perchè mi hai insegnato ad essere paziente e a sopportare, soprattutto quando eri piccolo. Ora invece che sei più grande sei anche diventato un esempio da seguire per la tua tenacia e forza di volontà nel superare le difficoltà che ti si pongono sulla tua strada. Devo ammettere che ti ammiro perchè quando ti metti in testa una cosa vai diritto per la tua strada e nessuno ti ferma finchè non raggiungi l'obiettivo. So che per te avere un fratello maggiore come me non è stato semplice, ma sono sicuro che questo ha forgiato il tuo carattere e ti ha dato la forza di dare il massimo sia a scuola che nella vita. Inoltre, sono felice che hai scelto di fare Ingegneria perchè sono più che sicuro che otterrai grandi risultati nella vita perchè questa è la strada più adatta a te.

Per ultimi, ma solo perchè sono i più importanti, voglio ringraziare i miei genitori, Franco e Nadia, per il supporto che mi hanno sempre dato, per aver sempre creduto in me in ogni istante della mia vita, anche quando nessuno, neanche io, ci credeva più, e per aver sempre lottato per farmi avere un futuro migliore possibile. Se sono la persona che sono diventato è solo merito vostro perchè fin dal primo giorno della mia vita mi avete sempre educato nel migliore dei modi e non mi avete mai fatto mancare niente, soprattutto in termini di affetto. Questo importante traguardo è anche merito vostro perchè con il vostro sostegno e con il vostro amore mi avete sempre spinto a superare tutte le difficoltà che mi si ponevano davanti. Spero che, se un giorno avrò dei figli, riuscirò ad essere un bravo genitore anche solo metà di quanto lo siete stati voi. Sarete sempre un esempio da seguire per me, anche ora che sono grande, e vi porterò sempre nel mio cuore.

Marco Ombrella
Göthenburg August 2014, Sweden

Contents

Chapter 1

Introduction

During the last millennium, the transport of people and goods became fundamental to the human development. As a consequence, not only transportation means became widespread, but they also significantly improved. A carriage becomes inefficient if a little volume of material or few people are transported in a single travel. For this reason it is important to fill up the transport vehicle at each trip, in this way it is possible to obtain the maximum benefit from the transport. The dimension of the vehicle depends on the type and the quantity of the transported material. In this thesis we focus our attention on trucks. Using a double trailer truck for the transport of goods is more convenient than using two single trailer trucks to transport the same amount of products. For this reason, Volvo has put in place projects to develop long combination trucks.

Figure 1.1: Nordic Combination.

The *Nordic Combination*, shown in Figure 1.1, consists of two trailers: the first is about 8 meters long and the second about 13 meters. The first trailer is connected to the cab, whereas the second is hooked at the first by a mechanical link. This connection system normally consists of four wheels, two per axis, and it is not able to steer. Starting from this configuration, Volvo wants to realize a new type of truck that is able to steer the Dolly's wheels; this increases the manoeuvrability at low speed and the vehicle stability at high speed.
To obtain this aim it is necessary to build a new connected mechanical part, called *Active Dolly*, shown in Figure 1.2.

Figure 1.2: Mechanical System: Dolly.

The purpose of this thesis is to design a low level steering control system for an *Active Dolly*, that is able to control the road steering angle. Particular attention is focused on the most important component of this machinery, the **Wheel**. This component introduces strong nonlinearities, making the control design problem challenging. In the literature different tire models can be found, some of these models are based on a **Physical Model** and some others are based on a **Semi-empirical Model**. The model, on which this project is based, is not so simple. This is due to the non-linearity of the equations that describe the system and to their dependence on velocity. The aim of this work is to design a stable controller for the nonlinear system that maintains the performance in different conditions of velocity, from the low to the high speed.
The contributions of this thesis are:

- The design of a PI controller and the analysis of the limitations in terms of stability and performance depending on the velocity variations;
- The design of an LPV controller by means of an LMI technique.

This thesis is structured as follows. Chapter 2 provides and explains the wheel equation. First the control system used in this thesis will be described. Afterwards, there is an introduction to a semi-empirical model, that describes in a mathematical form the forces and moments acting in the system. Many and different semi-empirical models are available. In this thesis the **Pacejka Model**, used by Volvo, is considered and developed. The first controller we consider, is discussed in chapter 3. This controller is the simpler and more widespread in the market, namely a PI Controller.

Therefore, in Chapter 4 we explain the need for a new controller, a LPV robust controller. Indeed, the PI controller and the sensitivity controller are not able to correctly control the system. The non-linearity of this analyzed system requires a LPV robust control, in order to obtain acceptable results.
Chapter 5 is devoted to the presentation of some simulations used to test the controller. Finally, in Chapter 6 the conclusions and future work are presented.

Chapter 2

Tire Modeling

The objective of this chapter is to provide a basic understanding of the physics, understanding the behavior of a tire in contact with the road. The material presented in this chapter has been distilled from [1] (chapter 1 from page 1 to 13, chapter 2, chapter 3 from 87 to 127 and chapter 4).

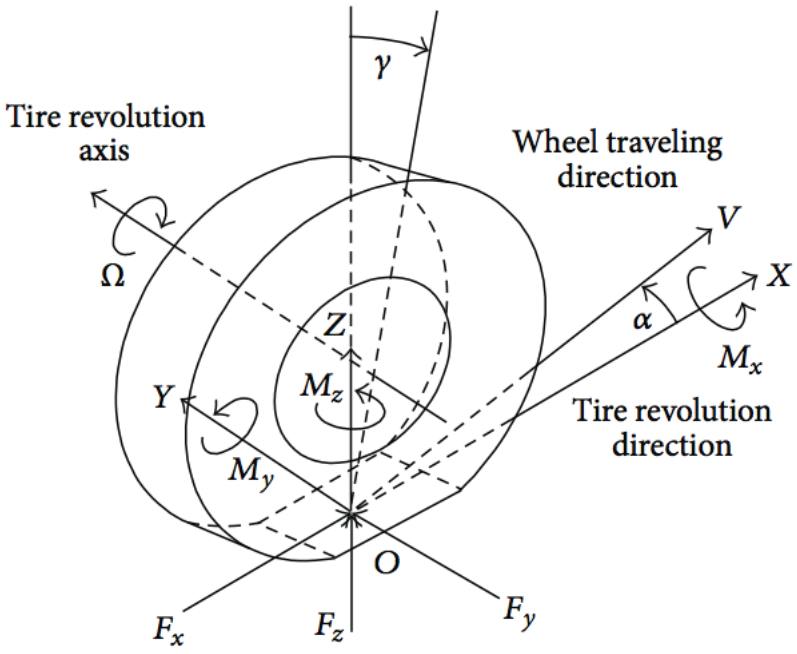

Figure 2.1: Tire Axis System [1]

Figure 2.1 represents the forces, moments and angles characterizing the behavior of the wheel.
The longitudinal force F_x acts along the X-axis, together with the moment M_x, which appears consequently to the oscillation of the tire. The angle between the X-axis and the velocity vector V is the *slip angle* α.
The lateral force F_y, the *speed of revolution* Ω and the moment M_y act along the Y-axis. Finally, along the Z-axis, the force F_z and the self aligning moment M_z are defined. In the presence of a deflection, the angle between the Z-axis and the normal axis of the wheel is the *camber angle* γ.

If the road surface is flat we can approximate the contact patch with a rectangle where $2a$ is the length and $2b$ is the width. Indeed the moment M_z value increases proportionally with the contact surface between the wheel and the road.

The purpose of this chapter is to describe the **Steering Dynamics** used to desing a control system. To this purpose, it will be useful to introduce the reference system and the input tire quantities and subsequently the most used semi-empirical model, called **Pacejka Model**. This model describes in an analytical way the wheel equation functioning and it is necessary to control the wheel system.
The **Pacejka Model**, shown in this thesis, is a distillate of the results contained in Pacejka's book [1].

2.1 Tire Steering Dynamics

The following sections will introduce and explain the input variables, the physical model and the semi-empirical model of the tire. We need this knowledge to derive an accurate description of the forces acting on the wheel. Preliminarly we derive the steering equation that we will use to design the controller.
The steering angle θ satisfies the differential equation:

$$I_w\ddot{\theta}(t) = -b\dot{\theta}(t) + \bar{M}_z(t, \kappa, \alpha, \mu, F_z) + T_{in}(t) \tag{2.1}$$

where I_w is the tire inertia, b is the damping coefficient, $\bar{M}_z$ is the disturbance and $T_{in}(t)$ is the control input and is the moment that the controller has to generate to control the system.

2.2 Reference Frame, Basic Terminology and Notation

After introducing the steering equation, we have to define the *Tire Reference System* that we use in this work. Figure 2.1 shows a reference frame, introduced with the origin in the point of contact between the road and tire and the most relevant variables. Assuming to be in the case of free rolling on a flat road and without an upright position ($\gamma = 0$) and without yaw rate ($\dot{\psi} = 0$), the velocity acting in the center of the wheel along the longitudinal direction is:

$$V_x = r_e\Omega, \tag{2.2}$$

where Ω is the rotating speed of the wheel and r_e is the effective wheel radius. In condition of braking and driving the longitudinal slip is different from zero and the contact patch will move with a longitudinal slip speed V_{sx} defined as:

$$V_{sx} = V_x - r_e\Omega. \tag{2.3}$$

The *longitudinal slip* or *slip ratio* κ is defined as the ratio between the longitudinal slip velocity V_{sx} of the contact patch and the speed of the wheel center V_x:

$$\kappa = -\frac{V_{sx}}{V_x} \Rightarrow \kappa = -\frac{V_x - r_e\Omega}{V_x}. \tag{2.4}$$

The sign of κ depends on the wheel state. During the tire driving the longitudinal force F_x is positive, then κ is positive, but when braking the sign of F_x changes and consequently even the sign of κ becomes negative. When the wheel is locked ($\Omega = 0$), the slip ratio

value saturates at -1.

When the tire proceed straight, there is only a longitudinal slip velocity V_{sx}, as shown before. During a curve manouvre, another slip velocity appears along the lateral axis, the lateral slip velocity $-V_{sy}$. The *lateral slip* or *slip angle* α is the arctan of the ratio between the lateral slip velocity $-V_{sy}$ and the longitudinal slip velocity V_{sx}:

$$\alpha = \arctan\left(-\frac{V_{sy}}{V_{sx}}\right). \tag{2.5}$$

The *spin slip* φ is obtained as the ratio of two terms: $-\omega_z$ absolute speed of rotation speed and the longitudinal velocity V_x. The expression of $-\omega_z$ is derived as the difference between the yaw rate $\dot{\psi}$ and the term $\Omega \sin\gamma$ that represents the camber reduction. In this way, we obtain for φ the following expression:

$$\varphi = -\frac{\omega_z}{V_x} = \frac{(\dot{\psi} - \Omega \sin\gamma)}{V_x}. \tag{2.6}$$

If the slip angle is constant ($\dot{\alpha} = 0$) and the road is fla, the expression of φ becomes:

$$\varphi = -\frac{1}{R} + \frac{\Omega}{V_x}\sin\gamma = -\frac{1}{R} + \frac{1}{r_e}\sin\gamma, \tag{2.7}$$

where r_e is the effective wheel radius.

2.3 Pacejka Model

In order to provide the necessary understanding of the tire forces and moments, a semi-empirical model is presented next. This is called **Pacejka Model**. This model consists of a number of *shape functions*, whose parameters are calculated using experimental data and whose evolution follows the real one.

2.3.1 Shape Functions

The forces and the moments, included the self aligning moment M_z, can be defined using a shape function with the following expression:

$$y(x) = D \sin\left[C \arctan\left\{Bx - E\left(Bx - \arctan Bx\right)\right\}\right], \tag{2.8}$$

where x is the input variable κ or α, B is the stiffness factor, C the shape coefficient, D the peak value and E the curvature coefficient. (2.8) generates a curve that passes through the origin, reaches a maximum and subsequently tends to an horizontal asymptote. However, the self aligning curve does not usually pass over the origin and shows an anti-symmetric shape respect to the origin. For this reason, we shift terms were introduced and therefore the curve shows an offset toward the axis origin:

$$\begin{aligned} Y(X) &= y(x) + S_V \\ x &= X + S_H \end{aligned} \tag{2.9}$$

where X is the input variable, such as $\tan\alpha$ or κ, Y is the output variable for example (F_x, F_y or M_z), S_V is the vertical shift and S_H is the horizontal shift.

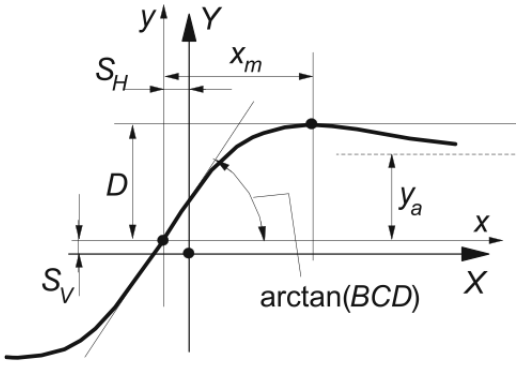

Figure 2.2: The meaning of the coefficient appearing in the Magic Formula curve. [1]

In Figure 2.2 the geometric interpretation of the coefficients in (2.8) is shown. $\arctan(BCD)$ corresponds to the slope of the curve, while the D coefficient represents the peak of the curve and the value of C changes the amplitude of the sine function. The E coefficient has different properties: it modifies the curvature at the peak and defines the position of the ascissa of the peak point. Finally, the B coefficient is used to determine the slope at the origin and is called stiffness coefficient.
The shape coefficient C may be computed as:

$$C = 1 \pm \left(1 - \frac{2}{\pi} \arcsin \frac{y_a}{D}\right), \tag{2.10}$$

where y_a is the height of the horizontal asymptote described in Figure 2.2.
On the other hand, the value of E is given by:

$$E = \frac{Bx_m - \tan[\pi/(2C)]}{Bx_m - \arctan[Bx_m]}, \tag{2.11}$$

where x_m is the peak point, as shown in Figure 2.2.

2.3.2 Representation of the Self Aligning Moment

The self aligning moment M_z is obtained as the sum of three terms:

$$M_z = -t(\alpha_{t,eq})F_y + M_{zr}(\alpha_{r,eq}) + s(F_y, \gamma)F_x. \tag{2.12}$$

The first term is the product of the side force F_y and the pneumatic trail t. The second term represents a small residual torque M_{zr}, as shown in Figure 2.3. The last term takes into account the contribute of the longitudinal force. Indeed, $s(F_y, \gamma)$ is the point of application of the force and F_x is the longitudinal force.
The side force F_y takes into account the influence of the longitudinal force and is therefore defined in the following way:

$$F_y = G_{y\kappa}F_y^{'} + S_{Vy\kappa}, \tag{2.13}$$

where $G_{y\kappa}$ is the weight function.
The generic weight function G is introduced to reproduce the interaction effect between F_y and κ or F_x and α and it is multiply the original pure slip function (2.8). The characteristic

of G is similar to an hill and it reaches its maximum value in case of pure slip (either κ or α equal to zero). The cosine version of (2.8) is used to represent the hill shaped function:

$$G = D\cos\left[C\arctan(Bx)\right]. \tag{2.14}$$

The residual force exhibits the same behavior of the pneumatic trail:

$$M_{zr}(\alpha_r) = D_r\left[\arctan(B_r\alpha_r)\right] \tag{2.15}$$

where:

$$\alpha_r = \tan\alpha + S_{Hf} \tag{2.16}$$

and S_{Hf} is the shift term with respect to the slip angle. We can observe that each element in (2.12) is modelled using the **Magic Formula** (2.8), upon replacing the sine function with the cosine function. In this way the peaks are shifted sideway and equation (2.15) produces a hill-shaped curve. The residual torque has the maximum value D_r at the slip angle when the side force becomes zero. This is shown in Figure 2.3.

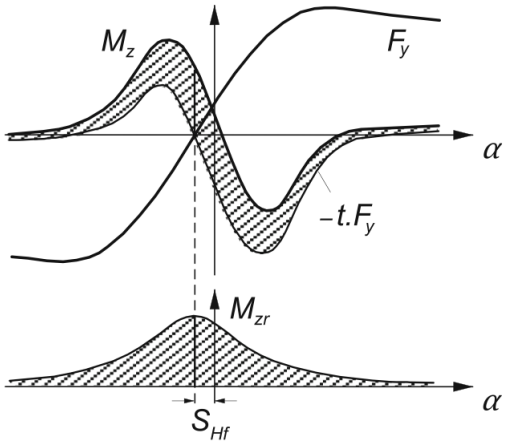

Figure 2.3: The self aligning torque composed from two term. [1]

The advantage of using (2.12), instead (2.8), to obtain the aligning torque is that in this way we can assess directly the function for the pneumatic trail needed to handle the combined slip situation.
The longitudinal force F_x is adjusted with the weighting function $G_{x\alpha}$: in this way also in the longitudinal force there is the interaction with the lateral force. The $\alpha_{t,eq}$ and $\alpha_{r,eq}$ terms, that appear in the equation of the pneumatic trail and the residual moment, are the equivalent slip angles incorporating effect κ on the composite slip. StOnce we define the value of α_t as:

$$\alpha_t = \tan\alpha + S_{Ht} \tag{2.17}$$

we can therefore introduce the terms $\alpha_{t,eq}$ and $\alpha_{r,eq}$, appearing in (2.12) and (2.15):

$$\alpha_{t,eq} = \sqrt{\alpha_t^2 + K^2\kappa^2} \tag{2.18}$$

where K is used to approximate the same effect on the degree of sliding in the contact patch. The expression of $\alpha_{r,eq}$ is similar to (2.18).

(2.12) describes the self aligning moment characteristic: due to the presence of the trigonometric function this curve has a non-linear characteristics.

2.3.3 Detailed Analysis of Self Aligning Moment

Section 2.3.1 explains how the self aligning curve was obtained. Now we want to analyze the main relationship between the self aligning moment and the input parameters described at the beginning of this chapter. Based on (2.12) described in 2.3.1, the self aligning moment can be written as a function of the following input parameters:

$$M_z = f_z(\kappa, \alpha, \mu, F_z, \gamma, \varphi) \tag{2.19}$$

where:

- κ = slip ratio;
- α = the slip angle. This depends on the steering angle δ and the vehicle states;
- μ = friction coefficient between wheel and road;
- F_z = normal force;
- γ = camber angle;
- φ = turn slip defined as:

$$\varphi = -\frac{1}{V_x}(\dot{\psi} + (1 - \varepsilon_\gamma)\Omega \sin\gamma), \tag{2.20}$$

where the $\dot{\psi}$ is the yaw rate, V_x is the longitudinal velocity or forward velocity, ε_γ is the camber reduction coefficient for the camber angle and Ω is the rotational velocity of the wheel. For trucks the value of ε_γ is approximately equal to 1, so (2.20) reduces to:

$$\varphi = -\frac{\dot{\psi}}{V_x} = \text{ (for constant angle of steering) } = -\frac{1}{R} \tag{2.21}$$

where R is the radius of the travelled path.
It should be noticed that φ decreases with V_x. Hence, M_z depends on φ at low speed only. In order to analyze how the three terms in the self aligning moment M_z equation (2.12) depend on the input variables, we present again the formula:

$$M_z = -tF_y + sF_x + M_{zr}, \tag{2.22}$$

where the $-tF_y$ term represents the lateral deformation that occurs in the wheel, sF_x the longitudinal one and the term M_{zr} represents the forces and moments acting on the wheel at a low speed. The dependencies of the input parameters are:

- $t = f_t(\kappa, \alpha, F_z, \gamma, \varphi)$ is the pneumatic trail;
- $F_y = f_{F_y}(\kappa, \alpha, \mu, F_z, \gamma, \varphi)$ is the lateral force;
- $s = f_s(F_y, F_z, \gamma)$ is the moment arm;
- $F_x = f_{F_x}(\kappa, \alpha, \mu, F_z, \gamma, \varphi)$ is the longitudinal force;
- $M_{zr} = f_{M_{zr}}(\kappa, \alpha, \mu, F_z, \gamma, \varphi)$ is the residual torque.

In the following, we analyze every single term of the moment's equation (2.22).

Term: $-t\,F_y$

The term $-t\,F_y$ models the moment on the tyre in a cornering manouvre.
The pneumatic trail is a shape function that decays with increasing side slip, and is described by the following nonlinear function:

$$t = f_t(\kappa, \alpha, F_z, \gamma, \varphi) \tag{2.23}$$

where:

- κ = slip ratio;
- α = slip angle;
- F_z = normal force on the wheel;
- γ = camber angle;
- φ = turn slip.

The pneumatic trail t is descripted using the shape function (2.8); the result is the following:

$$t = D_t cos[C_t arctan\{B_t\alpha_t - E_t(B_t\alpha_{t,eq} - arctan(B_t\alpha_{t,eq}))\}] \tag{2.24}$$

where:

- D_t is the peak value that depends on the variables F_z, γ and φ;
- C_t is a shape factor;
- B_t is the stiffness factor, depending on F_z and γ;
- E_t is the curvature factor, depending on F_z and α;
- $\alpha_{t,eq}$ is a combination of the slip ratio and the slip angle and is equal to $\sqrt{\alpha_t^2 + K^2\kappa^2}$, where K is a constant.

Figure 2.4 shows how the term t redefines the curve of the lateral force F_y as a function of $\alpha_{t,eq}$.

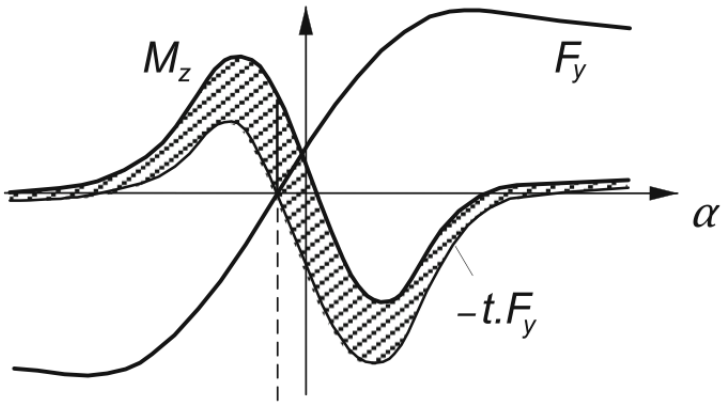

Figure 2.4: Effect of the trail t

It is interesting to observe that the value of camber angle γ is rather small in a vehicle/truck wheel (i.e. is around $1 \div 4$ degrees), hence in the formulas described in [1], it does not significantly affects on the term t. For this reason, we can simplify the equation of the trail and omit the value of the camber angle γ.
Hence equation (2.23) can be simplified as follows:

$$t = f_t(\kappa, \alpha, F_z). \tag{2.25}$$

The side force, or lateral force, F_y is the force acting on the tyre vehicle cornering and is defined in (2.13). We have only to describe the F_y term as a nonlinear function of the following variables:

$$F_y = f_{F_y}(\kappa, \alpha, \mu, F_z, \gamma, \varphi) \tag{2.26}$$

The lateral force F_y is described using the shape function (2.8); the result is the following:

$$F_y = D_y \sin\left[C_y \arctan\left\{B_y\alpha_{t,eq} - E_y(B_y\alpha_{t,eq} - \arctan(B_y\alpha_{t,eq}))\right\}\right] \tag{2.27}$$

where:

- D_y is the peak value that depends on the variables F_z, γ and φ;
- C_y is a shape factor;
- B_y is the stiffness factor, depending on F_z and γ;
- E_y is the curvature factor, depending on F_z and α;
- $\alpha_{t,eq}$ is a combination of the slip ratio and the slip angle and is equal to $\sqrt{\alpha_t^2 + K^2\kappa^2}$, where K is a constant.

where:

- κ = slip ratio,
- α = slip angle,
- μ = friction coefficient,
- F_z = normal force on the wheel,
- γ = camber angle,
- φ = turn slip.

Similar arguments hold for F_y, leading to the following simplified expression:

$$F_y = f_{F_y}(\kappa, \alpha, \mu, F_z). \tag{2.28}$$

An example of a lateral force as a function of α for given κ, μ and F_z is shown in Figure 2.4. Finally, we can write the expression using the formulas (2.25) and (2.28), as follows:

$$-t\, F_y = -f_t(\kappa, \alpha, F_z)\; t_{F_y}(\kappa, \alpha, \mu, F_z) \tag{2.29}$$

Term: $s\,F_x$

The second term in (2.22) models the effect on the moment M_z of the braking and driving force. This term is the product of the force arm s and the longitudinal force F_x. The force arm is defined as the nonlinear function:

$$s = f_s(F_y, F_z, \gamma) \tag{2.30}$$

So the s term is a shape function depending on the camber γ, the normal force F_z and the lateral tire deflection related to F_y, as shown in the following equation:

$$s = R_0 \left\{ K_{s1} + K_{s2}\frac{F_y}{F_z} + K_{s3}\gamma \right\}, \tag{2.31}$$

where R_0 is the wheel radius and K_{s1}, K_{s2} and K_{s3} are constant. As far as parameter t in Section 2.3.3 is concerned, we can neglect the camber angle γ in the final formula of s, obtaining the following expression for the force arm:

$$s = f_s(F_y, F_z). \tag{2.32}$$

The longitudinal force F_x is generated in a braking/driving condition and is expressed as:

$$F_x = f_{F_x}(\kappa, \alpha, \mu, F_z, \gamma, \varphi). \tag{2.33}$$

The longitudinal force is expressed by the equation (2.8) as follow:

$$F_x = D_x \sin\left[C_x \arctan\left\{B_x\alpha_{t,eq} - E_x(B_x\alpha_{t,eq} - \arctan(B_x\alpha_{t,eq}))\right\}\right] \tag{2.34}$$

where:

- D_x is the peak value that depends on the variables F_z, γ and φ;
- C_x is a shape factor;
- B_x is the stiffness factor, depending on F_z and γ;
- E_x is the curvature factor, depending on F_z and α;
- $\alpha_{t,eq}$ is a combination of the slip ratio and the slip angle and is equal to $\sqrt{\alpha_t^2 + K^2\kappa^2}$, where K is a constant.

where:

- κ = slip ratio;
- α = slip angle;
- μ = friction coefficient;
- F_z = normal force on the wheel;
- γ = camber angle;
- φ = turn slip.

As for the trail function t in (2.25), we can simplify the function of the longitudinal force and write the previous equation as:

$$F_x = f_{F_x}(\kappa, \alpha, \mu, F_z). \tag{2.35}$$

Finally, we can write the the second term in (2.22), by combining the formulas (2.32) and (2.35), as follows:

$$s\,F_x = f_s(F_y, F_z)\; f_{F_x}(\kappa, \alpha, \mu, F_z). \tag{2.36}$$

Term: M_{zr}

The residual torque M_{zr} models the moment acting on the tyre when the lateral and longitudinal forces become zero. Hence the forces F_y and F_x are assumed close to zero, as it can be seen in Figure 2.5. This term becomes particularly important in low speed manouvres, when the velocity is very close to zero and the effect of the first two terms in equation (2.22) is almost null.

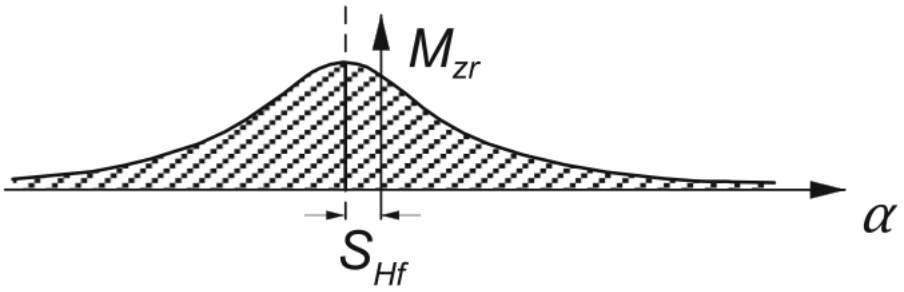

Figure 2.5: Description of the Moment M_{zr}

The term M_{zr} is defined in section 2.3.1 in (2.15) and it depends on:

- κ =slip ratio;
- α = slip angle;
- μ = friction coefficient;
- F_z = normal force on the wheel;
- γ = camber angle;
- φ = turn slip.

The value of α and κ appear in the residual torque M_{zr}, as reported in formula (2.18); the coefficient K is the ratio between the longitudinal and lateral slip stiffness.

$$\alpha_{r,eq} = \sqrt{\alpha_r^2 + K^2\kappa^2} \tag{2.37}$$

As for the terms t and F_y in $-t\,F_y$, we can simplify this equation by neglecting the effect of the variables γ and φ, following the same arguments. We then obtain the expression of the residual torque as:

$$M_{zr} = f_{M_{zr}}(\kappa, \alpha, \mu, F_z). \tag{2.38}$$

Following the aforementioned consideration, using (2.29), (2.36) and (2.38), the equation of the residual torque can be written as the equation of the self aligning moment:

$$M_z = -f_t(\kappa, \alpha, F_z)\; f_{F_y}(\kappa, \alpha, \mu, F_z) + f_s(F_y, F_z)\; f_{F_x}(\kappa, \alpha, \mu, F_z) + f_{M_{zr}}(\kappa, \alpha, \mu, F_z) \tag{2.39}$$

The dependence of the self aligning moment on the parameters κ, α, μ and F_z is shown in the Appendix A.

2.3.4 Effects of Velocity on Self Aligning Moment

In this section we analyze the effect of velocity V_x in (2.22). Indeed, equation (2.22) depends on φ only at low speed. To take this into account, we have to add the turn slip quantity φ into the model (2.22). In [1] the shape form ζ appears to introduce the dependence on φ in every term of (2.22). Now, it is shown how this term is introduced in each component of M_z and how it modifies the variables.
In Appendix B the complete formulas of ζ are reported.

Effect on the M_{zr} term

The M_{zr} term is the one most influenced by the ζ term. The equation of the residual moment was rewritten in section 2.3.1 using equation (2.15):

$$M_{zr}(\alpha_r) = D_r \left[\arctan(B_r \alpha_r)\right] \tag{2.40}$$

In every variable D_r, C_r, B_r and α_r there are different ζ shape functions that change their value together with the velocity.
In the expression (2.16) of α_r the coefficients ζ_2, ζ_3 and ζ_4 change the value of this angle.

$$\begin{aligned} \alpha_r &= \tan\alpha + S_{Hf} \\ S_{Hf} &= K_{\varphi 9}\zeta_4 + K_{\varphi 10}\zeta_2 \end{aligned} \tag{2.41}$$

where $K_{\varphi 9}$ and $K_{\varphi 10}$ are constant, and the terms ζ_2 and ζ_4 are defined as follow:

$$\begin{aligned} \zeta_2 &= \cos[\arctan(K_{\varphi 2}\varphi)] \\ \zeta_4 &= 1 + S_{Hy\varphi} - \frac{S_{Vy\gamma}}{K_{y\alpha}} \end{aligned} \tag{2.42}$$

where:

- $S_{Hy\varphi}$ is a shape factor and it depends on F_z and φ;
- $S_{Vy\gamma}$ is a term depending on F_z, γ and ζ_2;
- $K_{y\alpha}$ is a term depending on F_z and ζ_3.

At zero velocity, $S_{Vy\gamma}$ and $K_{y\alpha}$ are zero because there are ζ_2 and ζ_3 term that annul the value. Indeed, the $S_{Hy\varphi}$ term is approximately F_z because the ζ_4 term is equal to F_z if the velocity is zero. Instead, if the velocity is different from zero we have that $S_{Vy\gamma}$ and $K_{y\alpha}$ are more or less equal and their ratio is 1. The value of ζ_4 is close to zero because the $S_{Hy\varphi}$ term is about zero.
In the B_r term there is the ζ_6 variable and it is introduced in the way that changes the ampitude of the B_r. The ζ_6 variable changes the value of the arcotangent function and hence the value of the cosine, so at low speed (2.40) depends only of the term D_r. The expression of ζ_6 is the following:

$$\zeta_6 = \cos[\arctan(K_\varphi \varphi)] \tag{2.43}$$

In the C_r term there is the ζ_7 variable. This term changes the value of the cosine function and there is similar arguments hold for B_r. The expression of ζ_7 is the following:

$$\zeta_7 = \frac{2}{\pi} arcos(\frac{M_{z\varphi 90}}{D_{r\varphi}}) \tag{2.44}$$

where:

- $M_{z\varphi 90}$ is a term that depends on F_z, μ and φ;
- $D_{r\varphi}$ is a term that depends on F_z and φ.

In (2.44) if the velocity is close to zero the values of $M_{z\varphi 90}$ and $D_{r\varphi}$ are equal, more or less, to F_z and the term ζ_7 is zero, because the arcocosine value is zero. Whereas if the velocity is different from zero, the value of the $M_{z\varphi 90}$ term is zero and ζ_7 is equal to 1 because the arcocosine value is $\frac{\pi}{2}$.
At last, in the D_r term there are ζ_2 and ζ_8. These two terms influence the amplitude of in (2.40), indeed at low speed D_r is equal to the product of μ and F_z, while at high speed this term is equal to zero. The equation of ζ_8 is the following:

$$\begin{aligned} \zeta_8 &= 1 + D_{Dr\varphi} \sin(K_{\varphi 8}\varphi) \\ D_r &= \mu F_z \zeta_2 + \zeta_8 - 1 \end{aligned} \tag{2.45}$$

where $D_{Dr\varphi}$ depends on F_z and μ. If the velocity is close to zero equation (2.45) is equal to the product between F_z and μ. If the velocity is different from zero, (2.45) is equal to 1.
In the Figure 2.6 is shown as the velocity influences the residual moment characteristic. The M_{zr} term assumes high values when the velocity is close to zero. This behavior is due because the residual moment describes the force acting on the tire when the velocity is close to zero. For this reason, the value of M_{zr} is high for low speed. Increasing the velocity, M_{zr} descreases its values and becomes zero at high speed.
In conclusion, the residual moment M_{zr} describes the forces acting on the tire at low

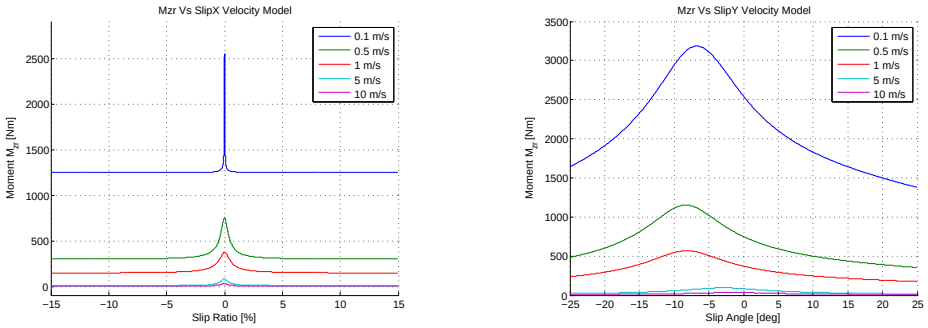

Figure 2.6: Characteristic of M_{zr} depending on the slip ratio on the left and depending on the slip angle on the right.

speed. This term assumes high value at low velocity and decreases its effect when the velocity increases.

Effect on the $-tF_y$ term

After the analysis of M_{zr} term in (2.22), we want to see how the velocity influences the combined term $-tF_y$, as shown in Figure 2.7. This term describes the forces acting on the tire when there is a cornering manouvre.
In Figure 2.7 on the left, it is shown the comparison between the influence that the velocity has on the $-tF_y$ term and the effect that the slip ratio κ has on the same term. When the velocity is low the $-tF_y$ term is zero for every value of κ, instead when the velocity is high this term has a peak close to the zero value of κ. This perfectly corrisponds to what we expected to see. The practical meaning of the graph is the following: at low speed, the lateral term is practically irrelevant; at high speed it becomes instead important, especially

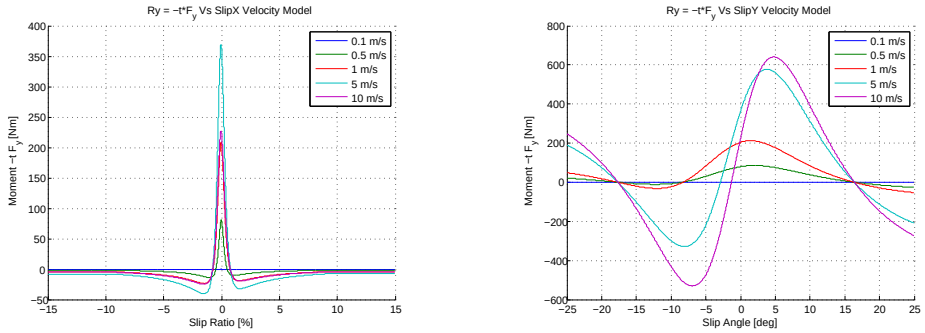

Figure 2.7: Characteristic of $-tF_y$. On the left it depends on the slip ratio, on the right depends on the slip angle.

in conditions of full adhesion, i.e. when κ is close to zero. In Figure 2.7 on the right, it is shown how the velocity influences the $-tF_y$ term comparing this influence to that that the slip angle α has on the same term. The behavior is equal to the one analized for the slip ratio κ. The $-tF_y$ characteristic respects the slip angle α meaning that at low velocity we do not have any effect of the term, increasing the velocity the effect of the velocity appears. At high velocity the curve has, more or less, the same waveform of the self aligning moment.
In conclusion, at low speed, the lateral term $-tF_y$ is practically irrelevant both for the slip ratio κ and for the slip angle α. At high speed it becomes instead important, especially in conditions of full adhesion, i.e. when κ is close to zero. Regarding the $-tF_y$ characteristic respects the slip angle α meaning that at high velocity the curve has, more or less, the same waveform of the self aligning moment.

Effect on the sF_x term

The last term of (2.22), that we are remained to analyze how the velocity influence its behavior, is the combined term sF_x, as shown in Figure 2.8. This term represents the forces acting on the tire when there is a braking/driving manouvre.

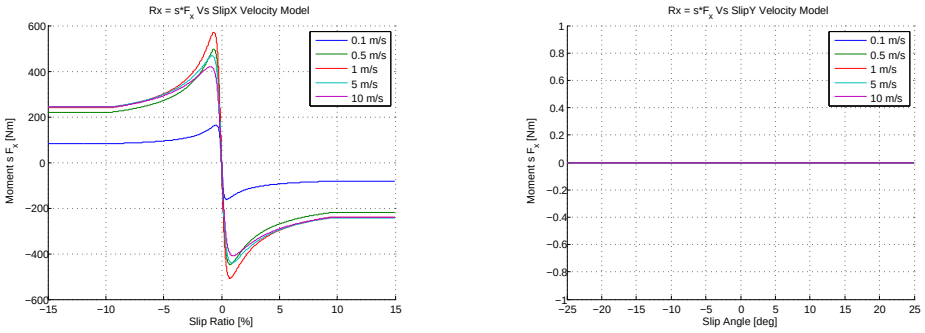

Figure 2.8: Characteristic of sF_x. On the left it depends on the slip ratio, on the right depends on the slip angle.

In Figure 2.8 on the left, it is shown how the velocity influences the sF_x term respect the slip ratio κ. We note that if the velocity changes its value from low to high speed, the curve increases its values. Instead, increasing the velocity, the adhesion term becomes higher, especially when the longitudinal slip, κ is close to zero. In Figure 2.8 on the right, it is shown how the velocity influences the sF_x term respect the slip angle α. The characteristic has a strange behaviour that we do not expect: the curve is zero for every value of α. This

is strange and the only possible explanation is that in case of slip angle changing the arm force s is zero and this causes the strange behavior.
In conclusion, the speed influences the sF_x term because it assumes higher values more as the velocity increases. In other words, the term that describes the longitudinal tire deformation depends on the velocity.

Effect on the M_z

At the end of our analysis of the effect of the velocity on (2.22), we show in Figure 2.9, as the characteristic of M_z changes with the velocity.
In Figure 2.9 on the left, it is shown how the self aligning moment characteristic changes

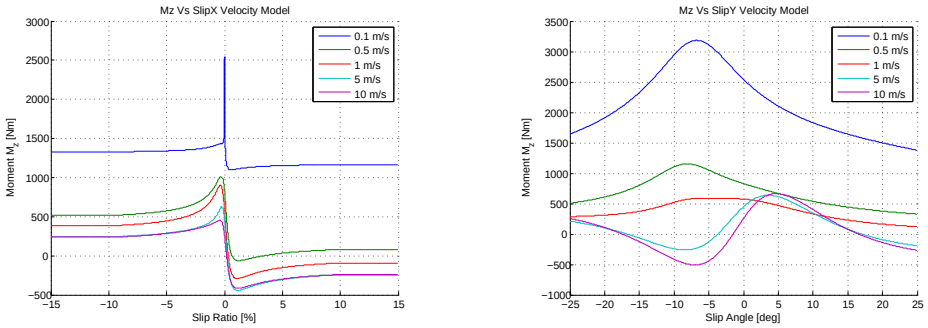

Figure 2.9: Characteristic of M_z. On the left it depends on the slip ratio, on the right depends on the slip angle.

with different velocities in relation with the slip ratio κ. We note that the curve is in particular the sum of two terms: M_{zr} at the low speed and sF_x at the high speed. Indeed, if we observe the Figure 2.6 and 2.8 on the left, we note the following behavior. At low speed the characteristic is very elevate and has a peak in corrispondence of the value $\kappa = 0$, but maybe this value is too elevate. At high velocity we have that the curve becomes equal to sF_x, this is an agreement with the previous description of the term sF_x and M_{zr}. Instead, in the Figure 2.9 on the right, it is shown how the self aligning moment characteristic changes with different velocity in realtion with the slip angle α. This time the curve is the sum of the residual moment term M_{zr} and the term $-tF_y$. Observing the right Figure of 2.8 and 2.6 we note that at low speed the curve depends on the value of M_{zr} and at high speed the characteristic assumes the same value as $-tF_y$.
We understand that the decription of the self aligning moment, described in the equation (2.39), depends on the value of the velocity.

Chapter 3

Baseline Controller

In this chapter we show the design of a baseline controller with the objective of:

1. Assessing the performance of the controller later designed in chapter 4;
2. Show the limitations of simple controller structures such as P or PI.

3.1 Problem Formulation

Consider the system:

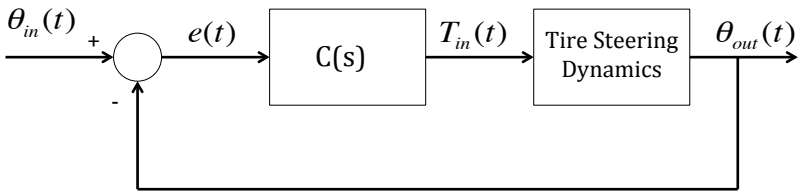

Figure 3.1: Initial Control System.

where the Tire Steering Dynamics are described by equation (2.1), the reference input $\theta_{in}(t)$ is the desired steering angle, the system output $\theta_{out}(t)$ is the actual steering angle, and $T_{in}(t)$ is the control input.
The objective of this chapter is to design a linear controller C(s) that makes the resulting controled loop satisfy the following specifications:

- M = 15 % (overshoot);
- Minimize the settling time t_s and the rise time t_r;
- Zero steady state error at the step;
- Limit the value of the control input below 200 Nm.

Two structures, namely P and PI controllers, will be considered.

3.2 Control Oriented Model

The Tire Steering Dynamic equation (2.1) is reported next:

$$I_w\ddot{\theta}(t) = -b\dot{\theta}(t) + M_z(t, \kappa, \alpha, \mu, F_z) + T_{in}(t). \tag{3.1}$$

Equation (3.1) is nonlinear due to the presence of the self aligning moment M_z. Next, we derive a linear model of the equation (3.1) to design a controller C(s) with standard the frequency domain techniques.
For constant κ, μ and F_z, M_z is a nonlinear function of α, as shown in Figure 3.2. Nevertheless, such nonlinear characteristics can be nicely approximated by a piece-wise linear function by partitioning the x-axis in three different regions and approximating the curve with three different lines, one for each region as shown in Figure 3.2.

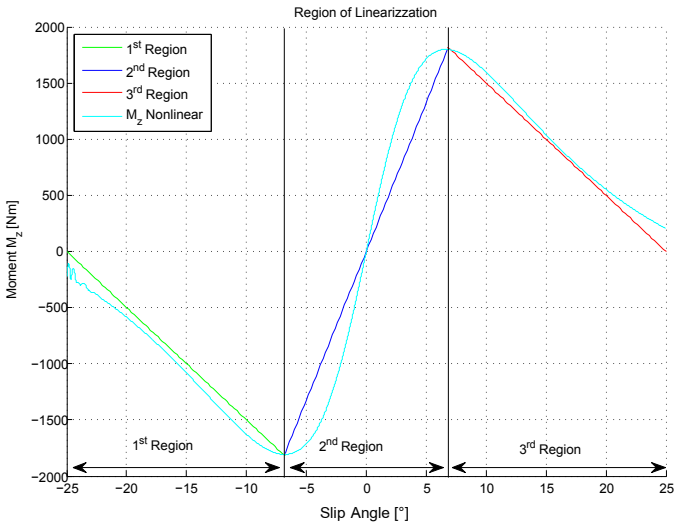

Figure 3.2: Self Aligning Moment Piecewise Line Characteristic.

The 2^{nd} region is the "linear" region and is characterized by a positive slope of the corrisponding linear approximation, while the 1^{st} and the 3^{rd} regions are called "saturation" regions and have a negative slope.
The description of the approximated self aligning moment characteristic with a piece-wise linear function is the following one:

$$M_z = \begin{cases} -C_{M\alpha,1}\alpha - \bar{M_{z,1}}, & -20° < \alpha < -6°, \\ C_{M\alpha,2}\alpha - \bar{M_{z,2}}, & -6° < \alpha < 6°, \\ -C_{M\alpha,3}\alpha + \bar{M_{z,3}}, & 6° < \alpha < 20°, \end{cases} \tag{3.2}$$

where $C_{M\alpha,1}$, $C_{M\alpha,2}$ and $C_{M\alpha,3}$ are positive coefficients. The constant terms $\bar{M_{z,1}}$, $\bar{M_{z,2}}$ and $\bar{M_{z,3}}$ are determinated via numerical linearization .
As we can see from Figure 3.2, it is clear that, one fixed the values for κ, μ and F_z, both $C_{M,\alpha,i}$ and $\bar{M}_{z,i}$ depend on α. Moreover, from equation (2.19) we conclude that $C_{M\alpha,i}$ and $\bar{M}_{z,i}$ depend on κ, μ and F_z as well:

$$M_z(t, \kappa, \alpha, \mu, F_z) = \bar{M}_z(\kappa, \alpha, \mu, F_z) + C_{M\alpha}(\alpha, \mu, F_z)\alpha(t). \tag{3.3}$$

The approximation (3.2) can be further manipulated to express M_z as a function of θ. Indeed, the slip angle $\alpha(t)$ is a function of the steering angle $\theta(t)$ as follows

$$\alpha(t) \simeq \arctan\left(\frac{V_y + d\dot{\psi}}{V_x} - \theta(t)\right), \tag{3.4}$$

where V_x and V_y are the longitudinal and lateral velocities of the wheel, d is the tire distance of the steering axis from the dolly center of gravity (COG) and $\dot{\psi}$ is the yaw rate, as shown in Figure 3.3.

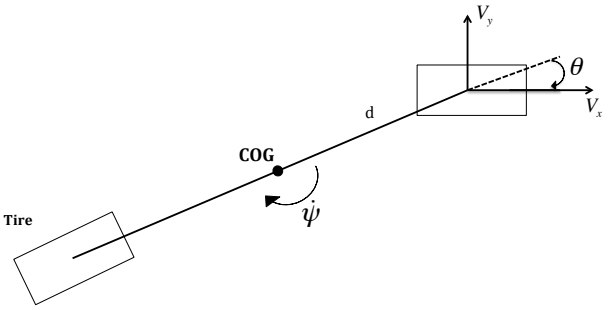

Figure 3.3: Simplifield dolly model.

In case of a small slip angle ($|\alpha| \leq 15°$), it is possible to approximate the arctan $\left(\frac{V_y+d\dot{\psi}}{V_x} - \theta(t)\right)$ with the argument of the arctan. At steady state, in a pure cornering manouvre (when the tire executes a curve manouvre at a constant velocity), the term $\frac{V_y+d\dot{\psi}}{V_x}$ is constant. Therefore, we can approximate equation (3.4) with the sum of a "constant" term, which depends on the value of $\frac{V_y+d\dot{\psi}}{V_x}$, and a variable term, which depends on the variable $\alpha(t)$. Following the aforementioned considerations, the equation (3.4) at steady state in case of little slip angle α becomes:

$$\alpha(t) \simeq -\theta(t) + c(V_x, V_y, \dot{\psi}). \tag{3.5}$$

Using equation (3.5), it is possible to substitute equation (3.5) in the approximated of self aligning moment characteristic with a piece-wise linear function (3.2) and we obtain:

$$M_z = \begin{cases} -C_{M\alpha,1}\theta - \bar{M_{z,1}} + \varepsilon_1, & -20° < \theta < -6°, \\ C_{M\alpha,2}\theta - \bar{M_{z,2}} + \varepsilon_2, & -6° < \theta < 6°, \\ -C_{M\alpha,3}\theta + \bar{M_{z,3}} + \varepsilon_3, & 6° < \theta < 20°, \end{cases} \tag{3.6}$$

where ε_1, ε_2 and ε_3 are unknown disturbances. These disturbances are due to two different types of event, that the terms $C_{M\alpha,i}$ and $\bar{M}_{z,i}$, $i = 1, 2, 3$, of equation (3.6) do not describe, and they are:

- **Constant input signals**: in particular constant disturbances as the banking (inclination of the road) and the unevenness of the road. So, we insert these disturbances in the terms ε_i, $i = 1, 2, 3$;
- **Linearization of the M_z characteristic**: the equation (3.5) depends on the term $\frac{V_y+d\dot{\psi}}{V_x}$ which varies according to different condition of working. In equation (3.2) the terms $C_{M\alpha,i}$ and $\bar{M}_{z,i}$, $i = 1, 2, 3$, are not constant in the nonlinear characteristic of M_z. So, we regroup these two approximations in the terms ε_i, $i = 1, 2, 3$.

In equation (3.7), the disturbances ε_i, $i = 1, 2, 3$, can be balanced out if the system has a particular controller configuration. Indeed, the two types of interferences assume constant values at steady state and ε_i, $i = 1, 2, 3$, can be approximated as constant terms. So, if the control synthesis uses a controller with a pole in the origin (i.e. integrator effect), we can eliminate the constant disturbance.
At steady state, therefore, equation (3.3) becomes:

$$M_z(t, \kappa, \alpha, \mu, F_z) = \begin{cases} -C_{M\alpha,1}\theta - \bar{M}_{z,1} + \varepsilon_1, & -20° < \theta < -6°, \\ C_{M\alpha,2}\theta - \bar{M}_{z,2} + \varepsilon_2, & -6° < \theta < 6°, \\ -C_{M\alpha,3}\theta + \bar{M}_{z,3} + \varepsilon_3, & 6° < \theta < 20°, \end{cases} \tag{3.7}$$

Indeed, by considering ε_i, i = 1, 2, 3, as unknown disturbances, we can describe

1. the effect of the approximation (3.5) of α given by equation (3.5);
2. the effect of the piece-wise linear approximation of M_z;
3. additional external disturbances, e.g., road banking.

In steady state maneuvers like, e.g., driving along a curve, ε_i, i = 1, 2, 3 can be well approximated by constant disturbance.
Substituting equation (3.7) into equation (3.1), we obtain the Tire Steering Dynamic equation in the Laplace domain for the different regions:

$$s^2 I_w \Theta(s) = T_{in}(s) + \bar{M}_{z,i} - C_{M\alpha,i}\Theta(s) - sb\Theta(s) + \varepsilon_i(s) \qquad \forall\, i = 1, 2, 3 \tag{3.8}$$

where $\Theta(s)$ and $T_{in}(s)$ are the Laplace trasfoms of $\theta(t)$ and $T_{in}(t)$ respectively. It is also possible to write equation (3.8) as follows:

$$\Theta_i(s) = P_i(s)T_{in}(s) + D(s)(\bar{M}_{z,i} + \varepsilon_i(s)) \qquad \forall\, i = 1, 2, 3 \tag{3.9}$$

where the plant $P_i(s)$ is described by the following equation:

$$P_i(s) = \frac{1}{s^2 I_w + sb + C_{M\alpha,i}} \qquad \forall\, i = 1, 2, 3. \tag{3.10}$$

3.3 System Specifications

The controller C(s) has to be designed to satisfy the specifications given in section 3.1. For reference signals $\theta_{in}(t)$ is generated by higher level controller. The spectrum of typical $\theta_{in}(t)$ obtained from experimental data is shown in Figure 3.4.
To limit the control input, C(s) should be designed to make the magnitude of the control sensitivity function $S_c(s)$, defined as:

$$S_c(s) = \frac{T_{in}(s)}{\Theta_{in}(s)} = \frac{C(s)}{1 + P(s)C(s)}, \tag{3.11}$$

in the frequency range [0,ω_θ] show in Figure 3.4. In particular, for a given amplitude of $\Theta_{in}(s)$ in [0,ω_θ], the objective is to maintain the control sensitivity bode diagram of the magnitude below a fixed value $|S_c|_{dB}$. This means that the control input is bounded at the value U_{max} for all frequencies below ω_θ.
The maximum value U_{max}, that the actuator is able to generate, sets the specification on the maximum value that the magnitude Bode diagram can assume previously the

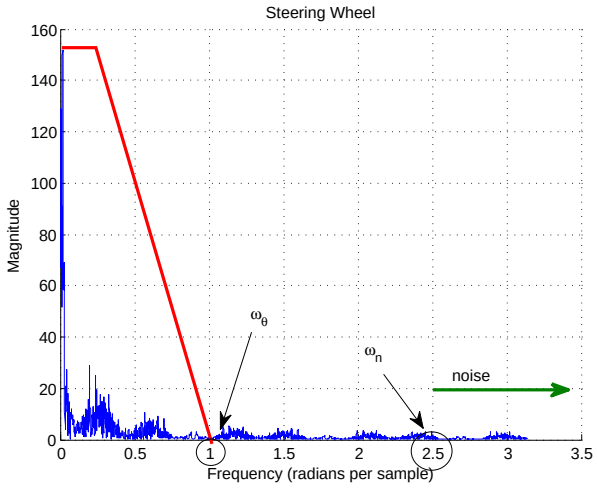

Figure 3.4: Steering spectrum.

frequency ω_θ. Since the actual technical specifications of the actuator are not available, we have assumed U_{max} around 200 Nm. With the formula (3.12) we can calculate the value of $|S_c|_{dB}$:

$$|S_c|_{dB} = 20 \log U_{max} = 20 \log 200 \simeq 46 \; dB \tag{3.12}$$

This specification allows us to limit the control input of the system. The control sensitivity function (3.11) has to satisfy the specification $|S_c|_{dB} \leq 46$ dB previously the frequency ω_θ. Using the ω_θ specification, it is possible to achieve the minimum time rise of the system. Indeed, we can make use of the empirical relationship:

$$\omega_\theta \geq \frac{0.35}{t_r} \rightarrow t_r = \frac{0.35}{\omega_\theta} \geq 0.35s \tag{3.13}$$

where t_r is the time rise. Starting with the rise time t_r, we can calculate the maximum natural phase ω_f of the system as follows:

$$\omega_f = \frac{1.8}{t_r} \leq 5.14[rad/s]. \tag{3.14}$$

The natural frequency ω_f is a specification in the frequency domain. To design a control system we need another specification in the frequency domain, the phase margin φ_{MF}. We obtain its value using the specification on the overshoot, as follows:

$$\varphi_{MF} = 2 \cos \left[\arctan \left(-\frac{\pi}{log(M)} \right) \right] \geq 1.18[rad] \tag{3.15}$$

Using the sensitivity function, it is possible to limit not only the control input, but also the noise affecting in the output $\theta_{out}(t)$. Indeed, if $|S_c(s)|_{dB}$ is small at the high frequencies, it is possible to achieve the reduction of the noise in the output $\theta_{out}(t)$.
In the following section the PI controller will be designed in the "linear" region and then the values found for the PI controller will be tested in the "saturation" one; it will be shown how the response of the wheel system changes in the different region.

3.4 Design of a Proportional Controller in the "Linear" and "Saturation" Region

A proportional controller allows to satisfy the specifications for the settling time, the rise time and the overshoot, introduced in section 3.1. However, with a proportional controller, is impossible to respect the specification about the zero steady state error. Indeed, without the integrator effect, the constant disturbances $\bar{M}_{z,i}$ and ε_i, $i = 1, 2, 3$, in (3.7) cannot be eliminated at steady state. Using the the *Final Value Theorem*, we obtain the result:

$$e(\infty) = \lim_{t\to\infty} e(t) = \lim_{s\to 0} s\, E(s) = \lim_{s\to 0} \frac{s}{1 + P_i(s)\, C(s)} \frac{1}{s} \neq 0^\circ \tag{3.16}$$

$i = 1, 2, 3$ and where $e(\infty)$ is the value of the error when the time t tends to infinity. This result is valid both in the "linear" and in the "saturation" region. Therefore, it is necessary to use a PI controller to obtain zero steady state error and reduce the control input.

3.5 Design of a PI Controller

We use a PI control to achieve zero steady state error and also the other specifications. We design the controller in the "linear" region, plant $P_2(s)$, and after we test the controller in the "saturation" regions, $P_1(s)$ and $P_3(s)$. To obtain the values of the coefficients K_P and K_I, we have to satisfy the following specifications:

$$\begin{aligned} &|P_2(j\omega_f)||C(j\omega_f)| = 1 \\ &\angle P_2(j\omega_f) + \angle C(j\omega_f) = \varphi_{MF} - 180^\circ \end{aligned} \tag{3.17}$$

where $|\cdot|$ and $\angle\cdot$ denote modulus and phase, respectively.
Using the second formula in equation (3.17), it is possible to use the following relation:

$$\angle C(j\omega_f) = \varphi_{MF} - 180^\circ - \angle P_2(j\omega_f) \tag{3.18}$$

Reminding that the $\angle C(j\omega_f)$ is equal to $\arctan\left(\frac{K_P\omega_f}{K_I}\right) - 90^\circ$, and it is possible to obtain the value of K_I from the following equation:

$$K_I = \frac{K_P\omega_f}{\tan(\varphi_{MF} - 90^\circ - \angle P_2(j\omega_f))} \tag{3.19}$$

After the value of K_I is derivatives, using the first equation of (3.17), it is possible to use the formula to derivate the K_P value, as shown in the following equation.

$$|C(j\omega_f)| = \frac{1}{|P_2(j\omega_f)|} \tag{3.20}$$

So, using the definition of $|C(j\omega_f)| = \sqrt{K_P^2 + \left(\frac{K_I}{\omega_f}\right)^2}$, it is possible to obtain the expression of the coefficient K_P:

$$K_P = \frac{1}{|P_2(j\omega_f)|\sqrt{1 + \left(\frac{K_I}{\omega_f}\right)^2}} \tag{3.21}$$

After K_P and K_I have been obtained from (3.21) and (3.19), we have to adjust these values to satisfy also the control sensitivity specification. In Figure 3.5 on the bottom, it

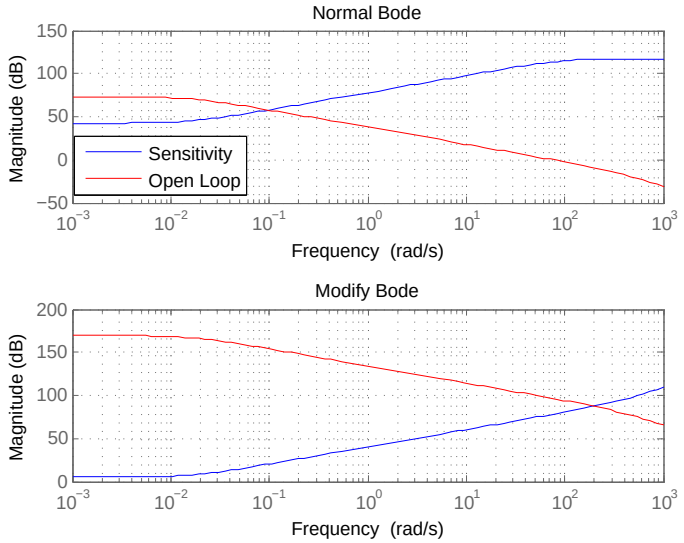

Figure 3.5: The Bode diagram of the open loop system and control sensitivity function. The top Figure is before the sensitivity analysis, down after the sensitivity analysis

is shown as, reducing the value of K_P and K_P, the limit input specification is satisfied. Indeed, the blu line, that represents the trasfer function $S_c(s)$, is lower the magnitude 46 dB previous the frequency ω_θ. After the adjustment with the sensitivity function, we obtain the following value for the Proportional and Integral coefficients:

$$K_P = 6658.6; \qquad K_I = 30.5. \tag{3.22}$$

To test the PI controller, we consider the control system in Figure 3.6.

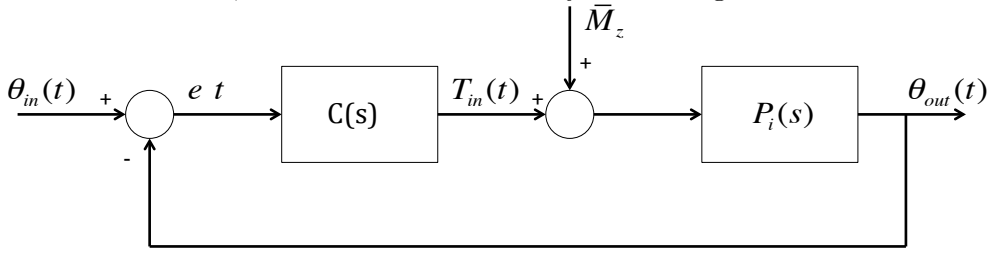

Figure 3.6: System of Control.

We want to analyze the behavior of the system when the self aligning characteristic is in the 2^{nd} "linear" region. For this reason we linearized this function with a straight line with slip angle from -6° to 6°, as shown in Figure 3.2.
We suppose the value of the slip angle α remains in the region of linearity. The M_z value is constant (condition of pure cornering) and it does not change within logitudinal accelerations and braking. In this condition the stiffness coefficient $C_{M\alpha,2}$ has a positive sign, as shown in Figure 3.7. In the equation (3.8) the term M_z is dependent on the following parameters: κ, α, μ and F_z. In the first analysis we suppose that this term is constant at the value $\bar{M}_{z,2}$. This constant value of the self aligning moment characteristic is zero because the slip angle α does not pass through the origin, as shown in Figure 3.8.
We also suppose that the values of μ and F_z remain constant.
Following the aforementioned considerations, we replace the terms μ and F_z in (3.8) formula with constant values and, after that, we adopt the Transfer Function $P_2(s)$ in the linear case, shown in equation (3.10).

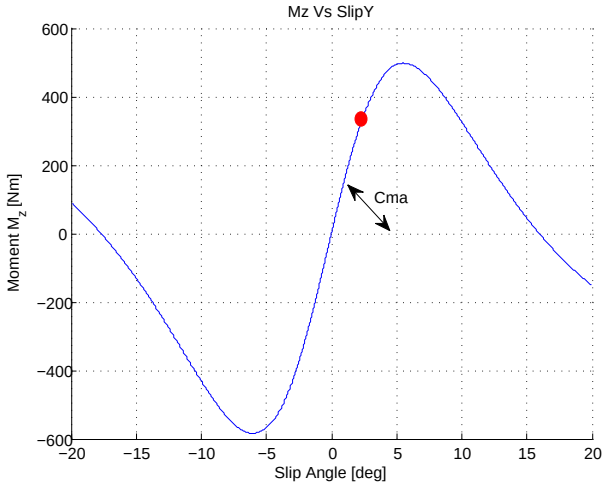

Figure 3.7: Charateristic of M_z.

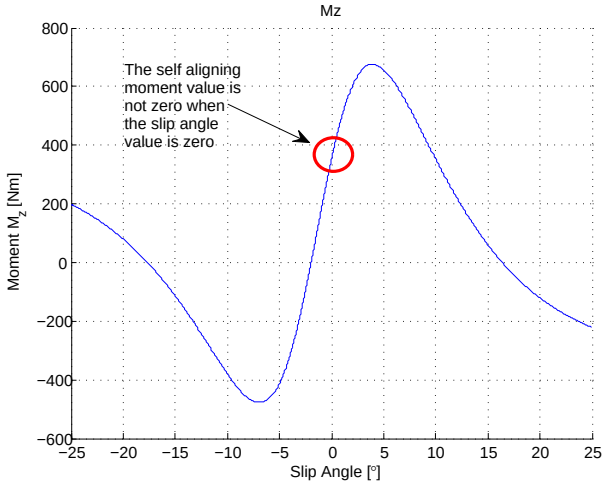

Figure 3.8: Charateristic of M_z.

For the control analysis we have to draw the root locus and the open loop Bode's diagram of the system in Figure 3.6, for C(s) = 1, as shown in Figure 3.9.
Figure 3.9 shows the poles of the transfer function $P_2(s)$. In Figure 3.9, every pole is on the left side of the real axis and this means that the system in the linear case is stable.
Afterward, in the wheel control system, in Figure 3.6, we insert in the controller the values of K_P and K_I given in (3.22) and the equation of the "linear" plant $P_2(s)$ expressed in the equation (3.10). In Figure 3.10, there are the root locus and Bode diagram for the system controlled with the PI controller.
As shown in Figure 3.10 on the left, the PI controller introduces a pole in zero, that does not modify the system stability. The Bode diagram, in Figure 3.10 on the right, changes with the application of the PI controller. We can note that the specifications on the natural frequency and the phase margin obtain at the end of the section 3.3 are satified.
Similarly, the output satisfies the project specifications in the time domain, as we see in the left plot of Figure 3.11.
On the right plot of Figure 3.11, the input control is shown and the value that its assume is large also using the sensitivity analysis. Indeed, we can see that the maximum value is around $7 \cdot 10^3$ Nm.
In the system with the PI controller there is not a steady state error, because the integral term has the property of guaranteeing the tracking input.

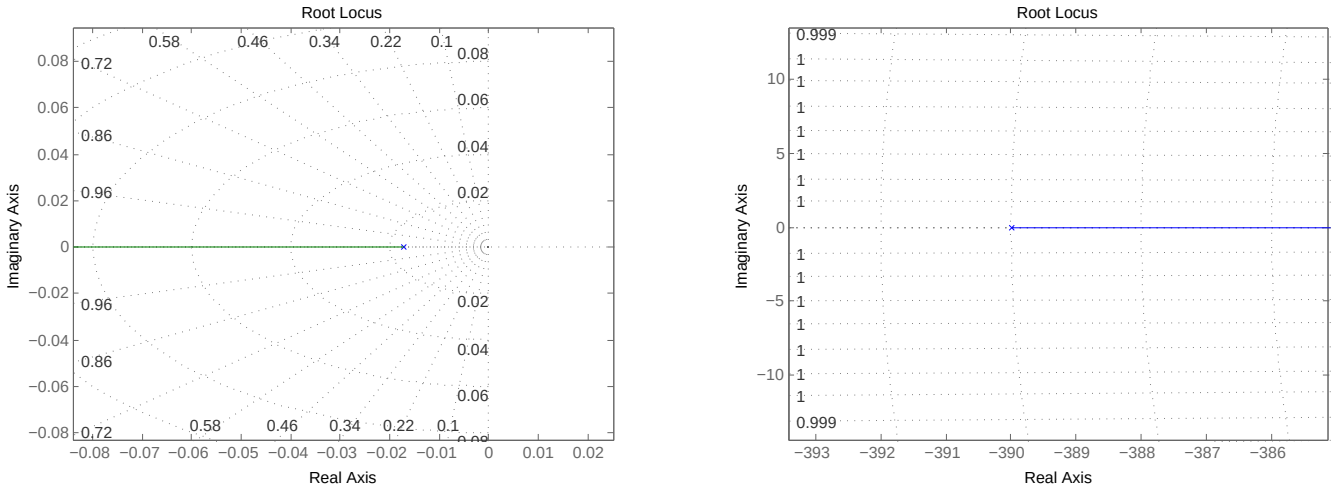

Figure 3.9: Zoom of the root locus diagram of the "linear" plant $P_2(s)$.

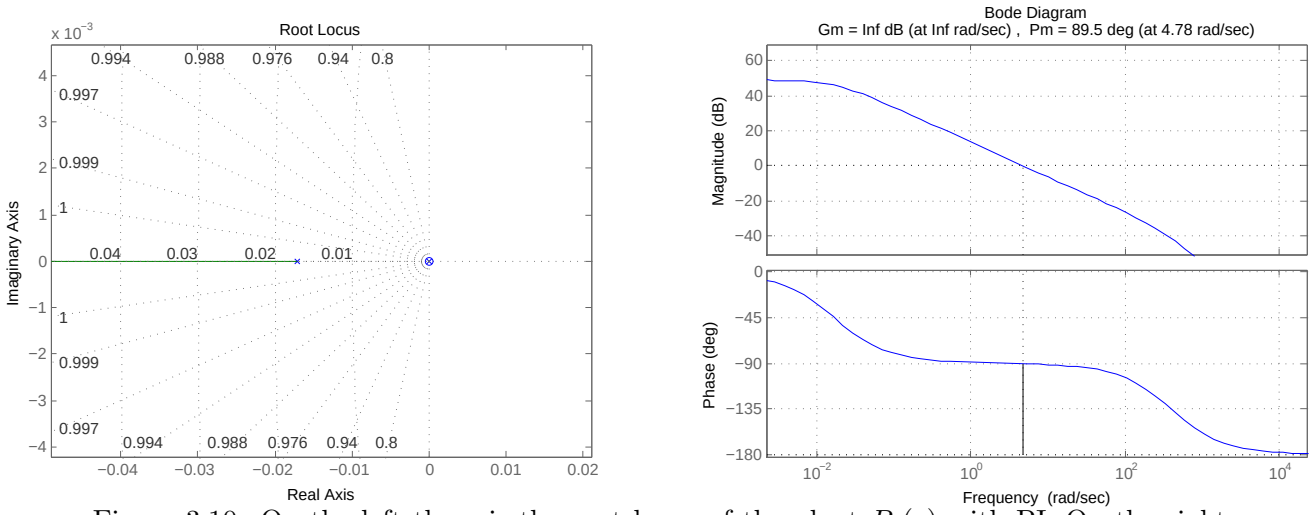

Figure 3.10: On the left there is the root locus of the plant $P_2(s)$ with PI. On the right the Bode's diagram of the plant $P_2(s)$ with PI.

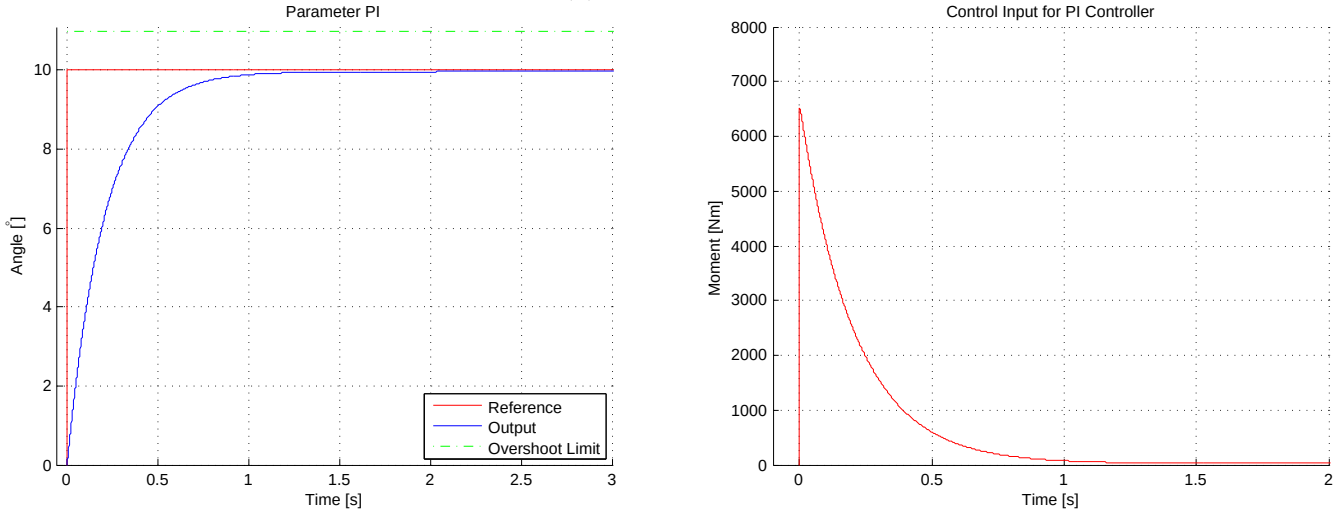

Figure 3.11: On the left there is the output of the PI Controller, on the right there is the input control of the PI Controller.

Therefore, the PI controller for the "linear" region satisfies every specification imposed in section 3.3, except for the bound on the control input. Now, we test the PI controller in

the "saturation" region in order to see if it satisfies the same specifications.

3.5.1 Analysis of a PI Controller in the "Saturation" Region

After the analysis of the system in the "linear" region, we apply the result found in the previous section in the case of the plant falling in the 1^{st} or 3^{rd} "saturation" regions. For this reason we have to analize the behavior of the system when the plant transfer function are $P_1(s)$ or $P_3(s)$, as shown in Figure 3.12.

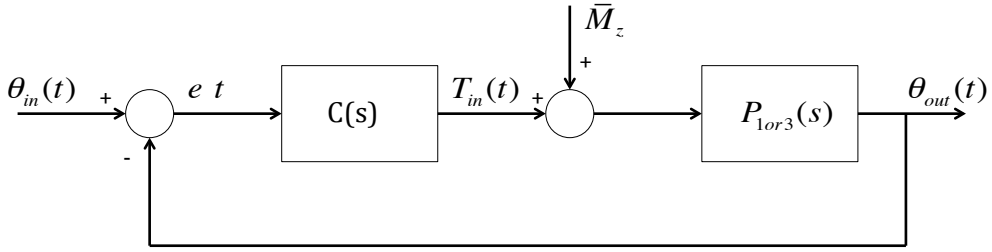

Figure 3.12: The wheel system in the "saturation" region.

Figure 3.13 shows the root locus of the plant $P_{1,3}(s)$ in close-loop without any controller in the "saturation" region.

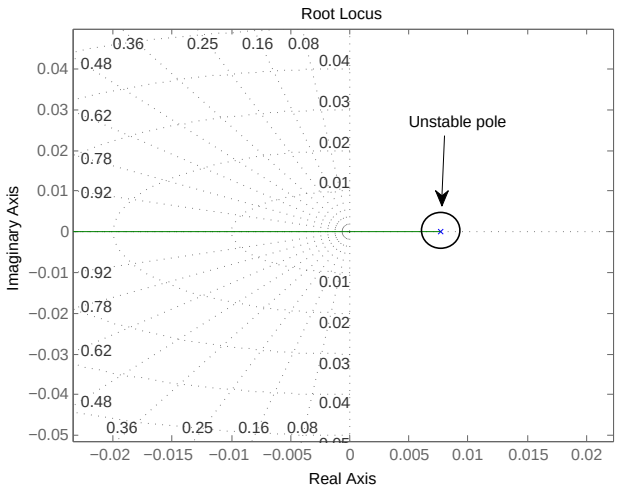

Figure 3.13: The zoom of the unstable pole in the "saturation" plant $P_{1,3}(s)$.

The root locus diagram, in Figure 3.13, shows the presence of an unstable pole. Indeed, the change of sign of the stiffness term leads to a pole in the right half-plane of the complex plane. This pole would make the system unstable, but the value of the pole is close to zero, threfore its effect could be eliminated with a large gain.
In the wheel control system in Figure 3.6, we insert in the controller the value of K_P and K_I found in (3.22) and the equation of the "saturation" plant $P_1(s)$ or $P_3(s)$ in given equation (3.10). The root locus and Bode diagram in the saturation case with the implementation of the PI controller are shown in Figure 3.14.
As shown in Figure 3.13, in the root locus an unstable pole appears. With a high gain introduced by the proportional coefficient of the PI controller and the zero pole added by the PI controller, it is possible to delete the effect of the unstable one, as shown in Figure 3.14. For this reason, and being the unstable pole closed to zero, the system becomes stable. The output of the system and the input control are shown in Figure 3.15.
Also the plant $P_{1,3}(s)$ in the "saturation" region is not stable, the high gain introduced

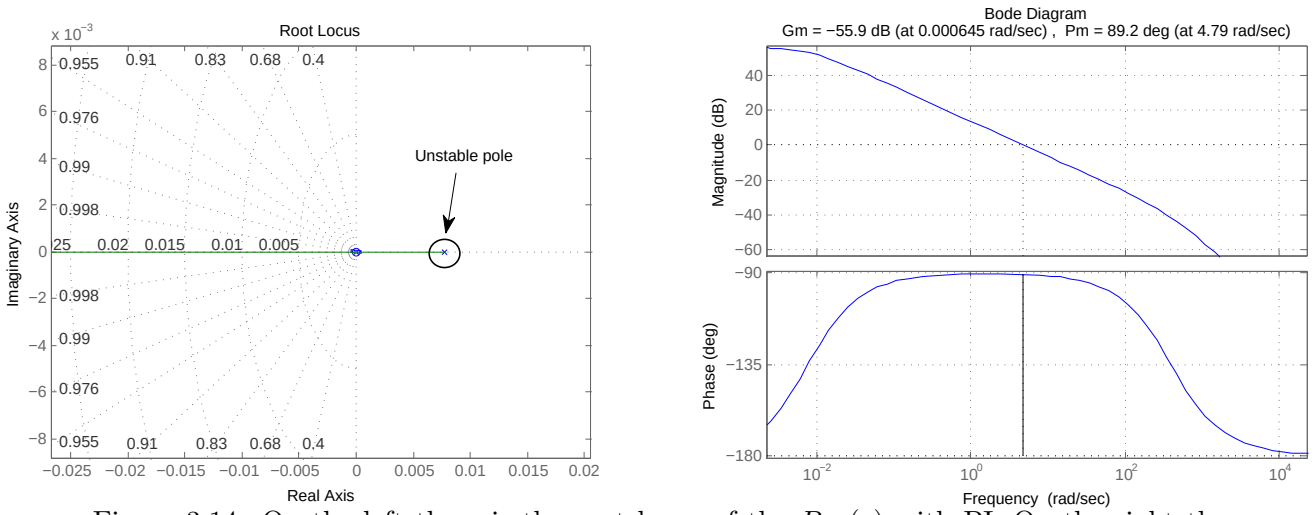

Figure 3.14: On the left there is the root locus of the $P_{1,3}(s)$ with PI. On the right the Bode diagram of the $P_{1,3}(s)$ with PI.

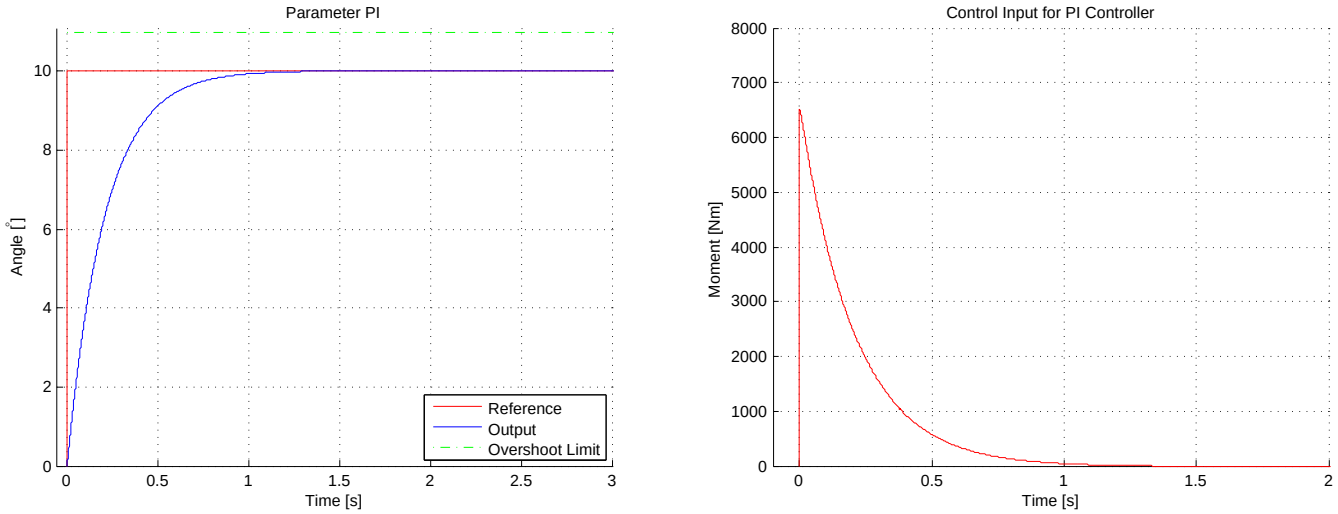

Figure 3.15: On the left there is the output of the PI Controller, on the right there is the input control of the PI Controller.

by the coefficients of the PI controller eliminated the effect of the unstable pole and the system becomes stable. The system output has a steady state error of 0°, but the control input remains always high as we observed in the linear case. This happens also because the values of K_P and K_I are too high to delete the effect of the unstable pole. Instead, the output characteistic in Figure 3.15 on the right is stable. At the end, the input control value remains always high, as shown in Figure 3.15 on the right.

3.5.2 Conclusion

In section 3.5 the PI controller was proved to be able to control an ideal wheel system in both regions. The output respects each specification imposed in section 3.3 but the control input does not satisfy the specification. This is because the PI controller has to introduce a high gain to eliminate the effect of the unstable pole in the "saturation" region.
In the next section we introduce in the system the actuator and we analyze its effect on the wheel system.

3.6 Effect of the Actuator Dynamics

Section 3.5 shows how the PI controller could be enough to control the system in both regions but accepting unrealistic elevate control input signal, also in presence of nonlinearty. The elevate control input signal is due because we do not considered the actuator dynamics in the analysis. Indeed, the actuator dynamics are able to decrease the elevate control input.
The actuator dynamics is the most important component omitted in the previous analysis. It is responsible to convert the control input generated by the controller and it implements the appropriate control action, as a moment to be applied to the system. The actuator is added after the PI control system, as shown in Figure 3.16.

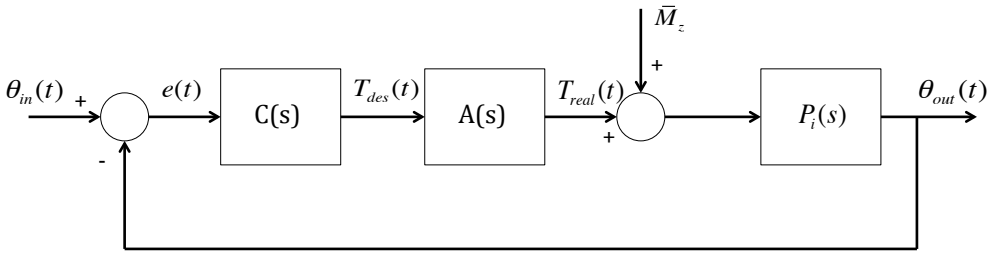

Figure 3.16: Control System with Actuator.

The actuator reduces the control input, therefore its dependence allows permit to obtain the desired input $T_{des}(t)$, calculated by the controller C(s), and the real input $T_{real}(t)$, i.e. the control input produced by the actuator.
The actuator is described as a low pass filter with gain 1 and frequency of 1 rad/s. The transfer function of the actuator is therefore:

$$A(s) = \frac{1}{\tau s + 1} \tag{3.23}$$

where τ is the time constant. The actuator Bode diagram, is shown in Figure 3.17.

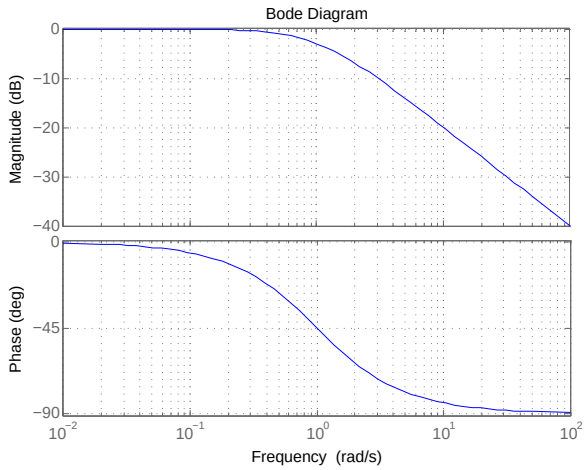

Figure 3.17: Actuator Bode Diagram.

The limitations introduced by the actuator are a reduction of the phase margin, the consequent reduction of the bandwidth of the close loop system and the decrease of the control

gain. Figure 3.16, which describes the control model used, explains how the introduction of the actuator modifies the system output. The tests in chapter 3.5 are replicated to understand the principal causes of changes.

3.6.1 PI Control with Actuator in "Linear" Region

At the begining, we consider the "linear" region of the plant characteristic, as done in section 3.5. It is possible to verify the effect of the actuator on the PI control system.
To implement the PI control with the actuator, we use the same values of K_P and K_I used in section 3.5. In Figure 3.18, there are the root locus and Bode diagram for the system with the actuator.

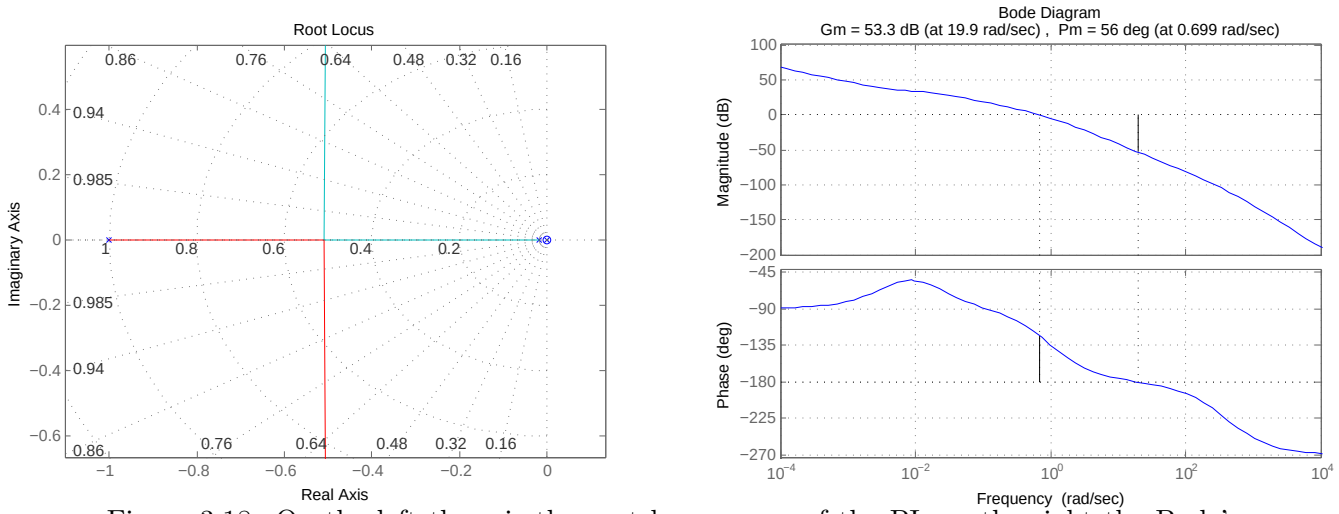

Figure 3.18: On the left there is the root locus zoom of the PI, on the right the Bode's diagram of the PI with the actuator.

As shown in Figure 3.18 on the left, the actuator changes the root locus diagram, and introduces a pole near the origin, so it affects the system stability. However, the actuator reduces the phase margin of the system and we have to reduce the controller gain to stabilize the system. This is not a problem for the "linear" plant, but for the "nonlinear" one we need a high gain to delete the unstable pole effect. Also the Bode diagram, the right plot of in Figure 3.18, changes with the application of the actuator. We can note that the frequency is the same obtain at the end of section 3.3, but the introduction of the actuator in the system reduces the phase margin and it makes the system more unstable. The aforementioned consideration reflected in the test for the constant angle, as shown in Figure 3.19.
In Figure 3.19 on the left, the introduction of the actuator in the system causes the output not to respect every specification imposed. The actuator modifies the root locus diagram and with an high gain, as we noticed for the PI controller in section 3.5, the system output response deteriorates. We have to reduce the gain of the system to make the system stable but, in this way, the system specifications are not satified. Also, the actuator has indeed a low pass characteristic, therefore cuts the control input high frequency but at the low frequencies the situation remains unchanged. The high frequency is important for the system readiness at the change of reference. The input still presents high values, even with the insert of the actuator (around $7 \cdot 10^2$ Nm), but losing one order of magnitude compared with the case without the actuator.
The wheel system with the actuator does not respect any specification imposed in the section 3.3.

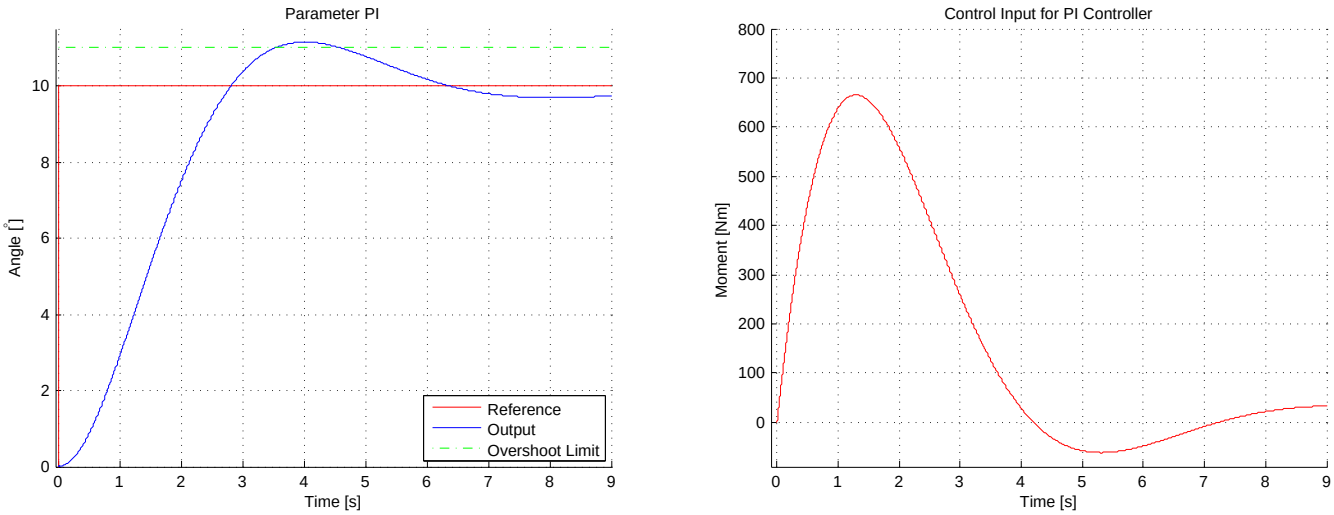

Figure 3.19: On the left there is the output of the PI Controller, on the right there is the input control of the PI Controller.

3.6.2 PI Control with Actuator in "Saturation" Region

As in section 3.5.1, the system is analyzed in the "saturation" region, namely when the stiffness coefficient $C_{M\alpha,1,3}$ changes its sign becoming negative and the trasfer function of the plant becomes unstable.
The simulation with constant input is run using the same values used before for K_P and K_I. In Figure 3.20, there are the root locus and Bode diagram for the system with the actuator.

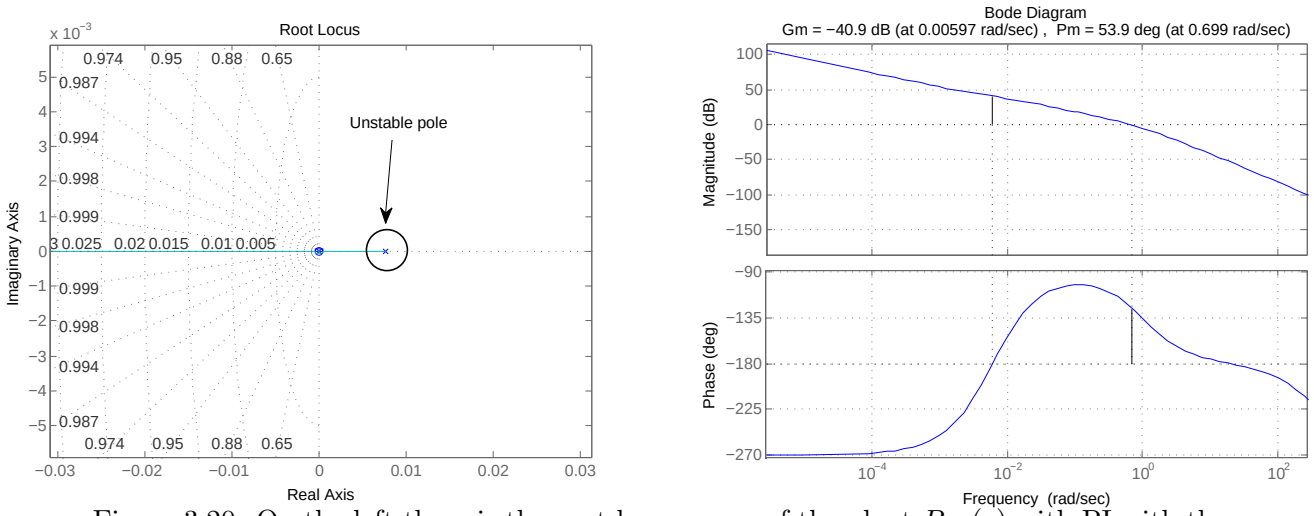

Figure 3.20: On the left there is the root locus zoom of the plant $P_{1,3}(s)$ with PI with the actuator, on the right the Bode's diagram of the plant $P_{1,3}(s)$ with PI with the actuator.

As shown in Figure 3.20 on the left, the actuator changes the root locus diagram, and introduces a pole near the origin, so it modifies the system stability and we have to reduce the controller gain to stabilize the system. But, if we reduce the control gain, it is not possible to stabilize the system in the "saturation" region. Indeed, it was dimostrated in the section 3.5.1, how an high gain is necessary to stabilize the system. Also the Bode diagram, the Figure 3.20 on the right, changes with the application of the actuator. Indeed, there is a reduction of the phase margin in Figure 3.20 with respect to Figure 3.14. We can note that the frequency is the same calculated at the end of section 3.3, but the introduction of the actuator in the system reduces the phase margin and it makes the

system unstable.
By appling a constant input, it is possible to obtain the results shown in Figure 3.21.

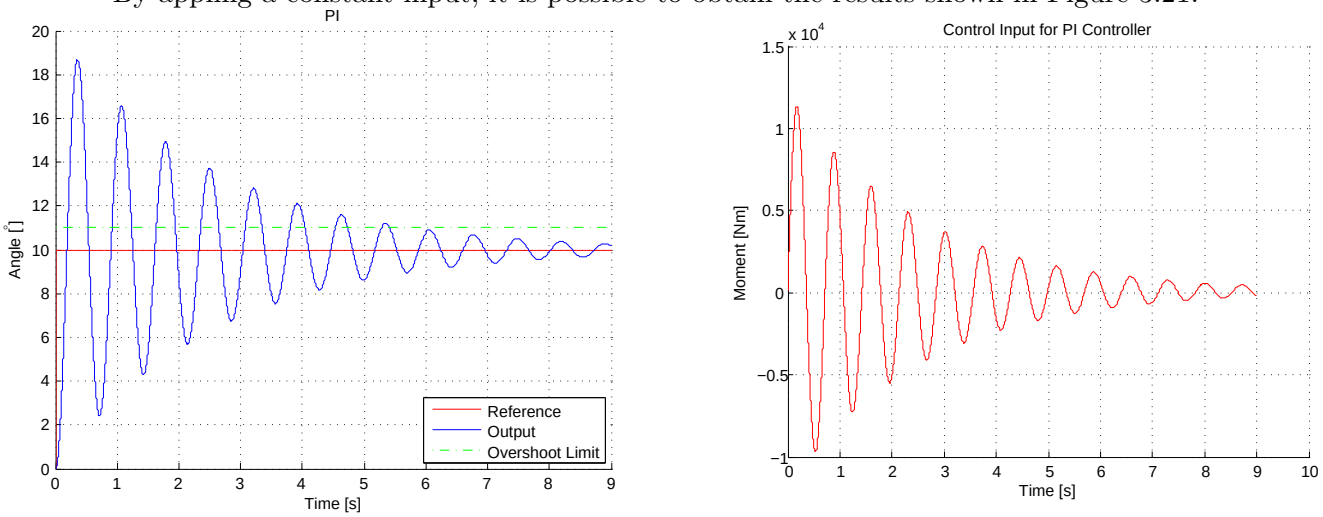

Figure 3.21: On the left there is the output of the PI Controller, on the right there is the input control of the PI Controller with the actuator.

In Figure 3.21 on the left, the introduction of the actuator in the system causes the output not to respect the specifications. The actuator modifies the root locus diagram and with an elevate gain, as we calculate for the PI controller in section 3.5, the system deteriorates the output behavior and becomes unstable. We have to reduce the gain of the system to make the system stable but, in this way, we do not respect the system specifications. This is because the actuator requires a low controller gain to respect the system specifications. However, a low control gain means the impossibility of stabiliazing the system in the "saturation" region because of the presence of the unstable pole.
The input takes high value with the insert of the actuator (around 10^4 Nm).
The wheel system with the actuator in the "saturation" region does not respect any specification imposed in the section 3.3.

3.6.3 Conclusion

The previuos results show that when introducing the actuator in the wheel system the PI controller is not able to follow the input with no steady state error. Indeed, the actuator introduction in the system deteriorates the phase margin and this produces the reduction of the gain to satisfy the specifications. In the wheel system and, in particular, when the plant is in the "saturation" region, it is necessary to insert a high gain to satisfy the specifications and to delete the effect of the unstable pole. The control input, in order to respect the specifications, is too high and the actuator limits the effect of the input. Therefore the controller we need, has to consider the minimization of the input control.

3.7 Summary of the results

In section 3.5 and 3.6 it is shown how it is necessary to build and analyze two different controls for each test, one for the "linear" and one for the "saturation" region. Indeed, with a unique PI controller, it is not possible to satisfy the specifications imposed at the beginning of the chapter. Moreover, the introduction of the actuator in the system reduces the phase margin and it is necessary to reduce the gain to respect the specifications. In the "saturation" region, we need an elevate gain to delete the unstable pole effect, but

this is not possible with the introduction of the actuator.
A new way of designing the controller must be found. In particular, the controller has to satisfy these specifications:

- Minimize the settling time t_s and the rise time t_r;
- Make the steady state error null at the step;
- Ensure that the input control is bounded below 200 Nm;
- The controller has to stabilize the system in both regions "linear" and "saturation".

In theory with a gain scheduling synthesis it is possible to satisfy these specifications. In pratice the uncertainty of the model, in particular in the "saturation" region, and the unmeasurable constant disturbance $\bar{M}_{z,i}$ do not permit to respect the previous specifications. To match the specifications we will introduce the robust control synthesis with LMI technique. The aim of the next section is to introduce the design of this type of control that is able to satisfy the mentioned specifications.

Chapter 4

LMI and LPV Control Synthesis

In recent years it has been shown that control problems are related to optimization problems [5], [9] and [19]. Indeed, the controller parameters and the input signals can be interpreted as a decision variables of an optimization problem. For this reason Linear Matrix Inequalities (LMI) first and Linear Parameter Varying (LPV) later emerged as powerful methods to solve control problems that appear difficult to resolve with traditional control methods. These two new control techniques not only solve a control problem, but are also able to build a controller that guarantees robust stability despite of parameters variations. Chapter 4 starts with the design of an LMI controller for the wheel equation. Subsequently, a robust LPV controller is built to control the wheel system.

4.1 LMI Synthesis for the Wheel Equation

In this section we show the controller designed with LMI technique for the wheel system (3.8). Using the theory shown in the appendix D, the controller designed with LMI technique for the wheel equation will be obtained. The controller is described by the following equation:

$$\begin{aligned} \dot{x}_c(t) &= A_c x_c(t) + B_c y(t) \\ T_{in}(t) &= C_c x_c(t) + D_c y(t) \end{aligned} \tag{4.1}$$

where $y(t)$ is the difference between θ_{out} and θ_{in}. The equation of the system are:

$$\begin{aligned} \dot{x}(t) &= Ax(t) + BT_{in}(t) + Hw(t) \\ e(t) &= Cx(t) + DT_{in}(t) + Ew(t) \\ y(t) &= Fx(t) + Gw(t) \end{aligned} \tag{4.2}$$

where $e(t)$ is the error, $w(t)$ is the disturbance, $T_{in}(t)$ is the control input and $y(t)$ is the measured output. The LMI technique consists of translating the wheel system control problem into an optimization problem, where the control problem specifications become the optimization problem constraints. The optimization problem is described as follows:

$$\begin{aligned} (A_c, B_c, C_c, D_c) &= argmin_{(A_c,B_c,C_c,D_c)}\ \gamma \\ \gamma &> \frac{\|e\|_{\mathcal{L}_2}}{\|w\|_{\mathcal{L}_2}} \end{aligned} \tag{4.3}$$

where γ is the variable which has to be minimized, $\|\cdot\|_{\mathcal{L}_2}$ is the energy of the signal (defined for a generic signal $p(t)$ as $\|p(t)\|_{\mathcal{L}_2} = \sqrt{\int_0^\infty \|p(t)\|^2\, dt}$), e is the error and w is

the disturbance. If the problem has a solution, the result ensures that the energy of the error $\|e\|_{\mathcal{L}_2}$ is at most γ times the value of the energy of the disturbance $\|w\|_{\mathcal{L}_2}$ in the system. To design the controller with LMI techinque we have to introduce the system in Figure 4.1.

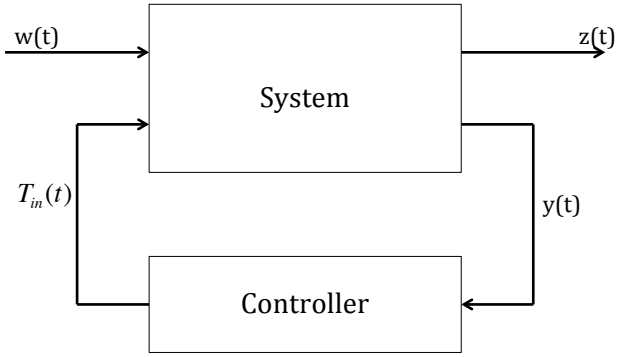

Figure 4.1: General plant configuration for an LMI problem.

As shown in Figure 4.1, the interconnection of the LMI system (4.2) and the LMI controller (4.1) has to be internally stable and to satisfy the desidered performance. A new state variable $\xi = [x, x_c]^T$ is introduced and the controlled system is simply described by the equation:

$$\begin{aligned} \dot{\xi}(t) &= \mathcal{A}\xi(t) + \mathcal{B}w(t) \\ z(t) &= \mathcal{C}\xi(t) + \mathcal{D}w(t) \\ \text{with } \left(\begin{array}{c|c} \mathcal{A} & \mathcal{B} \\ \hline \mathcal{C} & \mathcal{D} \end{array}\right) &= \left(\begin{array}{cc|c} A + BD_cF & BC_c & H + BD_cG \\ B_cF & A_c & B_cG \\ \hline C + DD_cF & DC_c & E + DD_cG \end{array}\right) \end{aligned} \tag{4.4}$$

By making use of **Theorem 2** and of the LMI inequality expressed in (D.16), in appendix D, the controller that stabilizes the system (4.4) can be found. It makes the $\mathcal{H}_\infty$-norm of the transfer matrix $\|w\|_{\mathcal{L}_2} \to \|e\|_{\mathcal{L}_2}$ smaller than γ if and only if there exists a matrix X such that

$$X \succ 0 \quad \text{and} \quad \begin{pmatrix} \mathcal{A}^T X + X\mathcal{A} & X\mathcal{B} & \mathcal{C}^T \\ \mathcal{B}^T X & -\gamma I & \mathcal{D}^T \\ \mathcal{C} & \mathcal{D} & -\gamma I \end{pmatrix} \prec 0 \tag{4.5}$$

where the first inequality guarantees stability and the second captures performance. So, substituting equation (4.5) in the initial problem (4.3), we obtain the optimization problem:

$$\begin{aligned} (A_c, B_c, C_c, D_c) &= argmin_{(A_c,B_c,C_c,D_c)}\ \gamma \\ X \succ 0 \quad \text{and} \quad & \begin{pmatrix} \mathcal{A}^T X + X\mathcal{A} & X\mathcal{B} & \mathcal{C}^T \\ \mathcal{B}^T X & -\gamma I & \mathcal{D}^T \\ \mathcal{C} & \mathcal{D} & -\gamma I \end{pmatrix} \prec 0. \end{aligned} \tag{4.6}$$

By solving the optimization problem, it is possible to translate the result into a solution for the control problem.
The controller of the system in Figure 4.1 has to satisfy the following specifications:

1. Minimize the settling time t_s and the rise time t_r;

2. Zero steady state error at the step;

3. Limit the value of the control input below 200 Nm;

4. The controller has to stabilize the system in both the "linear" and the "saturation" regions.

The specifications 1, 2 and 3 must be satisfied in both regions: "linear" and "saturation". Before introducing the conversion of the control specifications and the structure of the filters $W_1(s)$ and $W_2(s)$, we need to adapt the control system provided at the beginning of the section 3.5 to the LMI problem system, as shown in Figure 4.2.

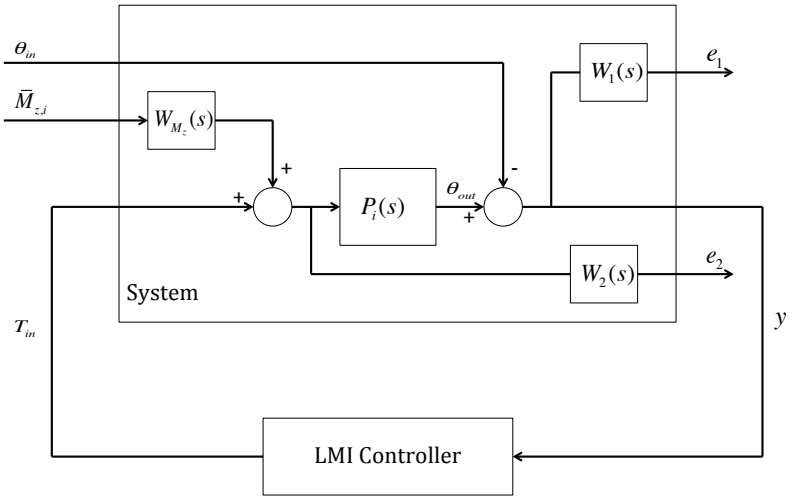

Figure 4.2: LMI Wheel Control System.

As deduced by Figure 4.2, the difference between the reference $\theta_{out}(t)$ and the output $\theta_{in}(t)$, that it is the tracking error y(t), times by a filter $W_1(s)$, giving as a result the error e_1. On the other side, the sum between the control input $T_{in}(t)$ and the disturbance $\bar{M}_{z,i}$ is multiplied by the filter $W_2(s)$, giving back the input control e_2. For the LMI problem the disturbance $\bar{M}_{z,i}$ is not measurable.
At this point we have to convert the specifications into constrains of the optimization problem. The second specification, zero steady state error at the step, is obtained by imposing the structure of the controller (4.1) has a pole in the origin. The pole in the origin has the same effect of the integrator in the PI controller. Indeed, the pole increase the precision at steady state and the robustness at the disturbances. In particular, we have zero steady state error at the reference signal or at constant disturbances. Therefore, the control matrix B_c has to satisfy the following description:

$$B_c = \begin{bmatrix} * \\ \vdots \\ * \\ 1 \\ * \\ \vdots \\ * \end{bmatrix}, \tag{4.7}$$

where * represents an irrelevant value. The other matrices A_c, C_c and D_c do not have any particular specification to satisfy.
The third specification, moderate the control input, is obtained immediately because of the structure of the optimization problem. Being the reference $\theta_{in}(t)$ a disturbance acting on the wheel system and the control input $T_{in}(t)$ an error of the system, minimizing γ coincides with a limited control input $T_{in}(t)$. Reducing the control input is possible by introducing a low pass filter $W_2(s)$ on signal $T_{in}(t)$, obtaining the error $E_2(s) = W_2(s)T_{in}(s)$. Scheduling the value of the filter $W_2(s)$, we change the control input value until the value of $T_{in}(t)$ satisfies the specification. In particular, increasing the $W_2(s)$ coefficients, especially the gain, we reduce the control input value. After that, using the theory shown in the appendix D.2.3 and, in particular the equations (D.24) and (D.27), it is possible to limit the input control of the controller.
The first specification, which imposes to minimize the settling and rise times, is conflicting with the third specification. Indeed, these two specifications are correlated to the input control. Instead, increasing the maximum value of the control input, it is possible to decrease the t_s and t_r values and viceversa. So, we have to increase the value of the control input to minimize the settling and rise time, but without exceed the maximum value of the control input (200 Nm). In this way, it is possible to satisfy both specifications: decrease the value of the settling and rise time and limit the value of the control input below 200 Nm. To obtain this specification we have to introduce a filter $W_1(s)$ on the signal $y(t)$, that is the difference between $\theta_{out}(t)$ and $\theta_{in}(t)$, and we achieve the error $E_1(s) = W_1(s)Y(s)$. Scheduling the value of the filter $W_1(s)$, we change the settling and rise time values. So, reducing the $W_1(s)$ coefficients, in particular the gain, the transitory may become slow but we limit the oscillations and viceversa.
The fourth specification, the design of a unique controller for both the "linear" and the "nonlinear" regions, is translated into an optimization problem introducing two different constrains. One of these constrains represents the condition for the problem in the "linear" region and the other the constraint for the "nonlinear" one. In this way, solving the optimization problem with these two different constrains, it is possible to obtain a controller that respects the specifications in both regions.
To satisfy the constrains and solve the LMI problem, we have introduced two filters. These filters have different effects on the system and allow to solve the optimization problem (4.3) in the frequency. Indeed, the filter $W_1(s)$ is associated to the settling and rise times and allows to modify the bandwidth of the system. The bandwidth is correlated with the rise and settling times. Changing the bandwidth, it is possible to satisfy the third specification. The filter output is described by the equation $E_1(s) = W_1(s)(\theta_{out}(s) - \theta_{in}(s))$ and allows to increase/decrease the bandwidth of the system. Therefore, the $W_1(s)$ transfer function has a low-pass characteristic. In this way, the constrain (4.6) assumes more importance in presence of low frequency. The filter $W_1(s)$ represents the limitation introduced by a sensitivity function in the system and the controller is allowed to use only a limited bandwidth of signal.
Instead, the filter $W_2(s)$ is associated to the control input signal $T_{in}(t)$. The filter output is described by the equation $E_2(s) = W_2(s)T_{in}(s)$ and allows to reduce the control input $T_{in}(t)$ and, also, to make the LMI problem feasible. To obtain these goals, we have to define the $W_2(s)$ transfer function as a low-pass filter. The low-pass definition permits to reduce the value of $e_2(t)$. Indeed, the value of $e_2(t)$ is related with the optimization problem $\|e_2\|_{\mathcal{L}_2} \leq \gamma\|\theta_{in}\|_{\mathcal{L}_2}$ and if the value of $e_2(t)$ is high, the $T_{in}(t)$ value is also high and the LMI problem becomes infeasible. Therefore, we choose a low-pass characteristic to reduce the value of the energy $e_2(t)$ in the LMI problem. In this way, we limit the

control input $T_{in}(t)$ and the LMI problem is feasible, so we can find a solution.
After introducing the conversion of the control specifications, we introduce the equation of the wheel system and the structure of the filters $W_1(s)$ and $W_2(s)$.
The equation of the wheel system in section 3.2 is adapted to obtain an LMI. The block $P_i(s)$ is the second order plant of the Tire Steering Dynamic described in equation (3.10). The equation (3.10) is rewritten as follows:

$$\begin{aligned} \begin{bmatrix} \dot{\theta}_{out}(t) \\ \ddot{\theta}_{out}(t) \end{bmatrix} &= \begin{bmatrix} 0 & 1 \\ -\frac{C_{M\alpha,i}}{I_w} & -\frac{b}{I_w} \end{bmatrix} \begin{bmatrix} \theta_{out}(t) \\ \dot{\theta}_{out}(t) \end{bmatrix} + \begin{bmatrix} 0 \\ \frac{1}{I_w} \end{bmatrix} \begin{bmatrix} T_{in}(t) \end{bmatrix} \\ y &= \begin{bmatrix} 1 & 0 \end{bmatrix} \begin{bmatrix} \theta_{out}(t) \\ \dot{\theta}_{out}(t) \end{bmatrix} + \begin{bmatrix} -1 \end{bmatrix} \begin{bmatrix} \theta_{in}(t) \end{bmatrix} \end{aligned} \qquad i = 1, 2, 3. \tag{4.8}$$

Equation (4.8) describes the Tire Steering Dynamic equation in both regions, "linear" and "saturation".
In the following part of the section, the descriptions of the two filters $W_1(s)$ and $W_2(s)$ will be given, in order to show how essential they are to satisfy the specifications about the settling and rise time and the control input, and therefore to solve the optimization problem.
The Laplace transform of the error e_1 is described by the relationship:

$$E_1(s) = W_1(s)Y(s) \qquad \text{where} \qquad W_1(s) = K_{sen}\frac{s+\omega_b}{s+\omega_z} \tag{4.9}$$

where the transfer function $W_1(s)$ plays the same role as the control sensitivity function used in the section 3.5. The filter $W_1(s)$ has a low pass characteristic and cuts the frequencies over the value ω_b. In this way, the system is not conditioned by the high frequency variations and this reduces the tracking errors. The frequency ω_b is the desired bandwidth of the feedback system, while ω_z is chosen to make the system stable and normally satisfies: $0 < \omega_z \ll \omega_b$. The wheel system is stable if the value of ω_b is chosen closed to the steer input frequency found in the section 3.5. In this way, the system is allowed to use every frequency of the reference, analized in Figure 3.4. The other term appearing in the definition of $W_1(s)$ is the gain K_{sen}, defined as $\frac{1}{S_\infty}$, where S_∞ represents the error at steady state. The S_∞ value is chosen lower than 50 to attenuate the effect of the error. The S_∞ value is achieved after some test and, with this value, we obtain the gain K_{sen}. Changing the S_∞ value and the bandwidth of the filter (frequency ω_b and ω_z), it is possible to modify the specifications about the rise and settling times. To satisfy these specifications, the filter $W_1(s)$ has the characteristic shown in Figure 4.3.

Figure 4.3 shows that the filter $W_1(s)$ emphasizes the low frequencies with respect to the high ones. The Laplace transform of the output variable e_1 can hence be expressed as:

$$\begin{aligned} E_1(s) &= K_{sen}\left(\frac{s+\omega_b}{s+\omega_z}\right) Y(s) \\ &= K_{sen}\left(1 + \frac{\omega_b - \omega_z}{s+\omega_z}\right)(\Theta_{out}(s) - \Theta_{in}(s)) \\ &= K_{sen}\left(\Theta_{out}(s) - \Theta_{in}(s) + X_3(s)\right) \end{aligned} \tag{4.10}$$

where:

$$X_3(s) = \frac{\omega_b - \omega_z}{s+\omega_z}(\Theta_{out}(s) - \Theta_{in}(s))$$

In the solution of the equation we introduced a new state variable x_3 that represents the sensitivity filter $W_1(s)$ state. Applying the Laplace inverse transform, the equation

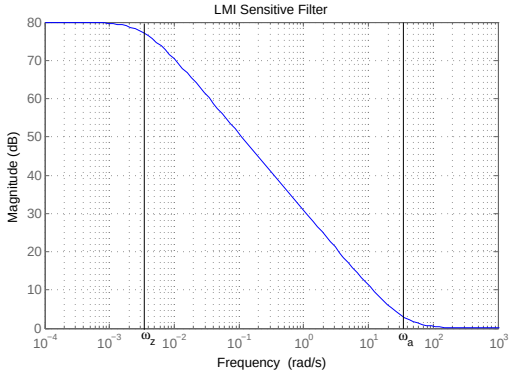

Figure 4.3: Magnitude plot of $W_1(s)$.

obtained in the time domain is:

$$\begin{aligned} \dot{x}_3(t) &= -\omega_z x_3(t) + (\omega_b - \omega_z)\theta_{out}(t) - (\omega_b - \omega_z)\theta_{in}(t) \\ e_1(t) &= K_{sen}(\theta_{out}(t) - \theta_{in}(t) + x_3(t)) \end{aligned} \tag{4.11}$$

The error e_2 is instead filtered by $W_2(s)$, in the following way:

$$E_2(s) = W_2(s)T_{in}(s) \qquad \text{where} \qquad W_2(s) = K_{act}\frac{s+\omega_a}{s+\omega_i} \tag{4.12}$$

where the transfer function $W_2(s)$ allows to limit the control input $T_{in}(t)$ and therefore makes the LMI problem feasible. Indeed, if the error energy $\|e_2\|_{\mathcal{L}_2}$ is high, the LMI problem becomes infeasible. The filter $W_2(s)$ has a low pass characteristic and cuts the frequency over the desired bandwidth value ω_a. This permits to attenuate the energy of the signal $e_2(t)$ and to reduce the control input amplitude, thus guaranteeing the feasibility of the LMI problem. In this case, the frequency ω_a is chosen close to the steer input frequency found in section 3.5. Thus, the controller uses the maximum bandwidth of the steer input signal. On the other hand, ω_i is the corner frequency and it is assumed to be greater than ω_a to obtain the low-pass characteristic. In this case $\omega_i = 0.0001\omega_a$. In addition, in the $W_2(s)$ characteristic there is the gain k_2 that allows to change the $e_2(t)$ signal amplitude. After some test, the k_2 value is chosen close to the value 30. In this way, we obtain the value of K_{act} from the relation:

$$K_{act} = \frac{\omega_i}{k_2\omega_a}$$

Changing the k_2 value and the bandwidth of the filter (frequency ω_a and ω_i), it is possible to modify the specifications on the control input and on the system feasibility. To satisfy these specifications, the filter $W_2(s)$ has the characteristic shown in Figure 4.4.

We are able to write the state equation in the Laplace domain for the output variable e_2:

$$\begin{aligned} E_2(s) &= K_{act}\left(\frac{s+\omega_a}{s+\omega_i}\right)T_{in}(s) \\ &= K_{act}\left(1 + \frac{\omega_a - \omega_i}{s+\omega_i}\right)T_{in}(s) \\ &= K_{act}\left(T_{in}(s) + X_4(s)\right) \end{aligned} \tag{4.13}$$

where:

$$X_4(s) = \frac{\omega_a - \omega_i}{s+\omega_i}T_{in}(s)$$

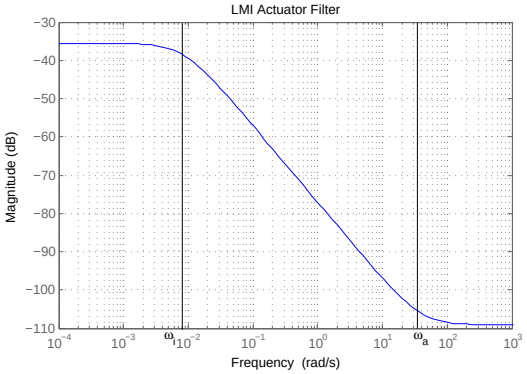

Figure 4.4: Magnitude plot of $W_2(s)$.

In the solution of the equation we introduced a new state variable x_4 that represents the filter state. Applying the inverse Laplace transform, the equation obtained in the time domain is:

$$\begin{aligned} \dot{x}_4(t) &= -\omega_i x_4(t) + (\omega_a - \omega_i) T_{in}(t) \\ e_2(t) &= K_{act}(u(t) + x_4(t)) \end{aligned} \tag{4.14}$$

The last filter used in the Figure 4.2 is the W_{M_z}, is a constant gain ε and it represents how much the disturbance is attenuated.
After the analysis of the filter, it is possible to write the equation of the wheel system in state form. We write the system in this form because the optimization synthesis for this type of systems is more easily implemented. The wheel system in state form is described as follows:

$$\begin{aligned} \dot{x}(t) &= \underbrace{\begin{bmatrix} 0 & 1 & 0 & 0 \\ -\frac{C_{M\alpha,i}}{I_w} & -\frac{b}{I_w} & 0 & 0 \\ \omega_b - \omega_z & 0 & -\omega_z & 0 \\ 0 & 0 & 0 & -\omega_i \end{bmatrix}}_{A} x + \underbrace{\begin{bmatrix} 0 \\ \frac{1}{I_w} \\ 0 \\ \omega_a - \omega_i \end{bmatrix}}_{B} T_{in} + \underbrace{\begin{bmatrix} 0 & 0 & 0 \\ 0 & \varepsilon & 0 \\ \omega_z - \omega_b & 0 & 0 \\ 0 & 0 & 0 \end{bmatrix}}_{H} w \\ e &= \underbrace{\begin{bmatrix} K_{sen} & 0 & K_{sen} & 0 \\ 0 & 0 & 0 & K_{act} \end{bmatrix}}_{C} x + \underbrace{\begin{bmatrix} 0 \\ K_{act} \end{bmatrix}}_{D} T_{in} + \underbrace{\begin{bmatrix} -K_{sen} & 0 & 0 \\ 0 & 0 & 0 \end{bmatrix}}_{E} w \\ y &= \underbrace{\begin{bmatrix} 1 & 0 & 0 & 0 \end{bmatrix}}_{F} x + \underbrace{\begin{bmatrix} -1 & 0 & \varepsilon \end{bmatrix}}_{G} w \qquad i = 1, 2, 3. \end{aligned} \tag{4.15}$$

where $x = [\theta_{out}, \dot{\theta_{out}}, x_3, x_4]^T$ and $w = [\theta_{in}, \bar{M}_{z,i}, n_1]^T$ and n_1 is the additional noise acting on the output. This noise is not measurable. As made for the PI synthesis, we fix the values of μ and F_z to a constant value. In this way, the system (4.15) allows to define the two differents contrains for the "linear" and "nonlinear" region. Introducing the $C_{M\alpha,2}$ value in (4.15), it is possible to build the system that describes the constrains for the "linear" region. Using the system for the "linear" region and the controller equation (4.1), it is possible obtain the optimization problem (4.6) for the wheel system in the "linear" region. To obtain the optimization problem (4.6) for the wheel system in the "saturation" region, we have to insert the value $C_{M\alpha,1}$ or $C_{M\alpha,3}$ in the system (4.15) and we use the same

procedure shown for the "linear" region. In this way, we design two different optimization problems, one for the "linear" region and one for the "saturation" one.
Using the *Matlab* function *hinfsyn*, it is possible to solve these two optimization problems introduced by the equation (4.6) and by respecting the associated constrains. This *Matlab* function implements the theory shown in section D.2.3. In particular, the function uses equations (D.24) and (D.27) to obtain a solution that solves simultaneously both optimization problems. The solution can be converted into a solution for the control problem and we obtain the matrices A_c, B_c, C_c and D_c. In this way, we solve the optimization problem (4.6) and we obtain the feedback controller designed with the LMI technique. The controller is described by equation (4.1).
We introduce the LMI controller in the system in Figure 4.2 and the result of the LMI synthesis is shown in Figure 4.5.

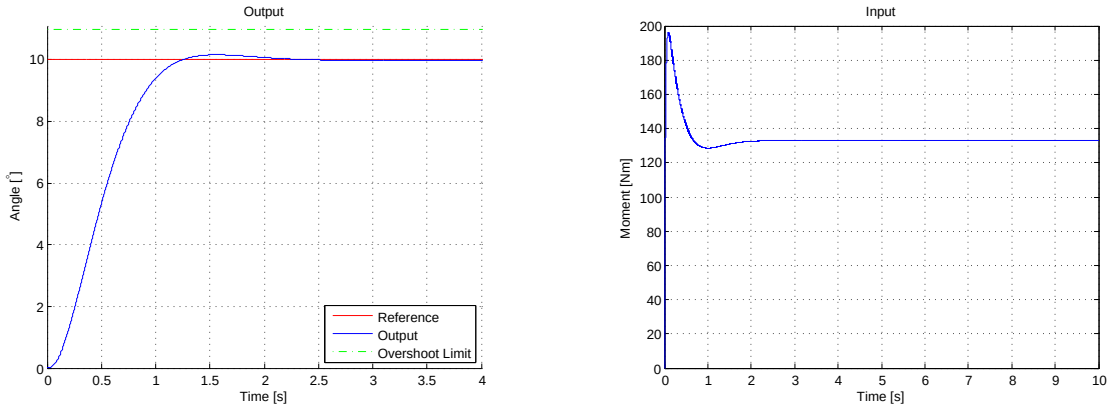

Figure 4.5: On the left there is the step responce, on the right there is the input control of the LMI feedback controller in "linear" region.

As shown in Figure 4.5, with a plant in the "linear" region, every specification imposed at the beginning of the section is satisfied.

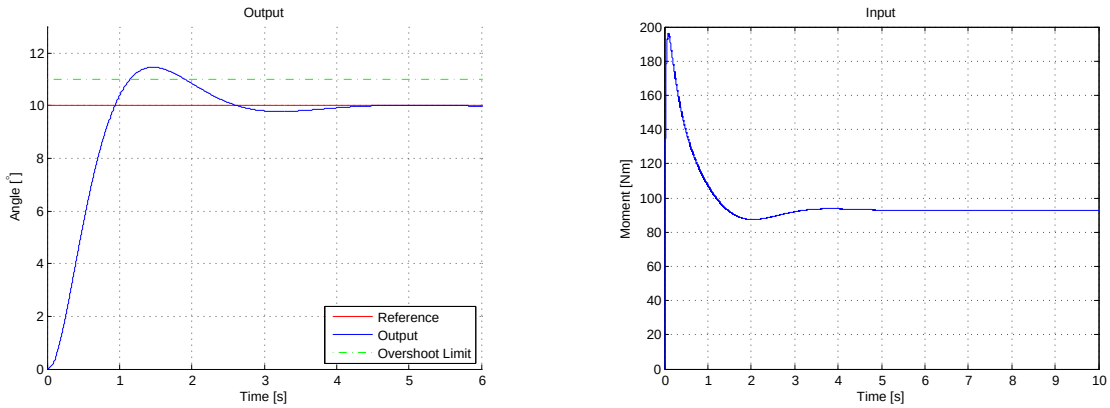

Figure 4.6: On the left there is the step responce, on the right there is the input control of the LMI state feedback controller in "saturation" region.

As shown in Figure 4.6, with a plant in the "saturation" region, the output employs more time to arrive at the steady state value respect to the one in the "linear" region. In fact, in order to reduce the control input, even the value of the controller matrix needs to be reduced. In the plant of the "saturation" region there is an unstable pole and this pole makes the system uncontrollable, as shown in section 3.5.1. The controller designed with

LMI technique controls the system output slower respect to the "linear" region, but the system has a stable behaviour and is controllable. With respect to the PI controller analysis, these results are a considerable progress.
In conclusion, the controller designed with the LMI technique has better performances for the wheel system than a controller designed with the PI synthesis.

4.2 LPV Synthesis for the Wheel System

In the previous section the controller designed with the LMI technique for the wheel system was built. This controller satisfies every specifications imposed in section 4.1. This controller does not take into account the possible variations of the $C_{M\alpha,i}$ term depending on the parameter μ and F_z. To meet also this constrain, it is necessary to introduce a controller designed with an LPV technique.

4.2.1 Linearization the Self Aligning Moment Characteristic

Before introducing the LPV synthesis for the wheel system, we have to linearize the Tire Steering Dynamic equation (3.9) for different values of μ and F_z. In this way, we find how the $C_{M\alpha,i}$ values change with different value of μ and F_z.
In section 3.2 the values of μ and F_z parameters were fixed to a constant values and the first self aligning moment linearization was deduced, in Figure 3.2. In that case, the self aligning characteristic was divided into three regions in order to describe the curve with a piece-wise linear curve.
Now, we have to built a robust controller that changes its value with the parameter μ and F_z. For this reason, the same division into regions is maintained but the values of μ and F_z change respectly from 0.6 to 0.9 and from 40000 N to 80000 N. The μ value represents the different conditions of wheel adhesion. Indeed, the friction coefficient for a weat road is close to 0.6 and for the dry one is close to 0.9. Instead, the F_z value represents the possible load on the wheel. Figure 4.7 shows the different waveforms of the self aligning moment for the minimum valuee, $\mu = 0.6$ and $F_z = 40000$ N, and for the maximum onee, $\mu = 0.9$ and $F_z = 80000$ N.

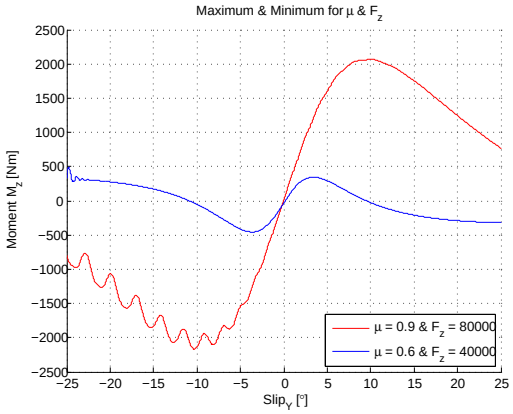

Figure 4.7: The self aligning moment for different value of μ and F_z.

As shown in Figure 4.7, the self aligning characteristic has a different waveform if the values of μ and F_z change from the minimum to the maximum value. Also the limit of the steering angle value $\theta(t)$, on the X-axis, changes with the value of these two parameters, indeed the maximum value of steering angle becomes 10°, for the minimum values of

the μ and F_z, and 20° for the maximum values of these parameters. At this point, it is possible to linearize the two different waveforms. Figure 4.8 shows the linearization for the minimum case (Figure 4.8 on the left) and the one for the maximum case (Figure 4.8 on the right). The linearization used the description of the self aligning moment with a piece-wise linear function, shown in equation (3.7). In this case, the values of $C_{M\alpha,i}$ and $\bar{M}_{z,i}$ change, not only with the steering angle $\theta(t)$, but also with the parameters μ and F_z from a minimum to a maximum value. We can define the variations as follows: $C_{M\alpha,i} \in [C_{M\alpha,i\ MIN}; C_{M\alpha,i\ MAX}]$ and $\bar{M}_{z,i} \in [\bar{M}_{z,i\ MIN}; \bar{M}_{z,i\ MAX}]$, $\quad i = 1, 2, 3.$

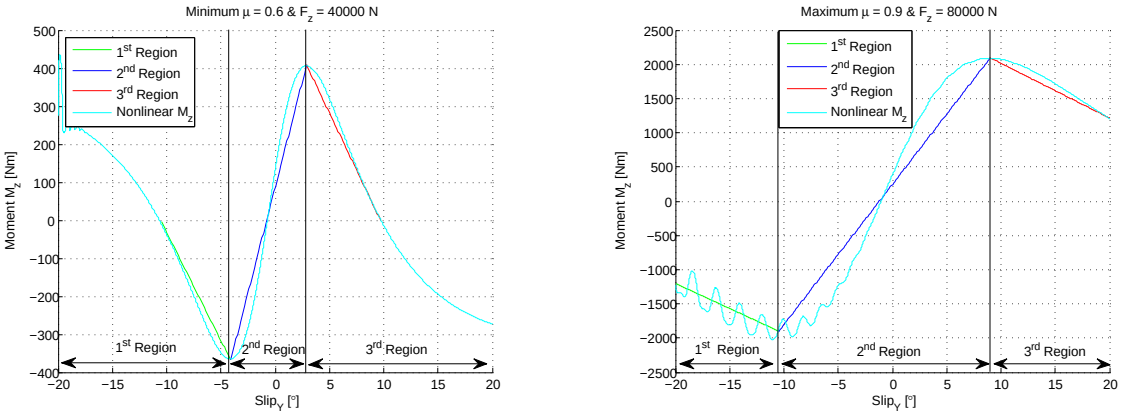

Figure 4.8: The self aligning moment linearization. On the left for $\mu = 0.6$ and $F_z = 40000$ N, on the right for $\mu = 0.9$ and $F_z = 80000$ N.

The linearization is necessary in order to know the value of the slope of the M_z curve. This value will be then inserted into the wheel equation (3.10). In this way, we can design a controller that changes its parameters with the value of $C_{M\alpha,i}$ and that operates in every curve region.
The self aligning moment equation (3.7) can be written as follows:

$$M_z(t, \kappa, \alpha, \mu, F_z) = \begin{cases} -C_{M\alpha,1}(\mu, F_z)\theta - \bar{M}_{z,1}(\mu, F_z) + \varepsilon_1, & -20° < \theta < -6°, \\ C_{M\alpha,2}(\mu, F_z)\theta - \bar{M}_{z,2}(\mu, F_z) + \varepsilon_2, & -6° < \theta < 6°, \\ -C_{M\alpha,3}(\mu, F_z)\theta + \bar{M}_{z,3}(\mu, F_z) + \varepsilon_3, & 6° < \theta < 20°, \end{cases} \tag{4.16}$$

We have to substitute the equation (4.16) in the Tire Steering Dynamic equation (2.1). The Tire Steering Dynamic equation in the Laplace domain for the different regions is defined as follows:

$$s^2 I_w \Theta(s) = T_{in}(s) + \bar{M}_{z,i}(\mu, F_z) - C_{M\alpha,i}(\mu, F_z)\Theta(s) - sb\Theta(s) + \varepsilon_i(s)\ i = 1, 2, 3 \tag{4.17}$$

Equation (4.17) is used to design the LPV controller.

4.2.2 LPV Problem for the Wheel Equation

The physical systems are variables, perturbed or uncertainties in the parameters at this lead the model uncertain. Often, these uncertainties change the values of the parameters or coefficients of the steady space model. Very small parameter variations have a great impact on the dynamics of the system, this reason is sufficient to derive a controller designed with LPV techniques. As shown in section 4.2.1, the self aligning moment curve changes its waveform with the variations of the parameters μ and F_z. Considering that the variations of μ and F_z have an influence on the $C_{M\alpha,i}$ value, we can assume that the

variation of μ and F_z is an uncertainty of our model.
The LPV design technique permits to realize a controller that adjust its parameters to the physical system uncertainty. So, the robust stability property can be guaranteed.
Using the theory shown in the appendix E and the self aligning moment linearization shown in the previous section, the controller designed with LPV technique for the wheel equation will be obtained.
The controller is described by the following equations:

$$\begin{aligned} \dot{x}_c(t) &= A_c(C_{M\alpha,i})x_c(t) + B_c(C_{M\alpha,i})y(t) \\ T_{in}(t) &= C_c(C_{M\alpha,i})x_c(t) + D_c(C_{M\alpha,i})y(t) \qquad i = 1,2,3 \end{aligned} \tag{4.18}$$

where $y(t)$ is the difference between θ_{out} and θ_{in}. The equations of the LPV system are:

$$\begin{aligned} \dot{x}(t) &= A(C_{M\alpha,i})x(t) + B(C_{M\alpha,i})T_{in}(t) + H(C_{M\alpha,i})w(t) \\ e(t) &= C(C_{M\alpha,i})x(t) + D(C_{M\alpha,i})T_{in}(t) + E(C_{M\alpha,i})w(t) \\ y(t) &= F(C_{M\alpha,i})x(t) + G(C_{M\alpha,i})w(t) \qquad i = 1,2,3 \end{aligned} \tag{4.19}$$

where $e(t)$ is the error, $w(t)$ is the disturbance, $T_{in}(t)$ is the control input and $y(t)$ is the measured output. The LPV technique consists of translating the wheel system control problem into an optimization problem, where the control problem specifications become the optimization problem constraints. The optimization problem is described as follows:

$$\begin{aligned} (A_c, B_c, C_c, D_c) &= argmin_{(A_c,B_c,C_c,D_c)}\ \gamma \\ \gamma &> \frac{\|e\|_{\mathcal{L}_2}}{\|w\|_{\mathcal{L}_2}} \end{aligned} \tag{4.20}$$

where in the matrices of equation (4.20) the dependency on the $C_{M\alpha,i}$ values is omitted. γ is the variable which has to be minimized, $\|\cdot\|_{\mathcal{L}_2}$ is the energy of the signal, e is the error and w is the disturbance. The solution of the optimization problem ensures that the energy of the error $\|e\|_{\mathcal{L}_2}$ is not greater than γ times the value of the energy of the disturbance $\|w\|_{\mathcal{L}_2}$ in the system, if and only if the solution exists. The LPV system has the same configuration of the LMI system shown in Figure 4.1. To satisfy the desired performance, the interconnection of the LPV system (4.19) and the LPV controller (4.18), in Figure 4.1, has to be internally stable. A new state variable $\xi = [x, x_c]^T$ is introduced and the controlled system is simply described by the equation:

$$\begin{aligned} \dot{\xi}(t) &= \mathcal{A}(C_{M\alpha,i})\xi(t) + \mathcal{B}(C_{M\alpha,i})w(t) \\ z(t) &= \mathcal{C}(C_{M\alpha,i})\xi(t) + \mathcal{D}(C_{M\alpha,i})w(t) \\ \text{with } \left(\begin{array}{c|c} \mathcal{A}(C_{M\alpha,i}) & \mathcal{B}(C_{M\alpha,i}) \\ \hline \mathcal{C}(C_{M\alpha,i}) & \mathcal{D}(C_{M\alpha,i}) \end{array}\right) &= \left(\begin{array}{cc|c} A + BD_cF & BC_c & H + BD_cG \\ B_cF & A_c & B_cG \\ \hline C + DD_cF & DC_c & E + DD_cG \end{array}\right) \end{aligned} \tag{4.21}$$

where in the matrices A, B, C, D, E, F, G, H, A_c, B_c, C_c and D_c the dependency on the $C_{M\alpha,i}$ parameters is omitted.
By making use of **Theorem 5** and of the LPV inequality expressed in (E.10) in appendix E, a controller that stabilizes the system (4.21) can be found. It makes the $\mathcal{H}_\infty$-norm of the transfer matrix $\|w\|_{\mathcal{L}_2} \to \|e\|_{\mathcal{L}_2}$ smaller than γ if and only if there exist $X(C_{M\alpha,i})$ satisfying

$$X \succ 0 \quad \text{and} \quad \begin{pmatrix} \mathcal{A}^T X + X\mathcal{A} & X\mathcal{B} & \mathcal{C}^T \\ \mathcal{B}^T X & -\gamma I & \mathcal{D}^T \\ \mathcal{C} & \mathcal{D} & -\gamma I \end{pmatrix} \prec 0 \tag{4.22}$$

where in the matrices X, $\mathcal{A}$, $\mathcal{B}$, $\mathcal{C}$ and $\mathcal{D}$ the dependency on the $C_{M\alpha,i}$ parameters is omitted. The first inequality guarantees stability and the second captures performance. So, by substituting equation (4.22) in the initial problem (4.20), we obtain the optimization problem:

$$\begin{aligned}(A_c, B_c, C_c, D_c) &= argmin_{(A_c,B_c,C_c,D_c)}\ \gamma \\ X \succ 0 \quad \text{and} \quad &\begin{pmatrix} \mathcal{A}^T X + X\mathcal{A} & X\mathcal{B} & \mathcal{C}^T \\ \mathcal{B}^T X & -\gamma I & \mathcal{D}^T \\ \mathcal{C} & \mathcal{D} & -\gamma I \end{pmatrix} \prec 0\end{aligned} \tag{4.23}$$

where in the matrices X, $\mathcal{A}$, $\mathcal{B}$, $\mathcal{C}$ and $\mathcal{D}$ the dependency on the $C_{M\alpha,i}$ parameters is omitted. By solving this optimization problem, it is possible to translate the result into a solution for the control problem.
The controller of the system in Figure 4.1 has to satisfy the following specifications:

1. Minimize the settling time t_s and the rise time t_r;
2. Zero steady state error at the step;
3. Limit the value of the control input below 200 Nm;
4. The controller has to stabilize the system in both regions "linear" and "saturation";
5. The control is robust to the variation of μ and F_z.

The specifications 1, 2 and 3 must be satisfied in both regions: "linear" and "saturation". At this point we have to convert the specifications into constrains of the optimization problem. Considering that the first four specifications are the same of the LMI synthesis, the way to translate these specifications into constrains is similar to the one shown in section 4.1. Also the filters $W_1(s)$ and $W_2(s)$ are introduced to design the controller with LPV technique and they have the same characteristics shown in section 4.1. However, we have to define how to convert the fifth specification.
As we made for the fourth specification in section 4.1, we have to introduce different constrains for the different values of μ and F_z to satisfy the fifth specification and guarantee the robust stability. Indeed, in section 4.2.1 we showed that with different values of μ and F_z it is possible to schedule several values of $C_{M\alpha,i}$. We have to introduce a polytopic region that describes how the $C_{M\alpha,i}$ values vary in the "linear" and "saturation" regions. For each region described in Figure 4.8, the maximum and minimum value of $C_{M\alpha}$ are extracted. With these $C_{M\alpha}$ values, it is possible to design a robust controller. Indeed, each $C_{M\alpha}$ values is translated into an optimization problem constrain. Solving the optimization problem with these different constrains, it is possible to obtain a controller that respects the robust stability property.
After having introduced the conversion of the control specifications, we need to adapt the control system provided at the beginning of the section 3.5 to the LPV problem system, as shown in Figure 4.9.

As it can be deduced from Figure 4.9, the difference between the reference $\theta_{in}(t)$ and the output $\theta_{out}(t)$, that it is the tracking error y(t), times a filter $W_1(s)$, giving as a result the error e_1. On the other hand, the sum of the control input $T_{in}(t)$ and the disturbance $\bar{M}_{z,i}$ times the filter $W_2(s)$, giving back the input control e_2. In the control system for the LPV synthesis in Figure 4.9 is introduced a noise in the input control. This noise is called n_2, it is not measurable and it represents the disturbance that can be present in the disturbance input $\bar{M}_{z,i}$ and then in the input control $T_{in}(t)$. In the LPV synthesis the

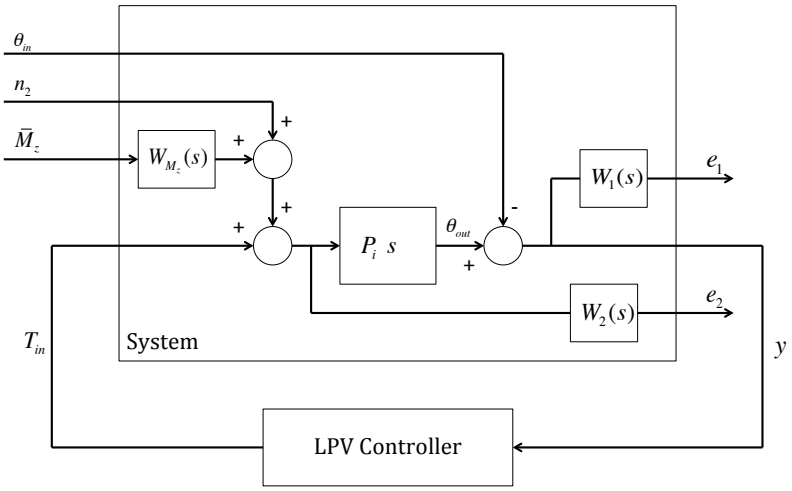

Figure 4.9: LPV Wheel Control System.

disturbance $\bar{M}_{z,i}$ is supposed to be measurable.
The block $P_i(s)$ is the second order model of the Tire Steering Dynamic described on the equation (4.17). As we made for the LMI synthesis, in the LPV implementation the state model is more appropriate. Equation (4.17) is rewritten as follows:

$$\begin{aligned}\begin{bmatrix}\dot{\theta}_{out}(t)\\ \ddot{\theta}_{out}(t)\end{bmatrix} &= \begin{bmatrix}0 & 1\\ -\frac{C_{M\alpha,i}(\mu,F_z)}{I_w} & -\frac{b}{I_w}\end{bmatrix}\begin{bmatrix}\theta_{out}(t)\\ \dot{\theta}_{out}(t)\end{bmatrix} + \begin{bmatrix}0\\ \frac{1}{I_w}\end{bmatrix}\left[T_{in}(t)\right]\\ y &= \begin{bmatrix}1 & 0\end{bmatrix}\begin{bmatrix}\theta_{out}(t)\\ \dot{\theta}_{out}(t)\end{bmatrix} + \left[-1\right]\left[\theta_{in}(t)\right]\end{aligned} \qquad i = 1, 2, 3. \tag{4.24}$$

Equation (4.24) describes the Tire Steering Dynamic equation in both regions, "linear" and "saturation".
The structure of the filters $W_1(s)$ and $W_2(s)$ does not change compared to the ones introduced in section 4.1. Indeed, The filters permit to reduce the steady state error and the input control, as shown in the LMI synthesis.
The error e_1 is described in equation (4.9), but the $W_1(s)$ filter characteristic changes to permit to the optimization problem the respect of every constrains. Indeed, to achieve robustness, in the LPV synthesis we have to insert more constrains. These constrains are very different respect to the LMI synthesis and we have to modify the ω_b, ω_z and S_∞ parameters in order to find a solution of the LPV synthesis that respects every constraints. So, we increase the ω_b and ω_z values of the bandwidth of the feedback system with respect to the ones used in the LMI synthesis. We also increase the gain error at steady state with respect to the LMI synthesis, modifying the S_∞ value.
The magnitude Bode plot of the filter $W_1(s)$ for the LPV synthesis is shown in Figure 4.10. Figure 4.10 shows that the filter $W_1(s)$ emphasizes the low frequencies with respect to the high ones. Remembering the equation of the filter $W_1(s)$ (4.9), it is possible to

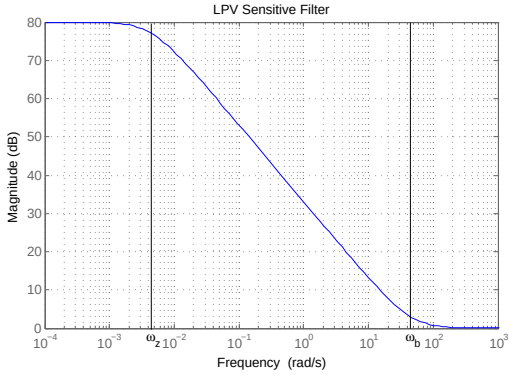

Figure 4.10: LPV Controller Magnitude plot of $W_1(s)$.

write the state equation in the Laplace domain for the output variable e_1:

$$\begin{aligned} E_1(s) &= K_{sen}\left(\frac{s+\omega_b}{s+\omega_z}\right)E(s) \\ &= K_{sen}\left(1+\frac{\omega_b-\omega_z}{s+\omega_z}\right)(\Theta_{out}(s)-\Theta_{in}(s)) \\ &= K_{sen}\left(\Theta_{out}(s)-\Theta_{in}(s)+X_3(s)\right) \end{aligned} \tag{4.25}$$

where:

$$X_3(s) = \frac{\omega_b-\omega_z}{s+\omega_z}(\Theta_{out}(s)-\Theta_{in}(s))$$

In the solution of the equation we introduced a new state variable x_3 that represents the sensitivity filter $W_1(s)$ state. Applying the inverse Laplace transform, the corresponding time domain equation is:

$$\begin{aligned} \dot{x}_3(t) &= -\omega_z x_3(t) + (\omega_b-\omega_z)\theta_{out}(t) - (\omega_b-\omega_z)\theta_{in}(t) \\ e_1(t) &= K_{sen}(\theta_{out}(t)-\theta_{in}(t)+x_3(t)) \end{aligned} \tag{4.26}$$

The error e_2 is defined by equation (4.12), but the $W_2(s)$ filter characteristic changes to permit to the optimization problem the respect of every constrains. As we made for the filter $W_1(s)$ we have to modify the ω_a, ω_i and k_2 parameters. So, we decrease ω_a and ω_i and increase the signal amplitude k_2 with respect to the ones used in the LMI synthesis. With these modifications, we satisfy the specifications about the control input and the system feasibility for different values of μ andF_z.
The magnitude Bode plot of the filter $W_2(s)$ for the LPV synthesis is shown in Figure 4.11. We are able to write the state equation in the Laplace domain for the output variable e_2:

$$\begin{aligned} E_2(s) &= K_{act}\left(\frac{s+\omega_a}{s+\omega_i}\right)(T_{in}(s)+\bar{M}_{z,i}(s)) \\ &= K_{act}\left(1+\frac{\omega_a-\omega_i}{s+\omega_i}\right)(T_{in}(s)+\bar{M}_{z,i}(s)) \\ &= K_{act}\left(T_{in}(s)+\bar{M}_{z,i}(s)+X_4(s)\right) \end{aligned} \tag{4.27}$$

where:

$$X_4(s) = \frac{\omega_a-\omega_i}{s+\omega_i}(T_{in}(s)+\bar{M}_{z,i}(s))$$

In the solution of the equation we introduced a new state variable x_4 that represents the filter state. By applying the inverse Laplace transform, the equation obtained in the time

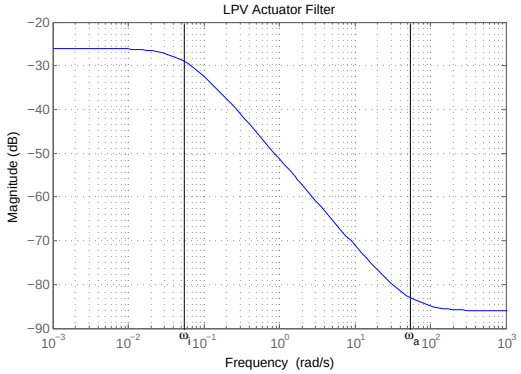

Figure 4.11: LPV Controller Magnitude plot of $W_2(s)$.

domain is:

$$\begin{aligned} \dot{x}_4(t) &= -\omega_i x_4(t) + (\omega_a - \omega_i)(T_{in}(t) + \bar{M}_{z,i}(t)) \\ z_2(t) &= K_{act}(T_{in}(t) + \bar{M}_{z,i}(t) + x_4(t)) \end{aligned} \tag{4.28}$$

The last filter used in Figure 4.9 is the W_{M_z}, is a constant gain ε and it represents how much the disturbance influences the system.
After the analysis of the filter, it is possible to write the equation of the wheel system in the state form. In the LPV synthesis, the disturbance $\bar{M}_{z,i}$ is supposed to be measurable. So it is necessary to add another output to the variable $y(t)$ in the control equation (4.29) of the LMI control because the LPV controller has also to evaluate the information of the disturbance $\bar{M}_{z,i}$ that influences the input control. The wheel system in state form is described as follows:

$$\dot{x}(t) = \begin{bmatrix} 0 & 1 & 0 & 0 \\ -\frac{C_{M\alpha}(\mu,F_z)}{I_w} & -\frac{b}{I_w} & 0 & \frac{\varepsilon_{n2}}{I_w} \\ \omega_b - \omega_z & 0 & -\omega_z & 0 \\ 0 & 0 & 0 & -\omega_i \end{bmatrix} x + \begin{bmatrix} 0 \\ \frac{1}{I_w} \\ 0 \\ \omega_a - \omega_i \end{bmatrix} T_{in} + \begin{bmatrix} 0 & 0 & 0 & 0 \\ 0 & \frac{\varepsilon}{I_w} & 0 & 0 \\ \omega_z - \omega_b & 0 & 0 & 0 \\ 0 & (\omega_a - \omega_i)\varepsilon & 0 & 0 \end{bmatrix} w$$

$$z = \begin{bmatrix} K_{sen} & 0 & K_{sen} & 0 \\ 0 & 0 & 0 & K_{act} \end{bmatrix} x + \begin{bmatrix} 0 \\ K_{act} \end{bmatrix} T_{in} + \begin{bmatrix} -K_{sen} & 0 & 0 & 0 \\ 0 & K_{act}\varepsilon & 0 & 0 \end{bmatrix} w$$

$$y = \begin{bmatrix} 1 & 0 & 0 & 0 \\ 0 & 0 & 0 & 0 \end{bmatrix} x + \begin{bmatrix} -1 & 0 & \varepsilon_{n1} & 0 \\ 0 & 1 & 0 & \varepsilon_{n2} \end{bmatrix} w \tag{4.29}$$

where the vectors are $x = [\theta_{out}, \dot{\theta_{out}}, x_3, x_4]^T$ and $w = [\theta_{in}, \bar{M}_{z,i}, n_1, n_2]^T$, n_1 is the additional noise in the output and n_2 is the additional noise in the input. These two noises are not measurable. System (4.29) allows to define the two different constrains to satisfy the robust stability property. Introducing the μ and F_z values, and therefore a specific value for $C_{M\alpha}(\mu, F_z)$, in (4.29), it is possible to build the system that describes a particular condition for the values μ and F_z. Using this system and the controller equation (4.18), it is possible obtain the optimization problem (4.23) for the wheel system. Following the same step, it is possible to define several optimization problems that satisfy the constrains for different values of $C_{M\alpha}$ both in the "linear" and in the "saturation" regions. In this way, finding a unique solution of these optimization problems, it is possible to guarantee

the robust stability property.
Using the *Matlab* function *hinfgs*, it is possible to solve all these optimization problems and respecting the associated constrains. This *Matlab* function implements the theory shown in section E.1.4. In particular, the function uses equation (E.20) to obtain a solution that solves simultaneously the optimization problems. The solution can be converted into a solution for the control problem and we obtain the matrices $A_c(C_{M\alpha})$, $B_c(C_{M\alpha})$, $C_c(C_{M\alpha})$ and $D_c(C_{M\alpha})$. In this way, we solve the optimization problem (4.23) and we design the feedback controller with the LPV technique. The controller is described by equation (4.18).
We introduce the LPV controller in the system in Figure 4.9 and the result of the LPV synthesis is shown in Figure 4.12. Figure 4.12 shows how the controller designed with

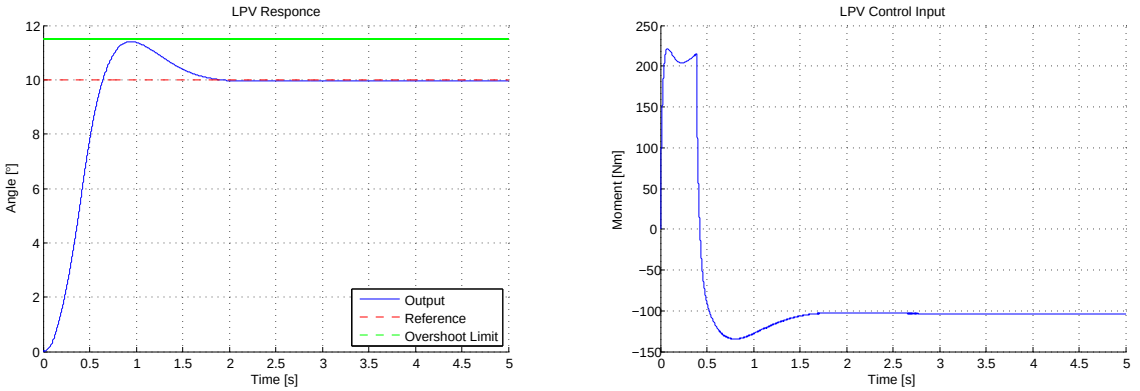

Figure 4.12: On the left there is the step responce, on the right there is the input control of the LPV state feedback controller.

LPV technique respects the specifications imposed at the beginning of this section. Reminding the M_z characteristic in Figure 4.8, the curve changes region, from the "linear" one to the "saturation" one, for values of steering angle θ included between 5° and 9°. So, the simulation shows how the controller designed with LPV technique controls the wheel system in both regions, "linear" and "saturation".
The LPV controller is tested with different values of μ and F_z, to show that the robust stability property is satisfied. The results are shown in Figure 4.13 and 4.14.

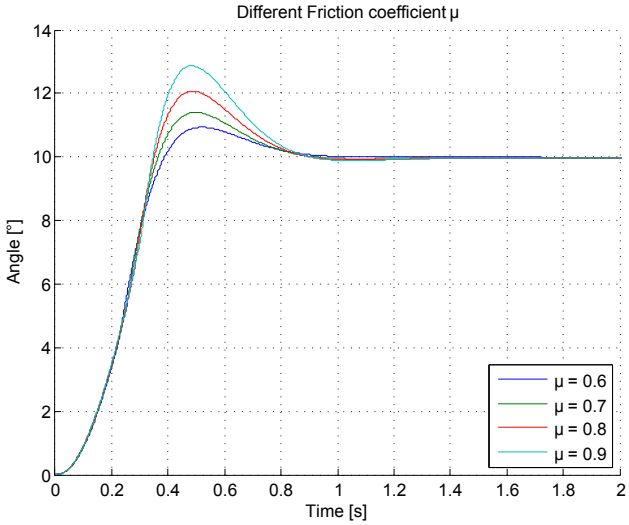

Figure 4.13: Simulation with different value of μ.

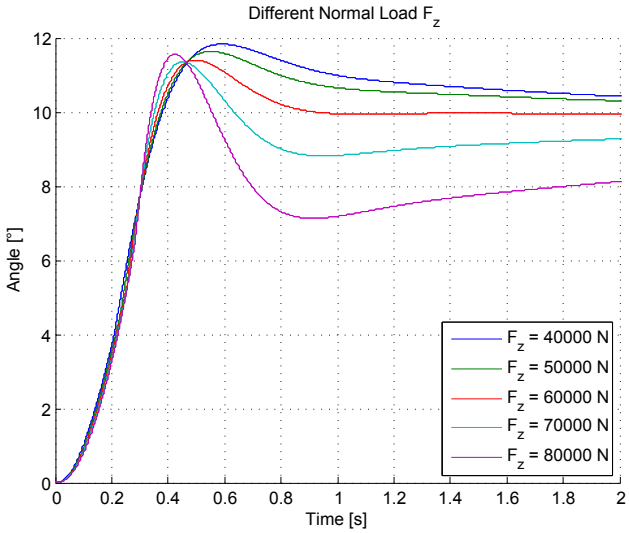

Figure 4.14: Simulation with different value of F_z.

Figure 4.13 shows that, for different values of μ, every specification is satisfied. Indeed, Figure 4.14 shows that the null steady state error specification is not respected for different values of F_z. We try to satisfy the steady state error specification also for the F_z values, but by adjusting the parameters of the filter it was not possible to find a better solution. In conclusion, the controller designed with LPV technique guarantees the robust property for different values of μ and F_z and controls the wheel system in both the "linear" and the "saturation" regions.

Chapter 5

LPV Controller Simulation

At the end of the previous chapter 4 the LPV controller for the wheel system was derived. It is very important now to test the controller in different cases. The simulation has to reproduce the possible real situations that the controller may face. So, at this point, some test on the LPV controller are made to reproduce some possible real events. In particular, the tests are divided into three parts and simulate three different conditions of the self aligning function:

1. The self aligning function is completely known and can be linearized as shown in section 4.2.1;
2. The self aligning characteristic is completely known and it is possible to calculate the derivate of M_z with respect to the slip angle α;
3. Only the empirical value of the self aligning characteristic and its uncertainty is known.

In the first two cases two different types of tests are made. The first one simulates a continuos change of steering, called run at zigzag, in a long period of 200 seconds. The second one compares the controller in different situations of adhesion and weight, in particular for the minimum and maximum values of friction coefficient μ and weight F_z. In this test there is always a continuous change of steering but the length of simulation is chosen shorter than the previous test, 60 seconds. For this controller, the test is repeated with different values of longitudinal velocity, especially focusing the attention on the low speed manoeuvre.
Instead, in the third case of simulations, the self aligning moment parameter is supposed completely unknown, but we know only the shape form of the characteristic and its uncertainty. In this case it is possible to make the test with uncertainty, the simulation has a length of 200 seconds.
In the following test a sinusoidal input is used because this type of input is closer to the real steering manoeuvre. Instead a step input does not represent in a good way the reality, but is good to check the control specific in the construction phase.

5.1 Linearizzed Self Aligning Moment Function

In this section the self aligning moment characteristic and every parameter, in particular μ and F_z, are supposed to be known. Chapter 2 explained how the self aligning moment curve presents a nonlinear behavior and must therefore be linearized with the procedure shown in section 4.2.1. The self aligning moment characteristic with a piece-wise linear

curve is composed by three straight lines; two lines have a negative slope, i.e. lines in the 1^{st} and 3^{rd} region of Figure 4.8, and the third one a positive slope, and is contained in the 2^{nd} region. With the linearization of the M_z curve it is also possible to obtain the value of the stiffness coefficient $C_{M\alpha}(\mu, F_z)$. In this condition normal values for μ and F_z are chosen and a test with a continuos change of steering is applied to the system, as shown in Figure 5.1. As shown in Figure 5.1 on the left, the controller tracks the input without

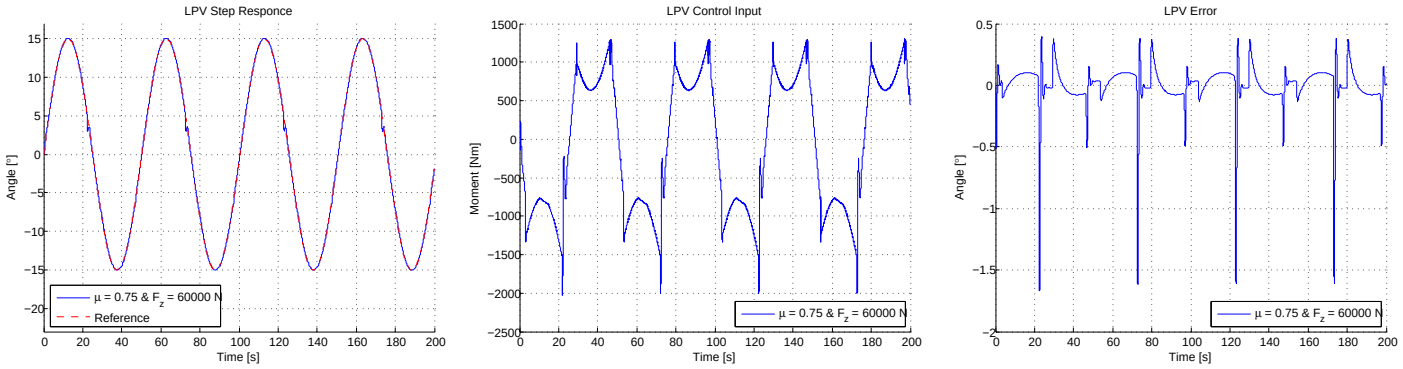

Figure 5.1: On the left there is the step response, in the middle there is the input control and on the right there is the error of the LPV state feedback controller with Linearized Self Aligning Moment Function.

delay and error in the characteristic, but in Figure 5.1 on the right the error becomes high in some point of the simulation. This behavior is due to the discontinuity of the linearized function, indeed the self aligning moment has a gradually change of slope from the positive value to the negative one. Instead, the linearized function has a sudden change and this causes a high value of the error and therefore a high value of the control input, as shown in Figure 5.1 on the center. Without this discontinuity the controller has the same behavior shown in the section 4.2.2.
After this first test other simulations are carried out, changing the value of the parameters μ and F_z. In particular, we want to analyze the limit case of these two values, that is when $\mu = 0.6$ and $F_z = 40000$ N and then when $\mu = 0.9$ and $F_z = 80000$ N. The results are shown in Figure 5.2. As shown in Figure 5.2 on the left, the controller tracks the reference

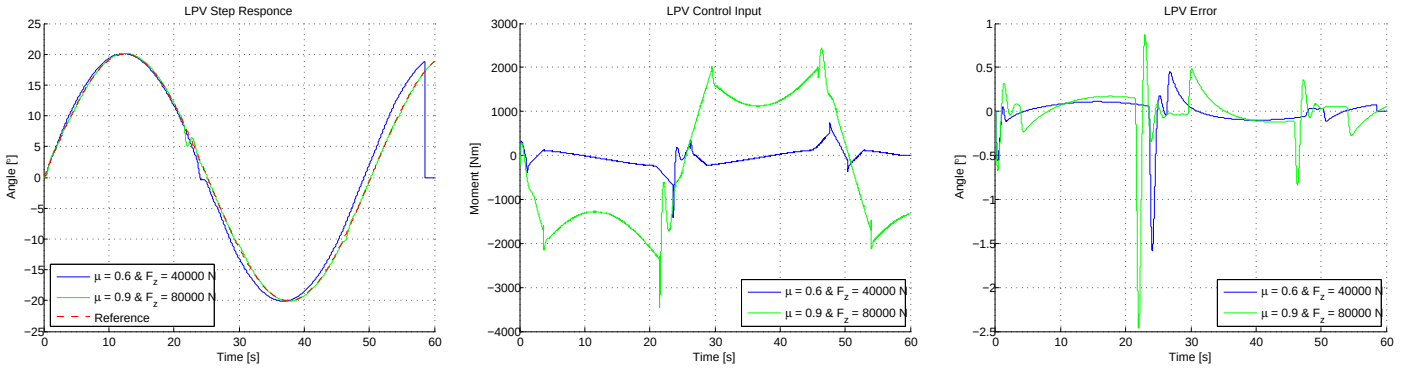

Figure 5.2: On the left there is the step response, in the middle there is the input control and on the right there is the error of the LPV state feedback controller with Linearized Self Aligning Moment Function.

also for different value of μ and F_z, but for the minimum parameters value there is an error at the end of the simulation. The reason is that the minimum value of the self aligning moment characteristic has a maximum value of slip angle of 10° and the simulation exceeds

that value. For this reason there is an error corresponding to high values of slip angle. In Figure 5.2 in the center, it is described as the control input increases when the friction coefficient and the weight increase, but this meets our expectations because an increase in the weight of the friction coefficient needs a higher control input in order to control the system. As analyzed in Figure 5.1 the discontinuity of the linearization causes a peak in the control input and in the error characteristic.
At last the linearized LPV controller has a good behavior in the reference tracking and has also a good behavior when the self aligning parameters change.

5.2 Derivate of Self Aligning Moment

Also in this section the self aligning characteristic is supposed to be known and it is possible calculate its derivate with respect to the slip angle α. This represents the stiffness coefficient value $C_{M\alpha}(\mu, F_z)$. The derivate calculations are shown in the Appendix C. With this type of simulation it is possible to test different values of velocity. In this condition normal values for μ and F_z are chosen and a velocity of 20 m/s is fixed. The first type of test is shown in Figure 5.3. As shown in Figure 5.3 on the left, the output has the same

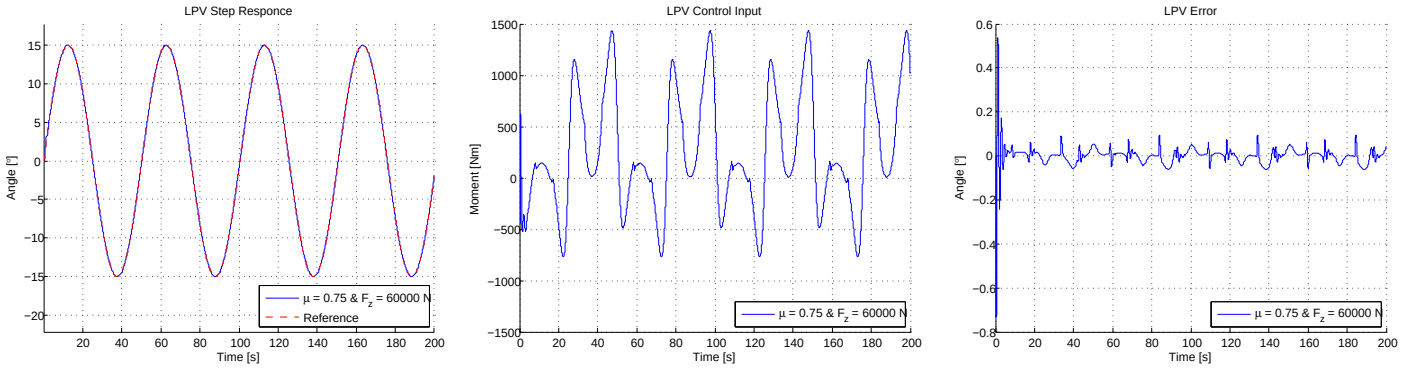

Figure 5.3: On the left there is the step response, in the middle there is the input control and on the right there is the error of the LPV state feedback controller with the Derivate Self Aligning Moment Function.

behaviour of the reference for the entire simulation. The control input remains limited for most of the time below the 1000 Nm, it has only a peak when the M_z characteristic slope changes sign. The error, after an initial transient, remains limited under the value 0.1°. The LPV controller with the derivate self aligning function satisfies the control specifics and generates a limited control input.
As we did before in 5.1, the value of the parameters μ and F_z are changed and some simulations are implemented. The limit cases of these two values are chosen to perform the tests, that is the case when the $\mu = 0.6$ and $F_z = 40000$ N and the one when $\mu = 0.9$ and $F_z = 80000$ N, the velocity remains at the value 20 m/s. The result is shown in Figure 5.4. As shown in Figure 5.4 on the right the output has the same behaviour of the reference also for different values of μ and F_z, but for the minimum parameters value there is an error at the end of the simulation. The reasons are the same exposed in the section 5.1. Also the comments about the control input and the error are the same of the previous section.

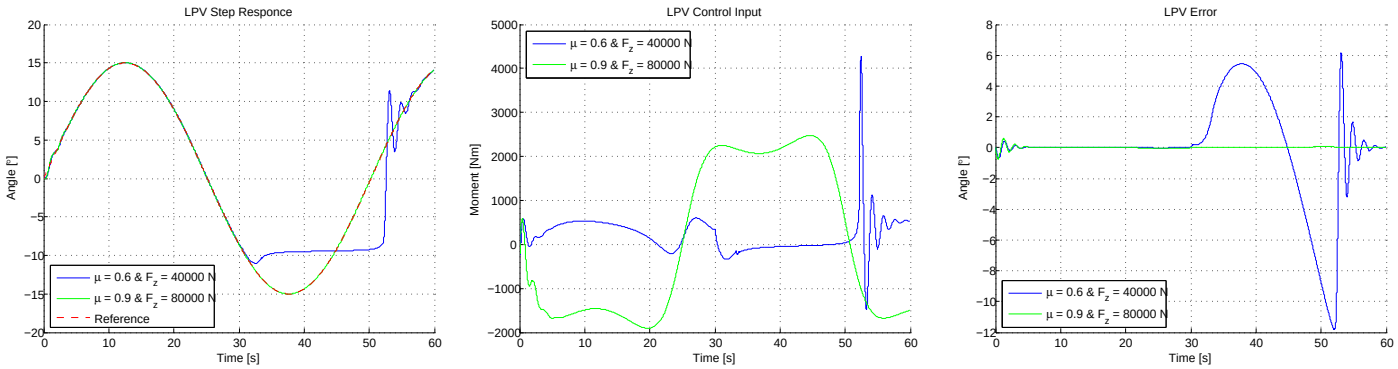

Figure 5.4: On the left there is the step response, in the middle there is the input control and on the right there is the error of the LPV state feedback controller with the Derivate Self Aligning Moment Function.

5.2.1 Velocity

We run the same tests we run before, but the value of the velocity, in this case, is different. Indeed, the Derivative LPV controller permits to simulate different velocities. The following tests are made assuming that the wheel is in a parking manouvre with 0.1 m/s velocity. The results are shown in Figure 5.5. As shown in Figure 5.5 on the left, the

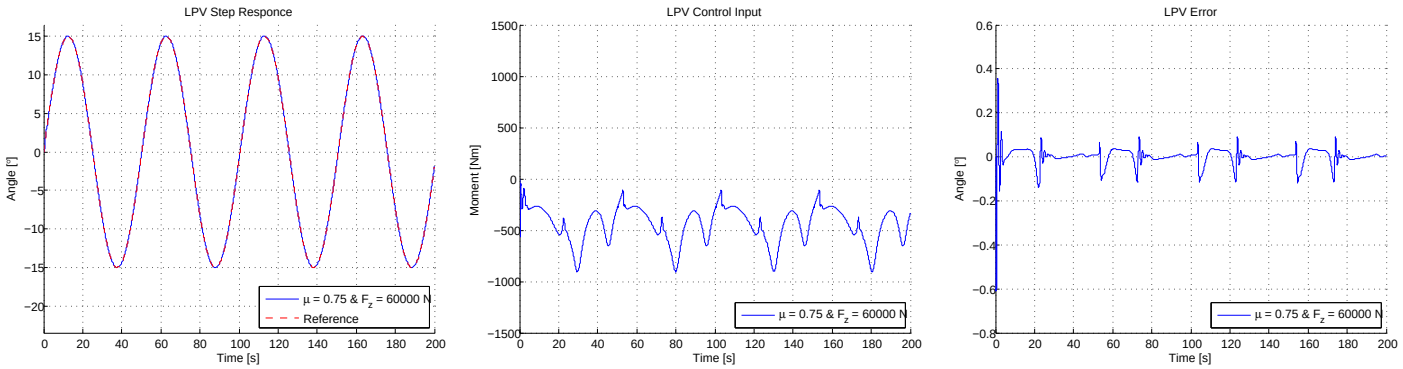

Figure 5.5: On the left there is the step response, in the middle there is the input control and on the right there is the error of the LPV state feedback controller for low velocity.

output has the same behaviour of the reference, but more importantly the control input at low speed, shown in Figure 5.5 on the center, is lower respect to the high velocity. This is an obvious result because if the speed is lower also the forces acting on the wheel decrease.
We want to test the LPV controller for the low velocity and different values of μ and F_z. The results are shown in Figure 5.6.
The behavior is the same as the one obtained for high speed, but as observed before the control input is smaller than the one at the high velocity.

At last, the system output with the derivate self aligning moment has the same behaviour of the reference and this behaviour is obtained also when the self aligning parameters change. This controller can be used to simulate the wheel manouvre at low speed.

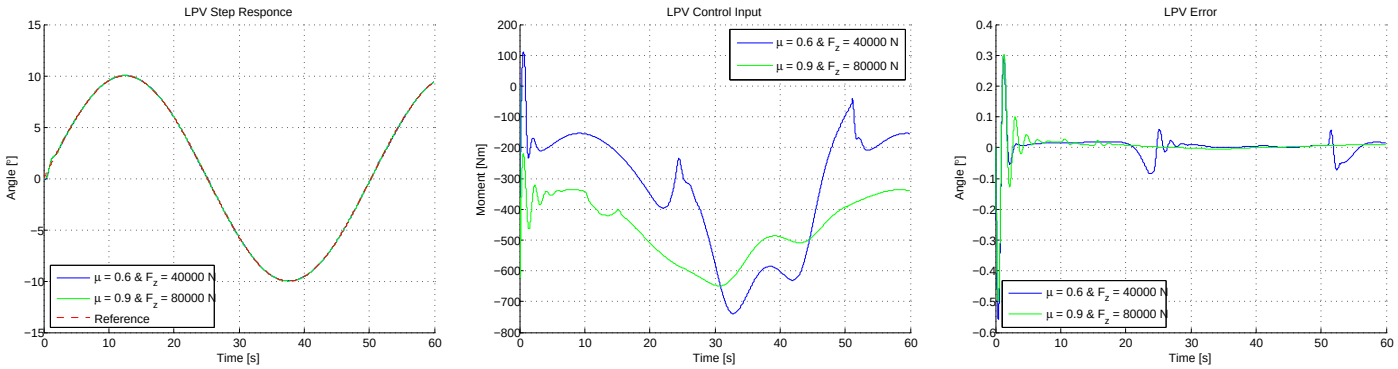

Figure 5.6: On the left there is the step response, in the middle there is the input control and on the right there is the error of the LPV state feedback controller for low velocity.

5.3 Uncertain Self Aligning Moment Function

In this section the self aligning moment characteristic is supposed not completely known and only the waveform of the curve and its uncertainty are known. We therefore simulate the case in which all the parameters of the system are unknown because impossible to be measured. Some tests can be performed on the system where some parameters are unknown. The simulations represent the continuos change of steering, shown in Figure 5.7. As shown in Figure 5.7 on the left the system output with this type of knowledge

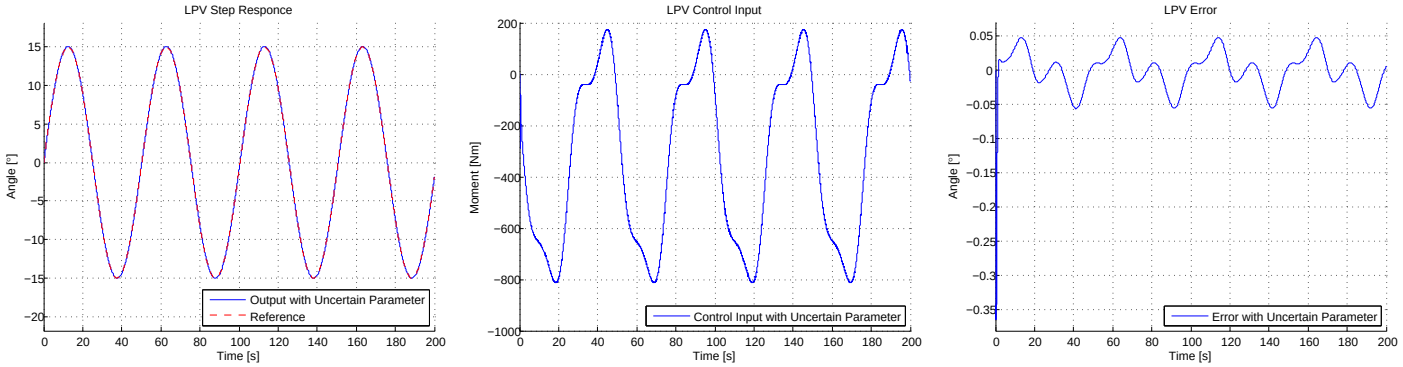

Figure 5.7: On the left there is the step response, in the middle there is the input control and on the right there is the error of the LPV state feedback controller with Uncertain Self Aligning Moment Function.

on the self aligning characteristic has the same behaviour of the reference. In Figure 5.7 on the center, the input control remains into the limit imposed and, in Figure 5.7 on the right, the error is not elevated, aside the initial transitory.
Also the Uncertain LPV controller satisfies the imposed specifics and has a good behavior in tracking the reference signal.

Chapter 6

Conclusion

This thesis has addressed the problem of building a robust controller for a wheel system. In particular it has shown how to design an LPV controller starting from a model with uncertain parameters. The dissertation begins introducing a semi-empirical tire model, the so-called **Pacejka Model**, used in order to calculate the steady-state forces and moment characteristics in the vehicle dynamics. Based on this model, the description of the self aligning moment has been extracted. This allowed therefore to deduce the formulation of the wheel system. Having the self aligning characteristic a nonlinear behavior, the synthesis of the controller has been more articulate, because of the difficulties of guaranteeing the controllability of a nonlinear function.
At this point of the work, all the components needed in the description of the wheel system were already introduced.
After having introduced the equation of the tire steering dynamics, the simplest controller available in the market, the PI controller, was used. Even though, the PI controller initially seemed sufficient for the wheel system, once the actuator had been applied to the wheel system, some problems emerged. Indeed, the input control values were too high and the nonlinearity of the self aligning moment function obliged us to build different controllers for different values of the self aligning moment itself. Also, the actuator reduces the system phase margin and, to stabilize the system, we have to reduce the system gain. Reducing the gain of the system is not possible when controlling the nonlinear plant. Indeed a high gain is necessary to delete the unstable pole effect.
It was clear at that point, that we needed a more complex controller to not only contain the control input and the noise, but also to satisfy certain specifications. To this purpose, controllers designed with LMI and LPV techniques were introduced to control the system. These types of controller work by correlating the control problem with an optimal problems Therefore, after imposing the control parameters and the input that represent the control specifications, these specifications can be interpreted as decision variables of an optimal problem. The control specifications and limit can be converted into constraints for the optimal problem, too. So, The controller designed with LMI technique for the wheel system was consequently designed. However, this system did not consider the variation of the self aligning characteristic. In order to introduce even this constraint into the controller, it was necessary to linearize the self aligning characteristic, to introduce the LPV synthesis and finally to build the controller designed with LPV technique for the wheel system.
As shown at the end of chapter 4, the controller designed with the LPV technique respects the specifications and limits the control input. Although, information about the wheel, the damping coefficient, the wheel inertia and the actuator limitation were obtained from the

literature, we did not have the opportunity to identify the correct values of these parameters and to solve the real problem concerning the wheel. However this thesis explains how to build a controller with LPV techniques for a theoretical wheel system. Having the real values of the parameters, it would easy to build the correct controller for the real system. Tests in chapter 5 show how the LPV controller tracks the reference with a bounded input control. Another advantage of this controller is the possibility of controlling the system at different values of speeds. This is fundamental especially when analyzing the case of a parking manoeuvre.

Appendix A

Dependence of M_z from the input quantities

Next, we highlight the dependency of M_z on (κ, α, μ and F_z) and every self aligning terms contain in the formula (2.39).

A.1 Self aligning Moment M_z

Slip Ratio κ

In this simulation we want to show as the slip ratio value influences the self aligning moment. The value of α, μ and F_z remain constant, respectively 0°, 1 and 40000 N, and the slip ratio changes between the values -5 to 5.

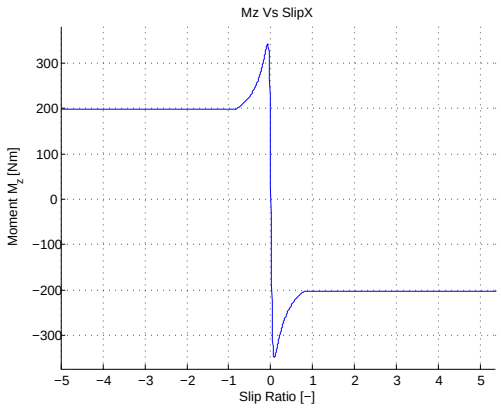

Figure A.1: Self aligning Moment with Slip Ratio

In Figure A.1, we observe that the characteristic of the self aligning moment remain constant for high and low slip ratio value. Instead for value close from -1 to 1, the curve changes very faster from the positive costant value to the negative one.

Slip Angle α

In this simulation we want to show as the slip angle value influences the self aligning moment. The values of κ, μ and F_z remain constant, respectively 0, 1 and 40000 N, and the slip angle changes between the value -20° to 20°.
The result shows in Figure A.2 is the same graphic report in the section 2.3.3.

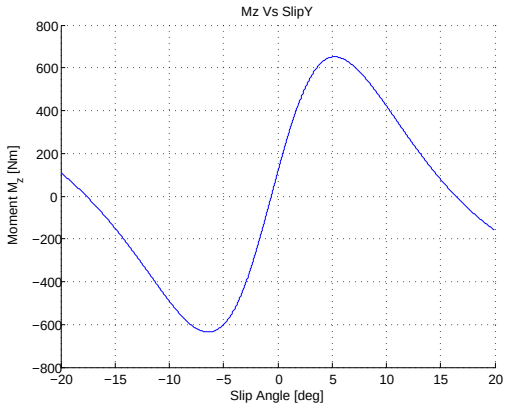

Figure A.2: Self aligning Moment with Slip Angle

Friction Coefficient μ

We want to explain the main relationship between the self aligning moment and the friction coefficient μ, for this reason we test different values of μ, in this case 0.6, 0.7, 0.8 and 0.9. In Figure A.3 on the left, the values of α and F_z remain constant, respectively 0 and 40000 N, while the slip ratio value changes between the value -4 to 4. Indeed, in Figure A.3 on the right, we have also the constant values for κ and F_z, while the slip angle value changes between the value -25° to 25°.

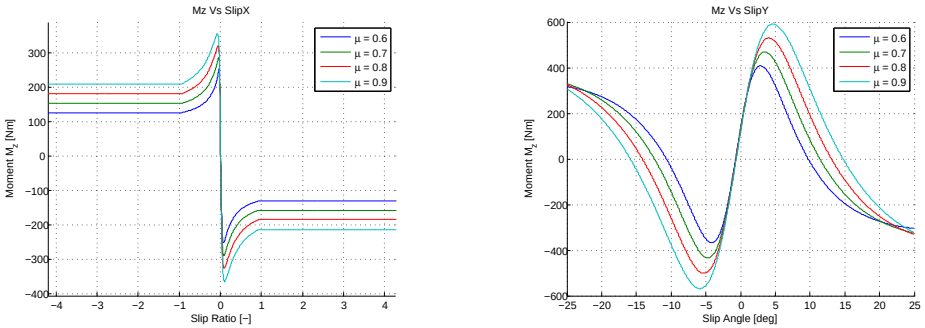

Figure A.3: The influence of parameter μ in the self aligning moment, on the left with different slip ratio value, on the right with different slip angle value.

We note, in Figure A.3, that if the coefficient friction value increases, the self aligning moment characteristic increases and we conclude that the value of the self aligning moment is realted with the coefficient friction value.

Normal Force F_z

We want to explain the main relationship between the self aligning moment and the normal force F_z, for this reason we test different values of F_z, in this case 40000 N, 50000 N, 60000 N, 70000 N and 80000 N.
In Figure A.4 on the left, the values of α and μ remain constant, respectively 0 and 1, while the slip ratio value changes between the value -10 to 10. Indeed, in Figure A.4 on the right, we have also the constant values for κ and μ, while the slip angle value changes between the value -25° to 25°.
In Figure A.4 on the left, we observe that, not only, the peak of self aligning moment decreases when the F_z value increases, but for high values of F_z the characteristic changes sign and become positive.

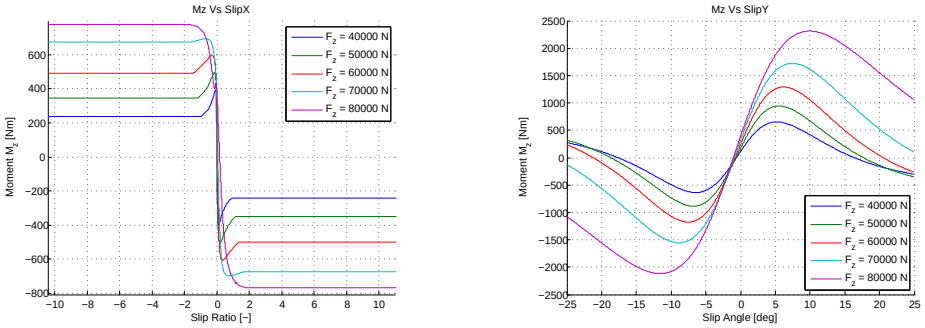

Figure A.4: The influence of parameter F_z in the self aligning moment, on the left with different slip ratio value, on the right with different slip angle value.

In the other graphic of Figure A.4, we observe that if the normal force value increases, the self aligning moment characteristic increases and we can conclude that the value of the self aligning moment is related with the normal force.

Conclusion

Following the aforementioned consideration, we obtain that the self aligning moment M_z depeds from the parameters κ, α, μ and F_z, as suppose in the section 2.3.3.

A.2 Pneumatic Trail t

Slip Ratio κ

In this simulation we want to show as the slip ratio value influences the pneumatic trail term. The values of α, μ and F_z remain constant, respectively 0°, 1 and 40000 N, and the slip ratio changes between the value -1 to 1.

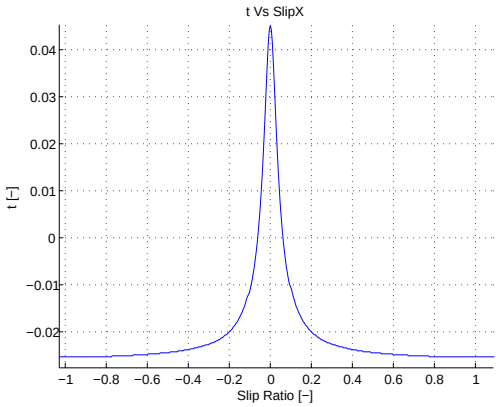

Figure A.5: The Pneumatic Trail with Slip Ratio

We note that the slip ratio value modifies the pneumatic trail characteristic when it is close to the interval [-1, 1]. Around these values the graphic has a positive peak and after these values the characteristic returns negative and it arrives at the asymptotical value.

Slip Angle α

In this simulation we want to show as the slip angle value influences the pneumatic trail term. The values of κ, μ and F_z remain constant, respectively 0, 1 and 40000 N, and the slip angle changes between the value -20° to 20°.

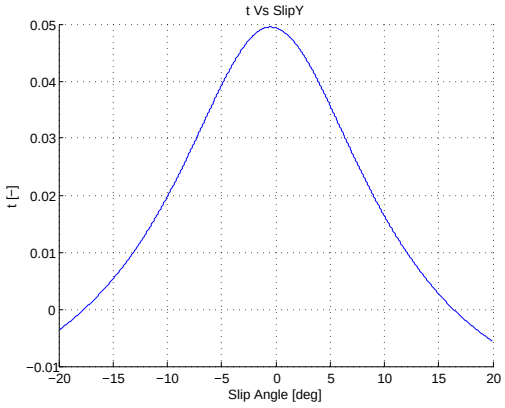

Figure A.6: The Pneumatic Trail with Slip Angle

As show in Figure A.6 the slip angle value influences the pneumatic trail characteristic, we note that the characteristic has the same waveform show for the slip ratio, but in this case the peak increase of the curve is more slow respect the previous case.

Friction Coefficient μ

We want to explain the main relationship between the pneumatic trail term and the friction coefficient μ, for this reason we test different values of μ, in this case 0.6, 0.7, 0.8 and 0.9.

In Figure A.7 on the left, the values of α and F_z remain constant, respectively 0 and 40000 N, while the value slip ratio changes between the value -1.5 to 1.5. Indeed, in Figure A.7 on the right, we have also the constant values for κ and F_z, while the slip angle value changes between the value -25° to 25°.

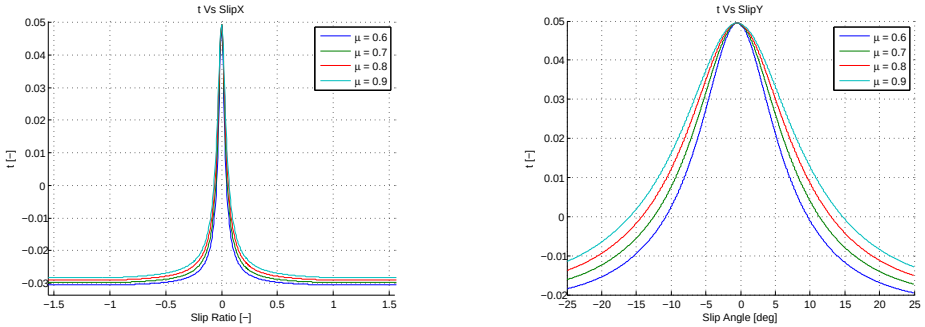

Figure A.7: The influence of parameter μ in the pneumatic trail, on the left with different slip ratio value, on the right with different slip angle value.

In Figure A.7, we note that the pneumatic trail value increases if the friction coefficient value increases. This phenomenon is valid for both the slip angle that the slip value.

Normal Force F_z

We want to explain the main relationship between the pneumatic trail term and the normal force F_z, for this reason we test different values of F_z, in this case 40000 N, 50000 N, 60000 N, 70000 N and 80000 N.
In Figure A.8 on the left, the values of α and μ remain constant, respectively 0 and 1, while the slip ratio value changes between the value -3 to 3. Indeed, in Figure A.8 on the right, we have also the constant values for κ and μ, while the slip angle value changes between the value -25° to 25°.

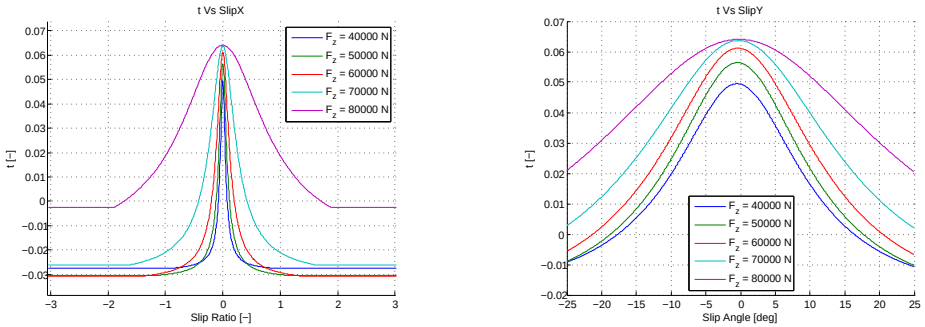

Figure A.8: The influence of parameter F_z in the pneumatic trail, on the left with different slip ratio value, on the right with different slip angle value.

We note, in Figure A.8, that if the normal force value increases, the pneumatic trail characteristic increases and we conclude that the value of the pneumatic trail is realted with the normal force value.

Conclusion

Following the aforementioned consideration, we obtain that the pneumatic trail t depeds from the parameters α and F_z, as suppose in the Section 2.3.3.

A.3 Lateral Force F_y

Slip Ratio κ

In this simulation we want to show as the slip ratio value influences the lateral force. The values of α, μ and F_z remain constant, respectively 0, 1 and 40000 N, and the slip ratio changes between the value -2 to 2. The characteristic of F_y has a very high negative peak

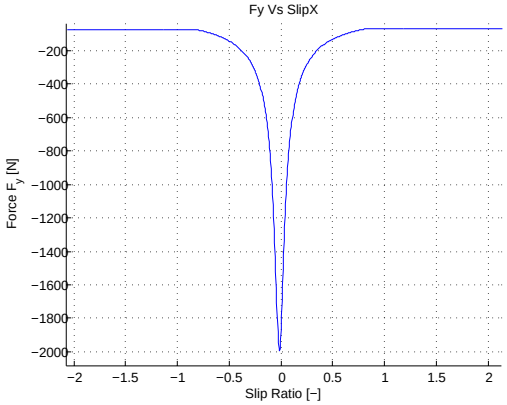

Figure A.9: The Lateral Force with Slip Ratio

close to the value 0, ideed there is a change of value from -100 to -2000. Before and after the peak the curve has an asymptotic value.

Slip Angle α

In this simulation we want to show as the slip angle value influences the lateral force. The values of κ, μ and F_z remain constant, respectively 0, 1 and 40000 N, and the slip angle changes between the value -20° to 20°.

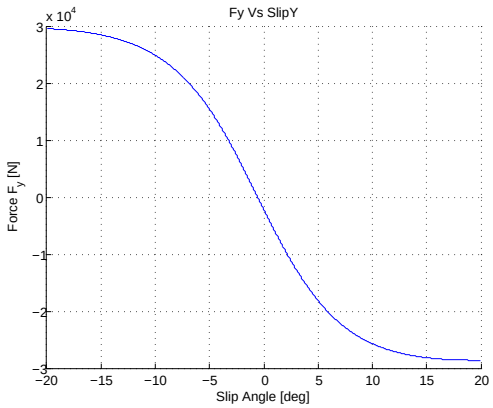

Figure A.10: The Lateral Force with Slip Angle

The F_y characteristic respect the slip angle α assume value elevate for elevate value of slip angle, at $\pm 20°$ arrives at the value of ∓ 30000 N. Instead, for value of slip angle close to zero, the lateral force becomes close to zero. This behavoir is what we expected from the laterl force. Indeed, the lateral force has the maximum value for elevate value of steering, but it becomes irrelevant for the little value of steering, and in consequence of elevate value of slip angle.

Friction Coefficient μ

We want to explain the main relationship between the pneumatic trail term and the friction coefficient μ, for this reason we test different values of μ, in this case 0.6, 0.7, 0.8 and 0.9. In Figure A.11 on the left, the values of α and F_z remain constant, respectively 0 and 40000 N, while the slip ratio value changes between the value -1 to 1. Indeed, in Figure A.11 on the right, we have also the constant value for κ and F_z, while the slip angle value changes between the value -25° to 25°.

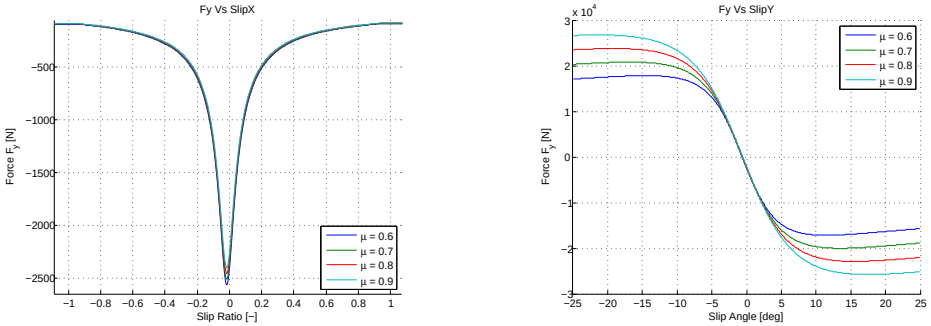

Figure A.11: The influence of parameter μ in the lateral force with different slip angle value.

We note, in Figure A.11 on the right, that if the friction coefficient value increases, the lateral force characteristic increases and we conclude that the value of the lateral force is realted with the friction coefficient value. Instead, in Figure A.11 on the left the value of the peak decreases when the coefficient μ increases.

Normal Force F_z

We want to explain the main relationship between the pneumatic trail term and the normal force F_z, for this reason we test different values of F_z, in this case 40000 N, 50000 N, 60000 N, 70000 N and 80000 N.
In Figure A.12 on the left, the values of α and μ remain constant, respectively 0 and 1, while the slip ratio value changes between the value -3 to 3. Indeed, in Figure A.12 on the right, we have also the constant values for κ and μ, while the slip angle value changes between the value -25° to 25°.
We note, in Figure A.12 on the right, that if the normal force value increases, the lateral

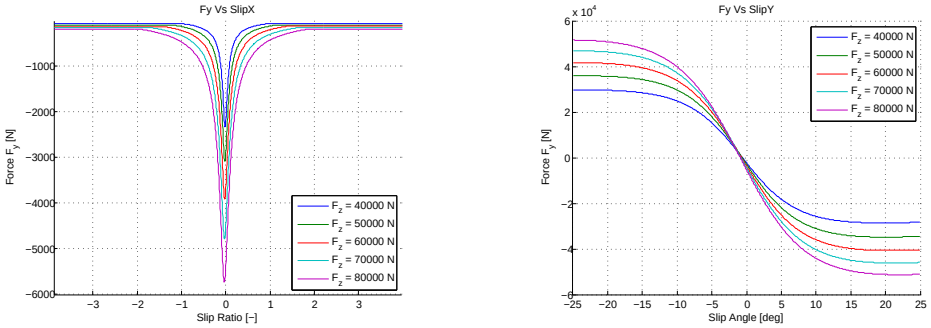

Figure A.12: The influence of parameter F_z in the lateral force with different slip angle value.

force characteristic increases. Also in Figure A.12 on the left the peak of the lateral force

characteristic increases when the normal force increases. We conclude that the value of the lateral force is realted with the normal force value.

Conclusion

Following the aforementioned consideration, we obtain that the lateral force F_y depeds from the parameters κ, α, μ and F_z, as suppose in the Section 2.3.3.

A.4 Arm Force s

Slip Ratio κ

In this simulation we want to show as the slip ratio value influences the force arm term. The values of α, μ and F_z remain constant, respectively 0°, 1 and 40000 N, and the slip ratio changes between the value -5 to 5.

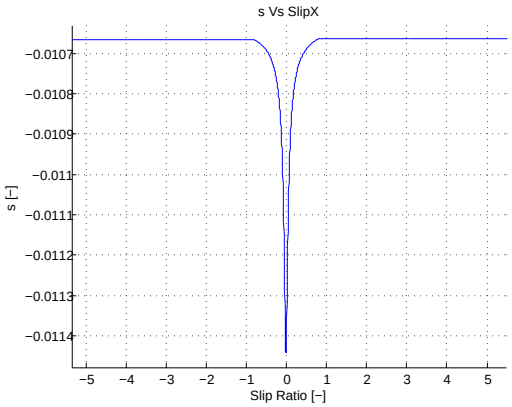

Figure A.13: The Force Arm with Slip Ratio

As show in Figure A.13 the arm force characteristic has a peak in corrispondence of the null slip ratio value and for the remaining values assume an asymptotic value.

Slip Angle α

In this simulation we want to show as the slip angle value influences the force arm term. The values of κ, μ and F_z remain constant, respectively 0, 1 and 40000 N, and the slip angle changes between the value -20° to 20°.

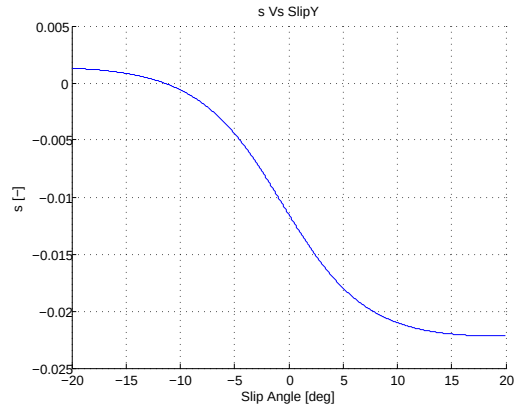

Figure A.14: The Force Arm with Slip Angle

We aspect that the arm force characteristic respects the slip angle will be symmetric and assumes the same value, only with different sign, for positive and negative value of the slip angle, but it is not so. This is due because the arm force definition introduce a shift and this means that the characteristic becomes non symmetric.

Friction Coefficient μ

We want to explain the main relationship between the self aligning moment and the friction coefficient μ, for this reason we test different values of μ, in this case 0.6, 0.7, 0.8 and 0.9.

In Figure A.15 on the left, the values of α and F_z remain constant, respectively 0 and 40000 N, while the slip ratio value changes between the value -1 to 1. Indeed, in Figure A.15 on the right, we have also the constant values for κ and F_z, while the slip angle value changes between the value -25° to 25°.

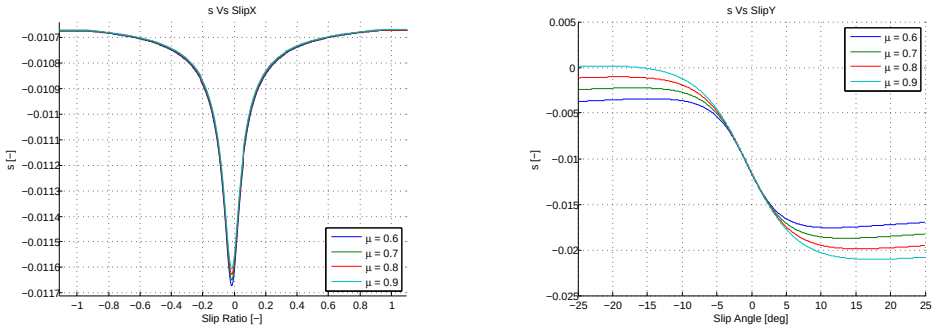

Figure A.15: The influence of parameter μ in the force arm, on the left with different slip ratio value, on the right with different slip angle value.

In Figure A.15 on the left we observe that the different μ values do not influence the arm force term respect the slip ratio, instead with the slip angle modifies the arm force characteristic. In Figure A.15 on the right we observe that the arm force value increases if the friction coefficient increases. After the aforementioned consideration we conclude that the arm force depends on the friction coefficient.

Normal Force F_z

We want to explain the main relationship between the self aligning moment and the normal force F_z, for this reason we test different values of F_z, in this case 40000 N, 50000 N, 60000 N, 70000 N and 80000 N.
In Figure A.16 on the left, the values of α and μ remain constant, respectively 0 and 1, while the slip ratio value changes between the value -2 to 2. Indeed, in Figure A.16 on the right, we have also the constant values for κ and μ, while the slip angle value changes between the value -25° to 25°.

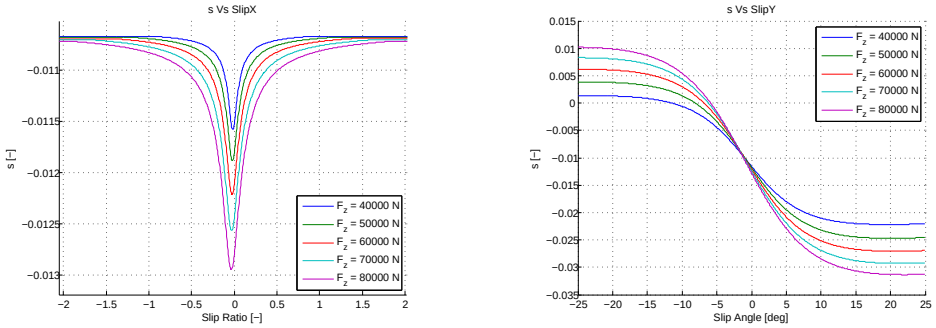

Figure A.16: The influence of parameter F_z in the force arm, on the left with different slip ratio value, on the right with different slip angle value.

In Figure A.16 on the left we observe that the different μ values influence the arm force term respect the slip ratio in a significant way. In Figure A.16 on the right we observe that the arm force value increases if the normal force increases.

Conclusion

Following the aforementioned consideration, we obtain that the arm force s depeds from the parameters F_y and F_z, as suppose in the Section 2.3.3.

A.5 Longitudinal Force F_x

Slip Ratio κ

In this simulation we want to show as the slip ratio value influences the longitudinal force. The values of α, μ and F_z remain constant, respectively 0°, 1 and 40000 N, and the slip ratio changes between the value -2 to 2.

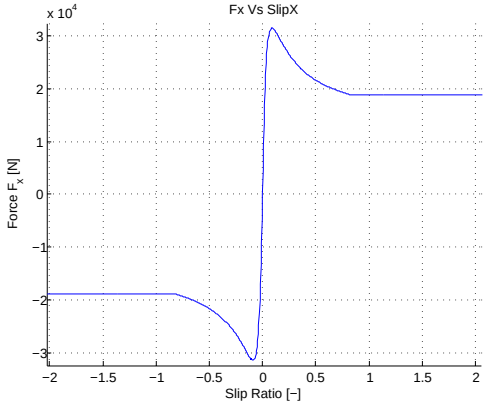

Figure A.17: Change of the Longitudinal Force with Slip Ratio

In Figure A.17 we note as the longitudinal force characteristic changes value when the slip ratio changes sign. It has a overshoot and then return to the asymptotic value.

Slip Angle α

The slip angle value does not influence the longitudinal force.

Friction Coefficient μ

We want to explain the main relationship between the longitudinal force and the friction coefficient μ, for this reason we test different values of μ, in this case 0.6, 0.7, 0.8 and 0.9. In the Figure A.18, the values of α and F_z remain constant, respectively 0 and 40000 N, while the slip ratio value changes between the value -1.5 to 1.5. The slip angle does not influence the longitudinal force. We note, in Figure A.18, that if the friction coefficient

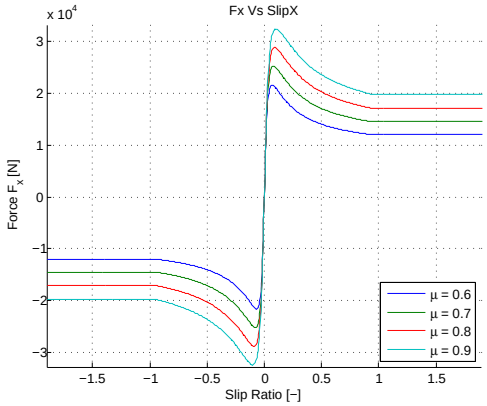

Figure A.18: The influence of parameter μ in the longitudinal force with different slip ratio value.

value increases, the longitudinal force characteristic increases and we conclude that the value of the longitudinal force is realted with the friction coefficient value.

Normal Force F_z

We want to explain the main relationship between the self aligning moment and the normal force F_z, for this reason we test different values of F_z, in this case 40000 N, 50000 N, 60000 N, 70000 N and 80000 N.
In the Figure A.19, the values of α and μ remain constant, respectively 0 and 1, while the slip ratio value changes between the value -10 to 10. The slip angle does not influence the longitudinal force. We note, in Figure A.19, that if the normal force value increases,

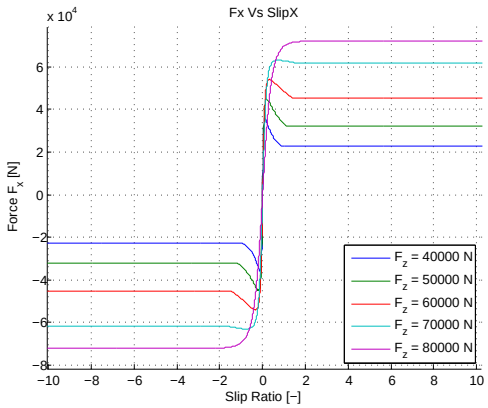

Figure A.19: The influence of parameter F_z in the longitudinal force with different slip ratio value.

the saturation value and the gradient of longitudinal force characteristic increases and we conclude that the value of the lateral force is realted with the normal force value.

Conclusion

Following the aforementioned consideration, we obtain that the longitudinal force F_x depeds from the parameters κ, α, μ and F_z, as suppose in the Section 2.3.3.

A.6 Residual Moment M_{zr}

Slip Ratio κ

In this simulation we want to show as the slip ratio value influences the residual moment. The values of α, μ and F_z remain constant, respectively 0°, 1 and 40000 N, and the slip ratio changes between the value -1 to 1.

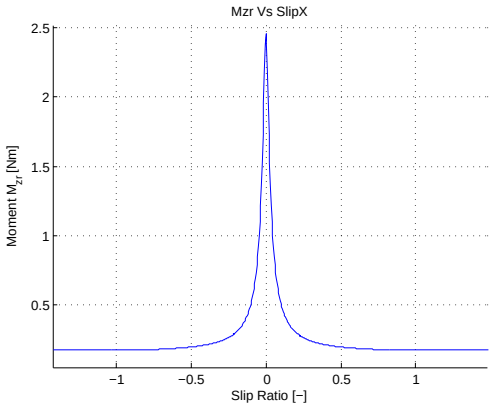

Figure A.20: The Residual Moment with Slip Ratio

We observe that more the the slip ratio value is close to zero, more it is the influence of the residual moment. This is what we aspect from the residual moment, it assumes great value when the slip ratio is zero.

Slip Angle α

In this simulation we want to show as the slip angle value influences the residual moment. The values of κ, μ and F_z remain constant, respectively 0, 1 and 40000 N, and the slip angle changes between the value -20° to 20°.

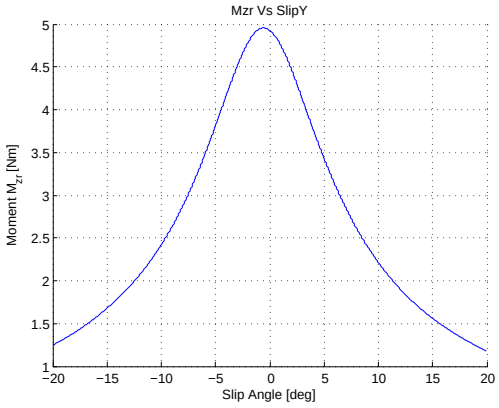

Figure A.21: The Residual Moment with Slip Angle

We observe that more the the slip angle value decreases, more it is the influence of the residual moment. This is what we aspect from the residual moment, it assumes great value when the slip angle is zero.

Friction Coefficient μ

We want to explain the main relationship between the residual moment and the friction coefficient μ, for this reason we test different values of μ, in this case 0.6, 0.7, 0.8 and 0.9.

In Figure A.22 on the left, the values of α and F_z remain constant, respectively 0 and 40000 N, while the slip ratio value changes between the value -0.2 to 0.2. Indeed, in Figure A.22 on the right, the values of κ and F_z remain constant, respectively 0 and 40000 N, while the slip angle value changes between the value -25° to 25°.

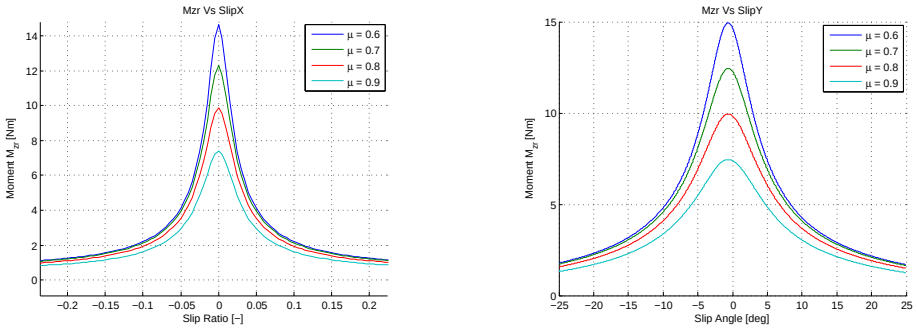

Figure A.22: The influence of parameter μ in the residual moment, on the left with different slip ratio value, on the right with different slip angle value.

We note, in Figure A.22, that if the friction coefficient value increases, the residual moment characteristic decreases and we conclude that the value of the residual moment is realted with the friction coefficient value.

Normal Force F_z

We want to explain the main relationship between the self aligning moment and the normal force F_z, for this reason we test different values of F_z, in this case 40000 N, 50000 N, 60000 N, 70000 N and 80000 N.
In Figure A.23 on the left, the values of α and μ remain constant, respectively 0 and 1, while the slip ratio value changes between the value -25 to 25. Indeed, in Figure A.23 on the right, the values of κ and μ remain constant, respectively 0 and 1, while the slip angle value changes between the value -25° to 25°.

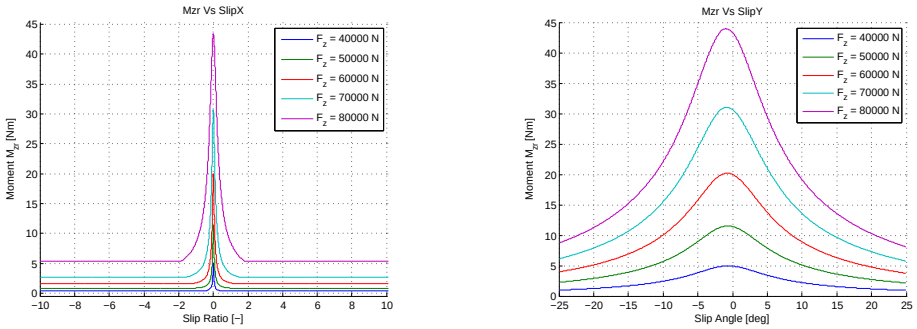

Figure A.23: The influence of parameter F_z in the residual moment, on the left with different slip ratio value, on the right with different slip angle value.

In Figure A.23, we observe that the peak of residual moment increases when the normal force F_z value increases. This behavior is what we aspect from the characteristic of the residual moment M_{zr}, it assumes the maximum value in corrispondence of null value of slip ratio but, above all, slip angle.

Conclusion

Following the aforementioned consideration, we obtain that the residual moment M_{zr} depeds from the parameters κ, α, μ and F_z, as suppose in the Section 2.3.3.

Appendix B

Formulas of Velocity

In this section is shown how the ζ coefficients are introduced in the self aligning moment equation.

$$\varphi = -\frac{1}{V_x}(\dot{\psi} - (1 - \epsilon_\gamma)\Omega \sin\gamma) \tag{B.1}$$

where:

- V_x is the longitudinal velocity;
- $\dot{\psi}$ is the yaw angle;
- ϵ_γ is the reduction coefficient for γ;
- Ω is the rotation velocity of the wheel;
- γ is the camber angle.

We introduce the equations for the ζ coefficient.

$$\zeta_1 = cos[arctan(B_{x\varphi}R_0\varphi)] \tag{B.2}$$

$$B_{x\varphi} = p_{Dx\varphi1}(1 + p_{Dx\varphi2}df_z)\cos[\arctan(p_{Dx\varphi3}\kappa)] \tag{B.3}$$

where $p_{Dx\varphi1}$, $p_{Dx\varphi2}$ and $p_{Dx\varphi3}$ are constant.

$$\zeta_2 = \cos[\arctan\{B_{y\varphi}(R_0|\varphi| + p_{Dy\varphi4}\sqrt{R_0|\varphi|})\}] \tag{B.4}$$

where $B_{y\varphi}$ is the sharpness factor:

$$B_{y\varphi} = p_{Dy\varphi1}(1 + p_{Dy\varphi2}df_z)\cos[\arctan(p_{Dy\varphi3}tan\alpha)] \tag{B.5}$$

The terms $p_{Dy\varphi1}$, $p_{Dy\varphi2}$, $p_{Dy\varphi3}$ and $p_{Dy\varphi4}$ are constant.

$$\zeta_3 = \cos[\arctan(p_{Ky\varphi1}R_0^2\varphi^2)] \tag{B.6}$$

where $p_{Ky\varphi1}$ is a constant.

$$\zeta_4 = 1 + S_{Hy\varphi} - \frac{S_{Vy\gamma}}{K_{y\alpha}} \tag{B.7}$$

where:

$$S_{Hy\varphi} = D_{Hy\varphi} sin[C_{Hy\varphi} \arctan\{B_{Hy\varphi} R_0\varphi - E_{Hy\varphi}(B_{Hy\varphi} R_0\varphi - \arctan(B_{Hy\varphi} R_0\varphi))\}] sgn(V_x) \tag{B.8}$$

where:

$$D_{Hy\varphi} = (p_{Hy\varphi 2} + p_{Hy\varphi 3} df_z) sgn(V_x) \tag{B.9}$$

$$C_{Hy\varphi} = p_{Hy\varphi 1} \qquad (> 0) \tag{B.10}$$

$$E_{Hy\varphi} = p_{Hy\varphi 4} \qquad (\leq 1) \tag{B.11}$$

where $p_{Hy\varphi 1}$, $p_{Hy\varphi 2}$, $p_{Hy\varphi 3}$ and $p_{Hy\varphi 4}$ are a constant.

$$B_{Hy\varphi} = \frac{K_{yR_\varphi 0}}{(C_{Hy\varphi} D_{Hy\varphi} K_{y\alpha o})} \tag{B.12}$$

$$S_{Vy\gamma} = F_z(p_{Vy3} + p_{Vy4} df_z)\gamma\zeta_2 \lambda_{Ky\gamma} \lambda'_{\mu y} \tag{B.13}$$

where p_{Vy3} and p_{Vy4} are constant.

$$K_{yR_\varphi 0} = K_{y\gamma 0} = F_z(p_{Ky6} + p_{Ky7} df_z)\lambda_{Ky\gamma} \tag{B.14}$$

where p_{Ky6} and p_{Ky7} are constant.

$$K_{y\alpha} = p_{Ky1} F'_{z0}(1 - p_{Ky3}|\gamma|) sin[p_{Ky4} \arctan\{\frac{\frac{F_z}{F'_{z0}}}{p_{Ky2} + p_{Ky5}\gamma^2}\}] \tag{B.15}$$

where p_{Ky1}, p_{Ky2}, p_{Ky3}, p_{Ky4} and p_{Ky5} are constant.

$$\zeta_5 = \cos[\arctan(q_{Dt\varphi 1} R_0\varphi)] \tag{B.16}$$

where $q_{Dt\varphi 1}$ is a constant.

$$\zeta_6 = \cos[\arctan(q_{Br\varphi 1} R_0\varphi)] \tag{B.17}$$

where $q_{Br\varphi 1}$ is a constant.

$$M_{z\varphi 90} = M_{z\varphi\infty} \frac{2}{\pi} \arctan(q_{Cr\varphi 2} R_0|\varphi|) \tag{B.18}$$

where $q_{Cr\varphi 2}$ is a constant.

$$\zeta_7 = \frac{2}{\pi} arc\cos[M_{z\varphi 90}/|D_{r\varphi}|] \tag{B.19}$$

$$\zeta_8 = 1 + D_{r\varphi} \tag{B.20}$$

where:

$$D_{r\varphi} = D_{Dr\varphi} \sin[C_{Dr\varphi} \arctan\{B_{Dr\varphi} R_0\varphi - E_{Dr\varphi}(B_{Dr\varphi} R_0\varphi - \arctan(B_{Dr\varphi} R_0\varphi))\}] \tag{B.21}$$

$$D_{Dr\varphi} = \frac{M_{z\varphi\infty}}{sin(0.5\pi C_{Dr\varphi})} \tag{B.22}$$

$$M_{z\varphi\infty} = q_{Cr\varphi1}\mu R_0 F_z \sqrt{\frac{F_z}{F'_{z0}}}\lambda_{M\varphi} \tag{B.23}$$

where $q_{Cr\varphi1}$ is a constant.

$$C_{Dr\varphi} = q_{Dr\varphi1} \tag{B.24}$$

where $q_{Dr\varphi1}$ is a constant.

$$E_{Dr\varphi} = q_{Dr\varphi2} \tag{B.25}$$

where $q_{Dr\varphi2}$ is a constant.

$$B_{Dr\varphi} = \frac{K_{z\gamma r0}}{\{C_{Dr\varphi}D_{Dr\varphi}\}} \tag{B.26}$$

$$K_{z\gamma r0} = F_z R_0\{q_{Dz8} + q_{Dz9}df_z + (q_{Dz10} + q_{Dz11}df_z)|\gamma|\}\lambda_{Kz\gamma} \tag{B.27}$$

where q_{Dz8}, q_{Dz9}, q_{Dz10} and q_{Dz11} are constant.

$$K_{z\gamma0} = K_{z\gamma r0} - D_{t0}K_{y\gamma0} \tag{B.28}$$

$$K_{zR\varphi0} = K_{z\gamma0} = F_z(p_{Ky6} + p_{Ky7}df_z) \tag{B.29}$$

where p_{Ky6} and p_{Ky7} are constant.

Appendix C

Derive the Pacejka Formula

The procedure to derivate the self aligning moment express in equation (2.39) is introduced. The formula is described as follow:

$$M_z(\kappa,\alpha,\mu,F_z) = -t(\kappa,\alpha,F_z)\ F_y(\kappa,\alpha,\mu,F_z) + s(F_y,F_z)\ F_x(\kappa,\alpha,\mu,F_z) + M_{zr}(\kappa,\alpha,\mu,F_z) \tag{C.1}$$

Starting with this formula is derived the equation respect the slip angle α. It is obtained the following result:

$$\frac{\partial M_z(\kappa,\alpha,\mu,F_z)}{\partial\alpha} = \frac{\partial[-t(\kappa,\alpha,F_z)\ F_y(\kappa,\alpha,\mu,F_z)]}{\partial\alpha} + \frac{\partial[s(F_y,F_z)\ F_x(\kappa,\alpha,\mu,F_z)]}{\partial\alpha} + \frac{\partial M_{zr}(\kappa,\alpha,\mu,F_z)}{\partial\alpha} \tag{C.2}$$

For simplicity the derivate of each term is calculated and after the final formula will be derived. Starting with the term $-tF_y$.

$$\frac{\partial[-t(\kappa,\alpha,F_z)\ F_y(\kappa,\alpha,\mu,F_z)]}{\partial\alpha} = \frac{\partial[-t(\kappa,\alpha,F_z)]}{\partial\alpha}F_y(\kappa,\alpha,\mu,F_z) - t\frac{\partial F_y(\kappa,\alpha,\mu,F_z)}{\partial\alpha} \tag{C.3}$$

At this point there are two different derivate in the formula (C.3), the derivation of $\frac{\partial -t}{\partial\alpha}$ is:

$$\begin{aligned}\frac{\partial[-t(\kappa,\alpha,F_z)]}{\partial\alpha} &= \frac{\partial}{\partial\alpha}\left[D_t\ \cos[C_t\ \arctan\{B_t\alpha_t - E_t(B_t\alpha_t - \arctan(B_t\alpha_t))\}]\right] \\ &= \frac{C_tD_t(E_t(B_t - \frac{B_t}{(B_t\alpha)^2+1}) - B_t)\cos(\alpha)\sin(C_t arctan(E_t(B_t\alpha - \arctan(B_t\alpha) - B_t\alpha)))}{(E_t(B_t\alpha - \arctan(B_t\alpha)) - B_t\alpha)^2 + 1} \\ &+ D_t\sin(\alpha)\cos(C_t\arctan(E_t(B_t\alpha - \arctan(B_t\alpha)) - B_t\alpha))\end{aligned} \tag{C.4}$$

Instead, the derivation of $\frac{\partial F_y}{\partial\alpha}$ is

$$\frac{\partial F_y(\kappa,\alpha,F_z)}{\partial\alpha} = \frac{\partial G_{y\kappa}}{\partial\alpha}F_y^{'} + \frac{\partial F_y^{'}}{\partial\alpha}G_{y\kappa} \tag{C.5}$$

Where the $\frac{\partial G_{y\kappa}}{\partial\alpha}$ is equal to zero, instead the $\frac{\partial F_y^{'}}{\partial\alpha}$ is equal to:

$$\frac{\partial F_y^{'}}{\partial\alpha} = \frac{C_yD_y(E_y(B_y - \frac{B_t}{(B_t\alpha)^2+1}) - B_y)\cos(C_y\arctan(E_y(B_y\alpha - \arctan(B_y\alpha)) - B_y\alpha))}{(E_y(B_y\alpha - \arctan(B_y\alpha)) - B_y\alpha)^2 + 1} \tag{C.6}$$

The second term of equation (C.2) has the following derivate:

$$\frac{\partial[s(F_y,F_z)\ F_x(\kappa,\alpha,\mu,F_z)]}{\partial\alpha} = \frac{\partial s(F_y,F_z)}{\partial\alpha}F_x(\kappa,\alpha,\mu,F_z) + \frac{\partial F_x(\kappa,\alpha,\mu,F_z)}{\partial\alpha}s(F_y,F_z) \quad \text{(C.7)}$$

but the term s does not depend on α so its derivate is zero, we have only to calculate the derivate of $\frac{\partial F_x(\kappa,\alpha,\mu,F_z)}{\partial\alpha}$:

$$\frac{\partial F_x(\kappa,\alpha,\mu,F_z)}{\partial\alpha} = \frac{\partial G_{x\alpha}}{\partial\alpha}F_x^{'} + \frac{\partial F_x^{'}}{\partial\alpha}G_{x\alpha} \quad \text{(C.8)}$$

where the $\frac{\partial F_x^{'}}{\partial\alpha}$ is equal to zero because the $F_x^{'}$ does not depend on α, so the derivate of the other term is:

$$\frac{\partial G_{x\alpha}}{\partial\alpha} = \frac{C_x(E_x(B_x - \frac{B_x}{(B_x\alpha)^2+a}) - B_x)\sin(C_x\arctan(E_x(B_x\alpha - \arctan(B_x\alpha)) - B_x\alpha))}{G_{ax0}((E_x(B_x\alpha - \arctan(B_x\alpha)) - B_x\alpha)^2 + 1)} \quad \text{(C.9)}$$

Te last term in the equation (C.2) is the residual moment derivate that it is calculated as follow:

$$\begin{aligned}\frac{\partial M_{zr}(\kappa,\alpha,\mu,F_z)}{\partial\alpha} &= \frac{\partial}{\partial\alpha}\left\{D_r\left[\arctan(B_r\alpha_r)\right]\right\} \\ &= -\frac{B_rC_rD_r\sin(C_r\arctan(B_r\alpha))}{(B_r\alpha)^2+1}\end{aligned} \quad \text{(C.10)}$$

Using the result found in the equation (C.4), (C.5), (C.6), (C.8), (C.9), and (C.10) the derivate of the self aligning moment M_z is obtained.

Appendix D

Background and Preliminaries of LMI Theory

D.1 Background and Preliminaries

The most important property, that the LMI problem uses, is the convexity. A normal constrain for the LMI is in the form:

$$F(x) := F_0 + x_1F_1 + \cdots + x_nF_n \prec 0 \tag{D.1}$$

where F_0, F_1, ..., F_n are real simmetric matrix and x = $[x_1, \cdots, x_n]$ is a column vector of unknown real scalar decision variables. The inequality $F(x) \prec 0$ means that the decision variable must render the symmetric matrix F(x) negative definite, so the maximum eigenvalue of F(x) should be negative. The equation (D.1) introduces two questions:

1. The LMI feasibility is guaranteed, if there are real variables $x_1, \cdots, x_n$ that satisfy the equation (D.1), then the LMI is feasibility;

2. The LMI optimization problem consists of the cost minimization of the cost function c(x) = $c_1x_1 + \cdots + c_nx_n$ for every $x_1, \cdots, x_n$ that satisfy the constraint (D.1).

This formulation is easy to find in the classical linear problem optimization, but also in the quadratic and convex quadratic problems of optimization.
Normally, the matrix variable in the control application are used instead of the vector variables. So, the LMI problem can be redefined in the more general form

$$F(X) \prec 0 \tag{D.2}$$

where X is a matrix defined in an arbitrary finite-dimension vector space χ of matrix and F: $\chi \rightarrow S^m$ is an affine function.
The different type of constrains becomes important in the pratical studying of the special form as in (D.1). There are different type of constrains, the first one is define the (D.1) as a convex constrain on the decisione variable. So the solution set S = $\{x \mid F(x) \prec 0\}$ of the LMI $F(x) \prec 0$ is convex. In this case the convex constrain $F(x) \prec 0$ on x has more useful property than the general convex sets. The second type of constrain is define for a finite set of LMIs

$$F_1(x) \prec 0, \cdots, F_n(x) \prec 0$$

and it is can also be represented as a single LMI $F(x) \prec 0$ by setting F(x) = diag$(F_1(x), \cdots, F_n(x))$.
There are different types of constrains used to find a solution for the equation (D.1), but

the most important constrain, is the partitioned LMI

$$F(x) = \begin{bmatrix} F_{11}(x) & F_{12}(x) \\ F_{21}(x) & F_{22}(x) \end{bmatrix} \prec 0$$

where the *Schur complements* is used to obtain the two expresion:

$$\begin{cases} F_{11}(x) \prec 0 \\ S_{22}(x) = F_{22}(x) - F_{21}(x)F_{11}(x)^{-1}F_{12}(x) \prec 0 \end{cases}$$

where $S_{22}(x)$ is the Schur complement of $F_{11}(x)$ and the equivalent one:

$$\begin{cases} F_{22}(x) \prec 0 \\ S_{11}(x) = F_{11}(x) - F_{12}(x)F_{22}(x)^{-1}F_{21}(x) \prec 0 \end{cases}$$

where $S_{11}(x)$ is the Schur complement of $F_{22}(x)$. If $F(x)$ is affine this equivalence, a specification types of rational inequalities and quadratic can be formulated as (D.1). The previous equation is due to a congruent transfomation of symmetric matrices that it leaves unchanged the number of the positive and negative eigenvalues.

D.1.1 LMI Stability

At the end of the 19^{th} century there was the beginning of study of the expansion and contraction motion property of dynamical system around an attractor point. The pioneer of this theory was Alksandr Mikhailovich Lyapunow and his studies become important for the control analysis. He found a function, called *Lyapunow Function*, that you can used to prove the stability equilibria of differential equations. This function used the idea that an invariant set of a differential equation attracts all nearby solutions and if you can find a function that is bounded and decreases along all solutions.
The differential equation, that it is supposed to be used, is:

$$\dot{x}(t) = f(x(t), t) \tag{D.3}$$

where $f : X \times \mathbb{R} \to X$ and $X = \mathbb{R}^n$ is a finite dimensional state space. The function f must be defined sufficiently smooth in order to guarantee the existence and uniqueness of the solution $x(x_0, t)$ that satisfy the initial condition $x(x_0, t_0) = x_0 \in X$, where the relation $x(0) = x_0$ is valid. The *time invariant* of the differential equation (D.3) is defined as

$$x(x_0, t_0 + \tau) = x(x_0, t_0)$$

for any $\tau \in \mathbb{R}$ and $t + \tau$ interval of existance. The equilibrium point $x^* \in X$ is defined as follow $x(x^*, t_0) = x^*$ and also satisfies the equation (D.3).
If the equilibrium point x^* exists, the equation (D.1) is called exponentially stable for all $t_0 \in \mathbb{R}$ and exist a positive numbers α, β and δ exist such that

$$\|x_0 - x^*\| \leq \delta \Rightarrow \|x(x_0, t_0) - x^*\| \leq \beta \|x_0 - x^*\| e^{-\alpha(t-t_0)} \qquad \forall t \geq t_0 \tag{D.4}$$

If the positive numbers α, β and δ do not depend on the initial time t_0, then we can say that x^* is uniformly exponentially stable. The equation (D.4) is called globally exponentially stable if δ can be choose in an arbitrary way. With this definition we can say that a fixed point is exponentially stable if every solution of the differential equation, with initial state

nearby x^*, converge to x^* with an exponential rate $\alpha > 0$.
The following results show how the exponential stability of linear time-invariant differential equations are related to the LMI feasibility. Let $A \in \mathbb{R}^{n\times n}$, the following statements are equivalent:

1. The origin is an exponentially stable equlibrium point of $\dot{x} = Ax$;
2. All eigenvalues $\lambda(A)$ belong to $\mathbb{C} := \{s \in \mathbb{C} \mid \Re(s) < 0\}$;
3. The LMIs $A^T X + XA \prec 0$ and $X \prec 0$ are feasible.

The 3^{rd} statement means that the solution X defines a quadratic function $V(x) = X^T Xx$ that solve a Lyapunow function of the differential equation $\dot{x} = Ax$ for the equilibrium point x^*. The derivative of the quadratic function $V(x)$ has a direction of decreasing as follow:

$$\frac{d}{dt}x(t)^T Xx(t) = \dot{x}(t)^T Xx(t) + x(t)^T X\dot{x}(t) = x(t)^T[A^T X + XA]x(t) \tag{D.5}$$

Recalling the previously considerations and using the formula (D.4), we can choose δ arbitrarily, $\beta = \sqrt{\lambda_{max}(X)/\lambda_{min}(X)}$ and $\alpha > 0$ has to satisfy the inequality $A^T X + XA + 2\alpha X \prec 0$. This consideration is important because in many control problem the interest is focused on the characterization of the eigenvalue location of A in a particular stability region of $\mathbb{C}$.

D.2 Introduction to LMI and Setting the LMI Controller

D.2.1 Performance Characterizations with LMI

The linear system considered in the LMI synthesis is:

$$\dot{x} = Ax + Hw, \qquad z = Cx + Ew, \qquad x(0) = 0 \tag{D.6}$$

where w is the undesired external disturbance and z is the error output. The control synthesis problem can be translated in a problem of reduction of the disturbance attenuation: the controller has the aim to decrease the disturbance w into the output error z as much as possible in the transfer function of the system given by

$$T(s) = C(sI - A)^{-1}H + E.$$

Using the equation (D.6), where A is Hurwitz and $E = 0$, and supposing that the number of the inputs is m, so H is the colum vector $(h_1, \cdots, h_m)$. The energy of the output trajectory for impusive inputs in all input components is:

$$\sum_{\nu=1}^{m} \int_0^\infty y_\nu(t)^T y_\nu(t)\, dt = \sum_{\nu=1}^{m} \text{Trace}(h_\nu^T Y_0 h_\nu) = \text{Trace}(H^T Y_0 H) \tag{D.7}$$

where Trace denotes the sum of the diagonal elements of a matrix and Y_0 is the observability Gramain, the unique solution of the Lyapunow equation:

$$A^T Y_0 + Y_0 A + C^T C = 0 \tag{D.8}$$

Using the Parseval's theorem we can explicit the formula of the observability Gramian (D.7) and we obtain the expression for the energy:

$$\|T\|_{\mathcal{H}_2}^2 = \frac{1}{2\pi} Trace \left\{ \int_{-\infty}^{\infty} [C(i\omega I - A)^{-1}H][C(i\omega I - A)^{-1}H]\, d\omega \right\}. \tag{D.9}$$

The $\|T\|^2_{\mathcal{H}_2}$ is called $\mathcal{H}_2$-norm on the transfer function T(s). We derive the impulse responce performance interpretation of the $\mathcal{H}_2$-norm.
The result is a stochastic interpretation of the $\mathcal{H}_2$-norm perform. If n is the noise with unity covariance, the asymptotic variance od the output process of (D.6) has to satisfy the following equation:

$$\lim_{t\to\infty} E[y(t)^T y(t)] = \text{Trace}\left(\lim_{n\to\infty} CE[x(t)x(t)^T]C^T\right) = \text{Trace}(CX_0C^T) \tag{D.10}$$

where X_0 is the controllability Gramian that it is obtain as the unique solution of the equation:

$$AX_0 + X_0A^T + HH^T = 0 \tag{D.11}$$

The transpose of the transfer function of the system (D.6) is defined as: $T^T(s) = H^T(sI - A^T)^{-1}C^T$. This means that the asymptotic output variance is equal to $\|T^T\|_{\mathcal{H}_2}$. This variance is the same used in the formula (D.9) and it is a dual version for computing the $\|T\|_{\mathcal{H}_2}$. The result found up to here are: If $E = 0$ and X_0 and Y_0 are the system's controllability and observability Gramains satisying the equations (D.8) and (D.11), then the solution is defined as follows: $\|T\|^2_{\mathcal{H}_2} = \text{Trace}(CX_0C^T) = \text{Trace}(H^TY_0H)$. This solution means that the sum of the energies of the output of the system (D.6) for the impulsive inputs in each input channel is limitated, if the input is a white noise with unity covariance, the solution is also equal to the asymptotic output variance of the system. Normally this solution is called $\mathcal{H}_2$ Performance. It is possible to introduce the following theorem:

Theorem 1: A is Hurwitz and $\|T\|_{\mathcal{H}_2} < \gamma$ if and only if $E = 0$ and exist X $= X^T$ and Y $= Y^T$ such that

$$\begin{pmatrix} A^TX + XA & XH \\ H^TX & -\gamma I \end{pmatrix} \prec 0, \qquad \begin{pmatrix} X & C^T \\ C & Y \end{pmatrix} \succ 0 \qquad \text{and} \qquad \text{Trace}(Y) < \gamma. \tag{D.12}$$

□

There is also another way to characterize the effect of the disturbance w on the output error z in the system (D.6). This approach expresses the energy in terms of the so-called energy gain and it is due by the formula:

$$\|T\|_{\mathcal{H}_\infty} = \sup_{0<\|w\|_{\mathcal{L}_2}<\infty} \frac{\|z\|_{\mathcal{L}_2}}{\|w\|_{\mathcal{L}_2}} \tag{D.13}$$

where $\|z\|_{\mathcal{L}_2}$ and $\|w\|_{\mathcal{L}_2}$ are respectly the finite eneregy of the error z and the disturbance d, defined as $\|x(t)\|_{\mathcal{L}_2} = \sqrt{\int_0^\infty \|x(t)\|^2\, dt}$. Equivalently, if Trace(Y) $< \gamma$ is replaced with Y $< \gamma$ in the **Theorem 1** the LMI formulation means that the system gain from finite energy input signals to the peak value of the output signal is bounded by γ:

$$\sup_{0<\|w\|_{\mathcal{L}_2}<\infty} \frac{\|z\|_{\mathcal{L}_\infty}}{\|w\|_{\mathcal{L}_2}} < \gamma \quad \text{with} \quad \|z\|_{\mathcal{L}_\infty} = \sup_{t\geq 0}\|z(t)\| \tag{D.14}$$

The equation (D.13) shows how the worst amplification of the disturbance input limits the output error and this means that the upper bound of a LMI characterization is $\|T\|_{\mathcal{H}_\infty} < \gamma$. As the previous solution, normally we call this $\mathcal{H}_\infty$ solution the $\mathcal{H}_\infty$ Performance. As shown for the $\mathcal{H}_\infty$, there is a similar theorem for the $\mathcal{H}_2$ also:

Theorem 2: A is Hurwitz and $\|T\|_{\mathcal{H}_\infty} < \gamma$ if and only if there exists $X \succ 0$ with

$$\begin{pmatrix} I & 0 \\ A & H \end{pmatrix}^T \begin{pmatrix} 0 & X \\ X & 0 \end{pmatrix} \begin{pmatrix} I & 0 \\ A & H \end{pmatrix} + \begin{pmatrix} 0 & I \\ C & E \end{pmatrix}^T \begin{pmatrix} -\gamma^2 I & 0 \\ 0 & I \end{pmatrix} \begin{pmatrix} 0 & I \\ C & E \end{pmatrix} \prec 0 \tag{D.15}$$

□

In the literature the LMI equation (D.15) is written in an equivalent and more common representation:

$$\begin{pmatrix} A^TX + XA + C^TC & XH + C^TE \\ H^TX + E^TC & E^TE - \gamma^2 I \end{pmatrix} \prec 0 \quad \text{or with Schur} \quad \begin{pmatrix} A^TX + XA & XH & C^T \\ H^TX & -\gamma I & E^T \\ C & E & -\gamma I \end{pmatrix} \prec 0 \tag{D.16}$$

Or equvalently using the Riccati inequalities $A^TX + XA + C^TC + (XH + C^TE)(\gamma^2 I - E^TE)^{-1}(H^TX + E^TC) \prec 0$ and $E^TE - \gamma^2 I \prec 0$.

D.2.2 Introduction to the Optimal Synthesis

After the introduction of the principal aspect about the $\mathcal{H}_2$ and $\mathcal{H}_\infty$ performance, the LMI system is introduced in Figure D.1.

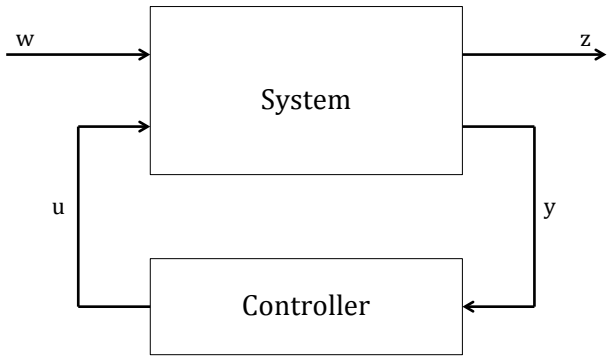

Figure D.1: General plant configuration for an LMI problem.

The system configuation permits to set different specifications, such as stability, error minimization and robust performance, and to find the more suitable controller to solve the problem. The equations of the LMI system are:

$$\begin{aligned} \dot{x} &= Ax + Bu + Hw \\ z &= Cx + Du + Ew \\ y &= Fx + Gw \end{aligned} \tag{D.17}$$

where z is the error, w is the disturbance, u is the control input and y is the measured output. Instead, the controller equations in the feedback synthesis are:

$$\begin{aligned} \dot{x}_c &= A_c x_c + B_c y \\ u &= C_c x_c + D_c y \end{aligned} \tag{D.18}$$

where y is the measured output of the LMI system and u is the input controller that controls the LMI system. As shown in Figure D.1, the interconnection of the LMI system (D.17) and the LMI controller (D.18) has to be internally stable and to satisfy the desidered performance. A new state system $\xi = [x, x_c]^T$ is created and the controlled system is simply

decribed by the equation:

$$\begin{aligned} \dot{\xi} &= \mathcal{A}\xi + \mathcal{B}w \\ z &= \mathcal{C}\xi + \mathcal{D}w \\ \text{with } \left(\begin{array}{c|c} \mathcal{A} & \mathcal{B} \\ \hline \mathcal{C} & \mathcal{D} \end{array}\right) &= \left(\begin{array}{cc|c} A + BD_cF & BC_c & H + BD_cG \\ B_cF & A_c & B_cG \\ \hline C + DD_cF & DC_c & E + DD_cG \end{array}\right) \end{aligned} \tag{D.19}$$

The equation (D.19) is really simple but inside this formulation is comprises many different specification configurations are included in this formulation and in this case it is necessary to build a controller with the reference tracking problem. A major emphasis is laid on shaping the sensitivity (reference to tracking error), under the constraint that the control effort (reference to control) does not peak too much and rolls off at high frequencies and we also guarentee the disturbance attenuation. In this section we try to build up a controller with the $\mathcal{H}_\infty$ performance.

D.2.3 State Feedback Synthesis

There are two different types of synthesis use to build up the controller: state feedback and output feedback. In the wheel system only the simplest one is needed the state feedback. In this technique of synthesis the equation of control (D.18) becomes:

$$\begin{aligned} \dot{x}_c &= A_c x_c + B_c x \\ u &= D_c x \end{aligned} \tag{D.20}$$

where the matrix C_c is equal to zero and the output y is equal to the state ($y = x$) of the LMI system (D.17). If the equation (D.20) is substituted in the LMI system (D.17) the following equation of control is obtained:

$$\begin{aligned} \dot{x} &= (A + BD_c)x + Hw \\ z &= (C + DD_c)x + Ew \end{aligned} \tag{D.21}$$

Using the **Theorem 2** and with the LMI synthesis expressed in (D.16) the controller that stabilizes the state feedback system (D.21) can be found. It renders the $\mathcal{H}_\infty$-norm of the transfer matrix $w \to z$ smaller than γ if and only if there are some X with

$$X \succ 0 \quad \text{and} \quad \begin{pmatrix} (A + BD_c)^T X + X(A + BD_c) & XH & (C + DD_c)^T \\ H^T X & -\gamma I & E^T \\ (C + DD_c) & E & -\gamma I \end{pmatrix} \prec 0 \tag{D.22}$$

where the first inequality guarantees stability and the second captures performance. The performance inequality is called bilinear matrix inequality problem. Normally this structure is required for some variety of design control problem, but in the LMI synthesis needs a convex bilinear inequelity. Exist a simple remedy to commute a normal bilinear problem in a convex one. The nonconvex bilinear matrix is turned, with a simple procedure, into a convex problem of LMI. This is realized by appling a nonlinear change of variables $(X, D_c) \to (Y, M)$ and a congruence transformation of (D.22). The new variables are defined:

$$Y := X^{-1} \quad \text{and} \quad M := D_c X^{-1} \tag{D.23}$$

So, the (D.22) is trasformed with a congruence transformation respectly X^{-1} for the left expression and a moltiplication for the diagonal matrix $\text{diag}(X^{-1}, I, I)$ for the right expression. After this transformation the variables, defined in (D.23), are substituted in the equation (D.22) and the following result is obtained:

$$Y \succ 0 \quad \text{and} \quad \begin{pmatrix} (AY + BM)^T + (A + BM) & H & (CY + DM)^T \\ H^T & -\gamma I & E^T \\ (CY + DM) & E & -\gamma I \end{pmatrix} \prec 0 \tag{D.24}$$

Obviously, the feasibility of the matrix (Y,M) has to guarantee the solution of the problem (D.24). If exists a solution of the problem (D.24), the previous system (D.22) for (X, D_c) can be solved inverting the equation of (D.23) where: $X = Y^{-1}$ and $D_c = MY^{-1}$. This means that, if the inequalities (D.24) are feasible, a couple of matrix (X, D_c) exists, that solves the problem. The matrix D_c stablizes the system and achieves the desired performance specification. If the inequalities (D.24) are not feasible, there is not exist a state feedback gain that satisfy the property.
Besides this contrains, in some control problem the control input is limited under a specific value β, to obtain this objective we have to add also this specifies at the equation problem (D.24). Starting for the inverse definition of $D_c = MY^{-1}$ the constrain $\|D_c\|^2 \leq \beta^2 I$ is imposed. This constrain is equal to $D_c D_c^T \leq \beta^2 I$. Now, at the last equation, the inverse definition of D_c is substituted, and obtain:

$$MY^{-1}Y^{-1}M^T \leq \beta^2 I \Rightarrow MY^{-2}M^T \leq \beta^2 I \tag{D.25}$$

At this point we can add and subtract the relation $M\phi^{-2}M^T$ at the left inequality of (D.25), where ϕ is a scalar. This operation does not change the inequality and the result is $M(Y^{-2} - \phi^{-2}I + \phi^{-2}I)M^T \leq \beta^2 I$. It is possible to divide the single inequality in two different inequelities as follow:

$$\begin{cases} M\phi^{-2}M^T \leq \beta^2 I \\ M(Y^{-2} - \phi^{-2})M^T \leq 0 \end{cases} \tag{D.26}$$

where the first is obtained considered only the ϕ^{-2} in the parentesis and the second with the remaining terms. Inverting the equation, the two constrain for the LMI problem are obtained:

$$Y \succ \phi \quad \text{and} \quad \begin{pmatrix} \beta\phi & M \\ M^T & \beta\phi \end{pmatrix} \prec 0 \tag{D.27}$$

The constrains find in the (D.27) add to the right contrain of the equation (D.24) guarantee the LMI solution for the bounded input.

Appendix E

Background of Robust LPV & Gain Scheduling Theory

E.1 Introduction to LPV and Setting the LPV Controller

In this section the principal LPV's property will be descirbed.

E.1.1 Polytopic Uncertainties and Robustness Analysis

The steady space model is used to describe the physical systems with various variables. Normally, the physical systems are variables, perturbed or uncertainties in the physical parameters at this lead the model uncertain. Often, this uncertain changes the value of the parameters or coefficients of the steady space model. The very small parameter variations have a great impact on the dynamics of the system, this reason is sufficient to analyze the parametric uncertainties of dynamical system. The vector $\delta = (\delta_1, \cdots, \delta_p)$ is defined and expresses the uncertain quantities of dynamical system. There are at least two distinct cases of interest:

1. *Time-invariant parametric uncertainties*: the vector δ is fixed but unknown element of an uncertainty set $\boldsymbol{\delta} \subseteq \mathbb{R}^p$;

2. *Time-varying parametric uncertainties*: the vector δ is an unknown time-varying function $\boldsymbol{\delta} : \mathbb{R} \to \mathbb{R}^p$ where values $\delta(t)$ belongs to an uncertainty set $\boldsymbol{\delta} \subseteq \mathbb{R}^p$, and there is also the possibility that they satisfy additional constrains.

Time-Invariant Parametric Uncertainty

The uncertain time-invariant system is defined as follow

$$\dot{x} = A(\delta)x \tag{E.1}$$

where A$(\cdot)$ is a continuos function of the real-valued parameter vector $\delta = col(\delta_1, \cdots, \delta_p)$ which is only known and is contained in an uncertain set $\boldsymbol{\delta} \subseteq \mathbb{R}^p$. The robust stability problem is made the uncertain system (E.1) exponentially stable for all $\delta \in \boldsymbol{\delta}$ around at a equilibrium point $x^* = 0$.
The quadratically stable for an uncertain system (E.1) is defined as: there exists $X = X^T$ such that

$$X \succ 0 \quad A(\delta)^T X + X A(\delta) \prec 0 \quad \forall \delta \in \boldsymbol{\delta} \tag{E.2}$$

The definition $V(x) := x^T X x$ is a quadratic Lyapunow function and that implies as $A(\delta)$ is Hurtwitz $\forall \delta \in \boldsymbol{\delta}$. Then, the equation (E.2) is quadratic stable and means that the uncertain system is robust exponentially stable against the time-invariant uncertainties $\delta \in \boldsymbol{\delta}$. This property is summarized in the following theorem:

Theorem 3: If $A(\delta)$ is affine in δ and $\boldsymbol{\delta} = co(\delta_1, \cdots, \delta_N)$ then $\dot{x} = A(\delta)x$ is quadratically stable if and only if there are some X such that

$$X \succ 0 \quad A(\delta^k)^T X + X A(\delta^k) \prec 0 \quad k = 1, \cdots, N \tag{E.3}$$

The theorem shows how the quadratic stability can be numerically verified testing the feasibility in a finite number of LMI problem.

□

Time-Varying Parametric Uncertainty

Normally the robust stability for time-varying uncertainties has more requirements than the previous one. The uncertain time-varying system is defined as follow:

$$\dot{x}(t) = A(\delta(t))x(t) \tag{E.4}$$

where δ is an uncertain parameter curve defined by the function $\delta : \mathbb{R} \to \boldsymbol{\delta}$. Now, we suppose that the time-invariant uncertain stability and the robust stability of the origin are guaranteed and this implies that the $A(\delta)$ is Hurwitz $\forall \delta \in \boldsymbol{\delta}$. In this case the uncertain system with time-varying parametric uncertainties is exponentially stable if an $X \succ 0$ exists such that the equation(E.2) is satisfied. The parameter curves $\delta(\cdot)$ normally are known to be continuously differentiable and constrained

$$\delta(t) \in \boldsymbol{\delta} \quad \dot{\delta}(t) \in \boldsymbol{\rho} \quad \forall t \in \mathbb{R} \tag{E.5}$$

In order to test the robust stability, it is necessary to introduce the parameter-dependent Lyapunow function. This function takes the form $V(x, \delta) := x^T X(\delta) x$ and requires to search a matrix function $X(\delta) = X(\delta)^T$ with $\delta \in \boldsymbol{\delta}$. Let introduce, for notational convenience, the "derivative"

$$\partial X(\delta, \rho) := \sum_{k=1}^{p} \partial_k X(\delta) \rho_k \quad (\delta, \rho) \in \boldsymbol{\delta} \times \boldsymbol{\rho} \tag{E.6}$$

where $\partial_k X(\cdot)$ is the partial derivative of the function X(·) respect to the kth entry of δ and ρ_k is the kth component of the vector ρ. As made for the time-invariant parametric uncertainties we can summarize the previous aspect in the following theorem:

Theorem 4: Supposing that $\boldsymbol{\delta}$ and $\boldsymbol{\rho}$ are compact subsets of $\mathbb{R}^p$ and that $X(\delta) = X(\delta)^T$ is a continuously differentiable matrix function that satisfies

$$X(\delta) \succ 0 \quad \partial X(\delta, \rho) A(\delta)^T X(\delta) + X(\delta) A(\delta) \prec 0 \tag{E.7}$$

$\forall\, \delta \in \boldsymbol{\delta}$ and $\forall\, \rho \in \boldsymbol{\rho}$, then the equation (E.4) is exponentially stable for all time-varying parametric uncertainties that satisfy (E.5).

□

E.1.2 Robust Performance

Section E.1.1 analyzes as the tests on robust stability influences the parametric uncertainties. The same generalization can be applied in order to obtain the conditions of robust performance. The uncertain parameter introduces a depending system

$$\begin{aligned} \dot{x}(t) &= A(\delta(t))x(t) + H(\delta(t))w(t) \\ z(t) &= C(\delta(t))x(t) + E(\delta(t))w(t) \end{aligned} \tag{E.8}$$

where $\delta(\cdot)$ is a continuously differentiable rate-bounded uncertainty that satisfies (E.5). In the $\mathcal{H}_\infty$ performance is demostrated which was the effect of the disturbance w on the error z in terms of the $\mathcal{L}_2$ gain of the system. In the equation (E.8), instead, the output z not only depends on the input w but also on the uncertainty $\delta(\cdot)$. We can say that the robust $\mathcal{L}_2$ gain is smaller than γ if:

- for w=0 and for every parameter curves $\delta(\cdot)$ that satisfies the (E.5), the point $x^* = 0$ is an exponentially stable equilibrium of the system (E.8);
- for $x(0) = 0$ it holds that

$$\sup_{\delta(\cdot) \text{ satisfies } (E.5)} \sup_{0<\|w\|_{\mathcal{L}2}<\infty} \frac{\|z\|_{\mathcal{L}2}}{\|w\|_{\mathcal{L}2}} < \gamma \tag{E.9}$$

With the time invariant parameter uncertainties (in case of $\boldsymbol{\rho} = \{0\}$) if the robust $\mathcal{H}_2$ gain is smaller than γ, the transfer function T_δ associated to the system (E.8) for the time invariant parameters $\delta(t) = \delta$ has to satisfy the inequality $\|T_\delta\|_{H\infty} < \gamma \ \forall \ \delta \in \boldsymbol{\delta}$. The following theorem is a generalization of the **Theorem 2** to robust $\mathcal{L}_2$ gain performance.

Theorem 5: supponing the existence of a continuously differentiable matrix function $X(\delta) = X(\delta)^T$ such that $X(\delta) \succ 0$ and

$$\begin{aligned} &\begin{pmatrix} \partial X(\delta,\rho) + A(\delta)^T X(\delta) + X(\delta)A(\delta) & X(\delta)B(\delta) \\ B(\delta)^T X(\delta) & 0 \end{pmatrix} \\ &+ \begin{pmatrix} 0 & I \\ C(\delta) & D(\delta) \end{pmatrix}^T \begin{pmatrix} -\gamma^2 I & 0 \\ 0 & I \end{pmatrix} \begin{pmatrix} 0 & I \\ C(\delta) & D(\delta) \end{pmatrix} \prec 0 \end{aligned} \tag{E.10}$$

$\forall \ \delta \in \boldsymbol{\delta}$ and $\rho \in \boldsymbol{\rho}$, then the uncertain system (E.8) has a robust $\mathcal{L}_2$ gain smaller than γ.

□

The **Theorem 5** has the main merit that converts the robust $\mathcal{L}_2$ gain performance to an algebraic property. The condition (E.10) requires to search with a numerical method the function matrix $X(\cdot)$ that needs to satisfy a partial differential LMI, as made for **Theorem 4**. Finally, we have to remark that the **Theorem 5** extends all performance specifications that we have mentioned in the section D.2.1.

E.1.3 Robust State Feedback

After the previous section, where we introduced the polytopic uncertainties and the robustness analysis, we have all element for introduce the *Robust State Feedback*. We consider

the system (E.16) whose it is described by matrix affected from time-dependent paremetric uncertainty $\delta(t) \in \mathbb{R}^p$.

$$\begin{aligned} \dot{x}(t) &= A(\delta(t))x(t) + B(\delta(t))u(t) + H(\delta(t))w(t) \\ z(t) &= C(\delta(t))x(t) + D(\delta(t))u(t) + E(\delta(t))w(t) \\ y(t) &= F(\delta(t))x(t) + G(\delta(t))w(t) \end{aligned} \tag{E.11}$$

We assume that the dependence of the system matrices is affine and bounded to the polytope:

$$\boldsymbol{\delta} := co(\delta^1, \cdots, \delta^N) \subset \mathbb{R}^p \tag{E.12}$$

The synthesis of the robust controller determines the feedback cotroller that guarantee the robust stability when the output y is measured and controlled from the input control u and it, also, guarantee the robust performance specification from the disturbance w to the output z of the controlled system. The robust state feedback synthesis problem is a particular case where the controller is a state feedback $u = D_c x$ with the gain D_c and it is suppose that we are able to measured the state (y=x). In this condition, the resulting close loop system becomes

$$\begin{aligned} \dot{x}(t) &= [A(\delta(t)) + B(\delta(t))D_c]x(t) + H(\delta(t))w(t) \\ z(t) &= [C(\delta(t)) + D(\delta(t))D_c]x(t) + E(\delta(t))w(t) \end{aligned} \tag{E.13}$$

At the equation (E.13) we apply the **Theorem 5** for a parameter indipendent $X(\delta) = X$ and, after that, we use the result of **Theorem 4** for the affine parameter dependence, we find the robust $\mathcal{L}_2$ gain of the controller system is smaller than γ if there exists $X = X^T$ such that

$$X \succ 0, \begin{pmatrix} [A(\delta^k) + B(\delta^k)D_c]^T X + X[A(\delta^k) + B(\delta^k)D_c] & XH(\delta^k) & [C(\delta^k) + D(\delta^k)D_c]^T \\ H(\delta^k)^T X & -\gamma I & E(\delta^k)^T \\ C(\delta^k) + D(\delta^k)D_c & E(\delta^k) & -\gamma I \end{pmatrix} \prec 0 \tag{E.14}$$

for all $k = 1, \cdots, N$. As made in the section D.2.3, we apply the nominal synthesis procedure with which we convert the bilinear problem in a convex one with a convexifying transformation. With reference at the equation (D.24) we perform a congruence transformation from $(X, D_c) \rightarrow (Y, M)$ and we can say that there exists (X, D_c) satisfying the (E.14) if and only if there exist (Y, M) that satisfying

$$Y \succ 0, \begin{pmatrix} [A(\delta^k)Y + B(\delta^k)M]^T + [A(\delta^k)Y + B(\delta^k)M] & H(\delta^k) & [C(\delta^k)Y + D(\delta^k)M]^T \\ H(\delta^k)^T & -\gamma I & E(\delta^k)^T \\ C(\delta^k)Y + D(\delta^k)M & E(\delta^k) & -\gamma I \end{pmatrix} \prec 0 \tag{E.15}$$

for all $k = 1, \cdots, N$.
We have also to solve the LMI feasibility problem in (Y, M). If the (Y, M) is a solution of the (E.15), the state feedback gain $D_c = MY^{-1}$ guaranteees the robust $\mathcal{L}_2$ gain that is smaller than γ for the close loop system.

E.1.4 Gain Scheduling Synthesis

An important generalization of the robust control synthesis problem shown in the previous section treated the depending of the controller on the parameter vector $\delta = col(\delta_1, \cdots, \delta_p)$. This means that there will be an online access to the time varying parameter $\delta(t)$ through an additional measurament by the controller. The aim of the classical *gain scheduling*

approach is this one: the controller has access in real time at the varying parameter $\delta(t)$ to associate a specific operating condition of the plant. For each condition $\delta \in \boldsymbol{\delta}$ a controller is designed and these are *scheduled* by the measurament information.
For the Linear Parameter-Varying (LPV) system

$$\begin{aligned} \dot{x}(t) &= A(\delta(t))x(t) + B(\delta(t))u(t) + H(\delta(t))w(t) \\ z(t) &= C(\delta(t))x(t) + D(\delta(t))u(t) + E(\delta(t))w(t) \\ y(t) &= F(\delta(t))x(t) + G(\delta(t))w(t) \end{aligned} \tag{E.16}$$

an LPV controller is defined as follow:

$$\begin{aligned} \dot{x}_c(t) &= A_c(\delta(t))x_c(t) + B_c(\delta(t))y(t) \\ u(t) &= C_c(\delta(t))x_c(t) + D_c(\delta(t))y(t) \end{aligned} \tag{E.17}$$

where $\delta(t)$ satisfies the constrains in (E.5). We want to design a LPV controller that make the controlled system robustly stable and establishes a desired robust performance specification. The close loop controlled system is obtained to the equation

$$\begin{aligned} \dot{\xi}(t) &= \mathcal{A}(\delta(t))\xi(t) + \mathcal{B}(\delta(t))w(t) \\ z(t) &= \mathcal{C}(\delta(t))\xi(t) + \mathcal{D}(\delta(t))w(t) \end{aligned} \tag{E.18}$$

where the system (E.18) has the same structure of the system (D.19). The LPV controller synthesis is closed to the one used to build up the LMI controller in section D.2.2. The robust stability and a robust $\mathcal{L}_2$ gain smaller than γ for the LPV synthesis problem is solved if we can find a controller and a smooth function $\mathcal{X}(\delta) = \mathcal{X}(\delta)^T$ such that for all $(\delta, \rho) \in \boldsymbol{\delta} \times \boldsymbol{\rho}$

$$\mathcal{X}(\delta) \succ 0, \quad \begin{pmatrix} \partial\mathcal{X}(\delta,\rho) + \mathcal{A}(\delta)^T\mathcal{X}(\delta) + \mathcal{X}(\delta)\mathcal{A}(\delta) & \mathcal{X}(\delta)\mathcal{B}(\delta) & \mathcal{C}(\delta)^T \\ \mathcal{B}(\delta)^T\mathcal{X}(\delta) & -\gamma I & \mathcal{D}(\delta)^T \\ \mathcal{C}(\delta) & \mathcal{D}(\delta) & -\gamma I \end{pmatrix} \prec 0 \tag{E.19}$$

where $\partial\mathcal{X}(\delta,\rho)$ is defined in (E.6). Afterwards a particular scenario is considered: the matrix B, D, F and G in the equation (E.16) become indipendent in δ. Moreover, the time varying parameters $\delta(t)$ are supposed to assume their values in a polytope without constraints on their rate of variation. The aim is finding a LPV controller in which the matrix functions (E.19) are affine in δ and the result matrix $\mathcal{X}$ is constant. All these assumptions imply that the close loop system becomes affine in δ. If the matrix of the close loop is affine imply that the equation (E.19) is verify $\forall\ \delta \in \boldsymbol{\delta}$ if and only if the generators $\delta = \delta^k$, k = 1,$\cdots$,N of the set $\boldsymbol{\delta}$ satisfy the (E.19). Hence, the robust $\mathcal{L}_2$ gain is smaller than γ if there is $\mathcal{X}$ such that

$$\mathcal{X} \succ 0, \quad \begin{pmatrix} \mathcal{A}(\delta^k)^T\mathcal{X} + \mathcal{X}\mathcal{A}(\delta^k) & \mathcal{X}\mathcal{B}(\delta^k) & \mathcal{C}(\delta^k)^T \\ \mathcal{B}(\delta)^T\mathcal{X} & -\gamma I & \mathcal{D}(\delta^k)^T \\ \mathcal{C}(\delta^k) & \mathcal{D}(\delta^k) & -\gamma I \end{pmatrix} \prec 0 \text{ and k} = 1,\cdots,\text{N} \tag{E.20}$$

The obtain system (E.20) is bilinear but not convex and for use the LPV synthesis we need a convex bilinear system. So, we apply a convexifying transformation

$$(\mathcal{X}, A_c(\delta^k), B_c(\delta^k), C_c(\delta^k), D_c(\delta^k)) \to (X, Y, K_k, L_k, M_k, N_k) := v_k$$

where k=1,$\cdots$,N. The (E.20) is transformed into

$$\begin{pmatrix} Y & I \\ I & X \end{pmatrix} \succ 0, \quad \begin{pmatrix} \mathbf{A}(v_k,\delta^k)^T + \mathbf{A}(v_k,\delta^k) & \mathbf{B}(v_k,\delta^k) & \mathbf{C}(v_k,\delta^k)^T \\ \mathbf{B}(v_k,\delta^k)^T & -\gamma I & \mathbf{D}(v_k,\delta^k)^T \\ \mathbf{C}(v_k,\delta^k) & \mathbf{D}(v_k,\delta^k) & -\gamma I \end{pmatrix} \prec 0, \text{ for all k=1,}\cdots,\text{N.} \tag{E.21}$$

In summary, the LPV controller design procedure consist of:

1. Test the feasibility of the synthesis inequalities (E.21) in the variables $v_k = (X, Y, K_k, L_k, M_k, N_k)$ for k=1,$\cdots$,N;
2. If the system is feasible, construct $\mathcal{X}$ as a standard state feedback procedure;
3. For this $\mathcal{X}$, find the controller parameter $\begin{pmatrix} A_{c,k} & B_{c,k} \\ C_{c,k} & D_{c,k} \end{pmatrix}$ that satisfies the (E.20) for each k=1,$\cdots$,N;
4. If $\delta \in \boldsymbol{\delta}$ is represented by $\delta = \sum_{k=1}^{N} \alpha_k \delta^k$ with $\alpha_k \geq 0$, $\sum_{k=1}^{N} \alpha_k = 1$, then we obtain the controller matrix are equal to:

$$\begin{pmatrix} A_c(\delta) & B_c(\delta) \\ C_c(\delta) & D_c(\delta) \end{pmatrix} = \sum_{k=1}^{N} \alpha_k(t) \begin{pmatrix} A_{c,k} & B_{c,k} \\ C_{c,k} & D_{c,k} \end{pmatrix}$$

with $\mathcal{X}$ indipendent of δ and $\partial\mathcal{X}(\delta, \rho) = 0$.

So, the LPV controller is obtained by taking time varying comvex combination of the N controllers defines by the quadruples $(A_{c,k}, B_{c,k}, C_{c,k}, D_{c,k})$. The controller equation (E.19) are obtained by the equation:

$$\begin{pmatrix} A_c(\delta(t)) & B_c(\delta(t)) \\ C_c(\delta(t)) & D_c(\delta(t)) \end{pmatrix} = \sum_{k=1}^{N} \alpha_k(t) \begin{pmatrix} A_{c,k} & B_{c,k} \\ C_{c,k} & D_{c,k} \end{pmatrix}$$

where the parameter $\delta(t)$ at time t is represented as $\delta(t) = \sum_{k=1}^{N} \alpha_k(t)\delta^k$ with $\alpha_k(t) \geq 0$, $\sum_{k=1}^{N} \alpha_k(t) = 1$.

Bibliography

[1] Hans B. Pacejka, *Tyre and vehicle dynamics*, Third Edition, British Library, 2009.

[2] U. Kiencke and L. Nielsen, *Automotive Control Systems*, For Engine, Driveline and Vehicle, Germany, Springer, 2005

[3] R. Rajamani, *Vehicle Dynamics Control*, Second Edition, London, Springer, 2012

[4] J. Y. Wong, *Theory of Ground Vehicles*, Third Edition, United States of America, John Wiley & Sons., 2001

[5] J.S. Shamma, *An overview of LPV systems*, in Control of Linear Parameter Varying Systems with Applications, Germany, Springer, 2012

[6] B. Vanek, B. Kulcsàr, P. Falcone and G. Balas, *Yaw Control via Combined Braking and Steering*, European Control Conference (ECC), Budapest, Hungary, 23-26 August 2009

[7] W. J. Rugh and J. S. Shamma, *Research on Gain Scheduling*, Automatica 36 (2000) 1401-1425, 6 December 1999

[8] J. S. Shamma and M. Athans, *Gain Scheduling: Potential Hazards and Possible Remedies*, Control Systems IEEE, vol. 12, no. 3, pp. 101-107, June 1992

[9] M. Athans and J. S. Shamma, *Analysis of Gain Scheduled Control for Nonlinear Plants*, IEEE Transactions on Automatic Control, vol. 35, no. 8, pp. 898-907, August 1990

[10] M. Doumiati, O. Sename, L. Dugard, J. Martinez, P. Gaspar and Z. Szabo, *Integrated Vehicle Dynamics Control via Coordination of Active*, European Journal of Control, vol. 19, no. 2, pp. 121-143, 2013

[11] G. Cai, G. Duan and C. Hu, *A Velocity-Based LPV Modeling and Control framework for an Airbreathing Hypersonic Vehicle*, International Journal of Innovative Computing of Information and Control, vol. 7, no. 5, pp. 2269-2281, May 2011

[12] J.-M. Biannic and P. Apkarian, *Missile Autopilot Design via a Modified LPV Synthesis Technique*, Aerospace Science and Technology, vo. 3, no. 3, pp. 153-160, April 1999

[13] M. Chilali, P. gahinet and P. Apkarian, *Robust Pole Placement in LMI Regions*, IEEE Transactions on Automatic Control, vol. 44, no. 12, December 1999

[14] S. Scalzi, A. Benine-Neto, M. Netto, W. Pasillas-Lepine and S. Mammar, *Active Steering Control Based on Piecewise Affine Regions*, American Control Conference (ACC), Baltimore MD, pp. 5362-5367, July 2010

[15] S.C. Baslamisli, I. Polat and I. E. Kose , *Gain Scheduled Active Steering Control Based on a Parametric Bicycle Model*, IEEE Intelligent Vehicles Symposium, Istanbul, pp. 1168-1173, 13-15 June 2007

[16] Y. Ikeda, *Active Steering Control of Vehicle by Sliding Mode Control*, IEEE International Conference on Control Applications (CCA), Yokohama, pp. 1660-1665, 8-10 September 2010

[17] J. Ackermann and W. Sienel, *Robust Yaw Damping of Cars with Front and Rear Wheel Steering*, IEEE Transactions on Control Systems Technology, vol. 1, no. 1, pp. 15-20, March 1993

[18] M. Arrambide and E. Durling, *Design of a side-slip observer for single-unit heavy trucks*, Chalmers University of Technology, Master's Thesis, 2010

[19] F. Wu, *Control of Linear Parameter Varying System*, University of California at Berkeley, Ph.D Thesis, 1995

[20] J. S. Shamma, *Analysis and Design of Gain Scheduled Control Systems*, Massachusetts Institute of Technology, Ph.D Thesis, May 1998

[21] A. U. genc, *Linear Parameter-Varying Modelling and Robust Control of Variable Cam Timing Engines*, University of Cambridge, Ph.D Thesis, November 2002

[22] F. Bruzelius, *Linear Parameter-Varying System* an approach to gain scheduling, Chalmers University of Technology, Ph.D Thesis, 2004